An effective MPPT control techniques for active and reactive power control in grid connected PV system

A thesis submitted in fulfillment of the requirements for the award of the degree of

DOCTOR OF PHILOSOPHY

in

ELECTRICAL & INSTRUMENTATION ENGINEERING

submitted by

VINIT KUMAR

(Registration No: 901504017)

Under the guidance of

Dr. MUKESH SINGH

Associate Professor, EIED

THAPAR INSTITUTE
OF ENGINEERING & TECHNOLOGY
(Deemed to be University)

Electrical & Instrumentation Engineering Department

Thapar Institute of Engineering and Technology, Patiala.

(Deemed-to-be-University)

Punjab (India)-147004

November 2020

CERTIFICATE

I, Vinit Kumar, Registration No. 901504017, hereby declare that the thesis entitled **"An effective MPPT control techniques for active and reactive power control in grid connected PV system"**, submitted to the Electrical and Instrumentation Engineering Department at Thapar Institute of Engineering and Technology, Patiala, Punjab (India) is an authenticated record of my own work for the award of the degree of "**Doctor of Philosophy**" under the supervision of Dr. Mukesh Singh. This Thesis has not been submitted to any other Institute or University for the award of any other degree or diploma.

Vinitkumar

Vinit Kumar
Registration No. 901504017

Place: Patiala
Date: 06/11/2020

This is to certify that the above statement made by the candidate is correct to the best of our knowledge.

Verified by:

Mukesh

Dr. Mukesh Singh
Associate Professor
EIED, Thapar Institute of
Engineering and Technology

ACKNOWLEDGEMENTS

First and foremost, I would like to thank the almighty God who gave me strength and courage to overcome all the obstacles and complete this endeavour. The successful completion of any task would be incomplete without acknowledging the people who made it possible. I would like to take this opportunity to express my gratitude to all those who made this journey possible. Words are often too less to express one's deepest regards, but let's give it a go.

I offer my sincerest gratitude to my supervisors, Dr. Mukesh Singh (Associate Professor, EIED), who have supported me throughout my Ph.D. work with their patience and knowledge; while providing me the room to work in my own way. I had the pleasure to visit South Korea with him and one simply could not have wished for better and friendlier supervisors. They led me to the correct direction at every stage of this research work. Apart from providing me with excellent supervision, strong cooperation and constant encouragement throughout this journey, they also shared their invaluable experiences with me to succeed in life. They have truly been the source of real inspiration for me and I will always remain indebted to him.

I am also grateful to the head of department, Prof. R.S. Kaler, the former head, Prof. Ravindra Agarwal, Ph.D. Coordinator, Prof. Mandeep Singh and members of my doctoral committee, Prof. S. K. Jain, Prof. Kulbir Singh and Dr. Parag Nijhawan for their constructive suggestions and ensuring the correct pace of my work. I sincerely thank to Ms. Manbir Kaur, Dr. Shakti Singh and all other faculty and support staff of Electrical and Instrumentation Engineering Department as well for their constant help whenever required. I am also obliged to the Director, Prof. Prakash Gopalan, DoRSP, Prof. Rafat Siddique, Associate DoRSP Prof. Kulvir Singh and the management of Thapar Institute of Engineering and Technology, who provided me with all the necessary resources and facilities to complete my work.

The chain of my gratitude will definitely be incomplete if I forget to thank my parents, Shri Krish Nandan Singh and Smt. Shanti Devi, for their unconditional love, support and encouragement in every phase of my life. It was due to my father's faith and encouragement that I started my Ph.D. in the first place. Since then, he stood by me through thick and thin,

and gave me courage at the times when I felt really low. His constant motivation showed me the silver lining in the dark clouds. I would also like to express heartfelt thanks to my friend Ms. Neha Rawat who always believed in me and whose love have truly played the role of game changer in my life. I would like to pay my sincere regards to all my relatives and cousins for their constant motivation and support. They made this journey easier with words of encouragement which helped me in finishing my work.

I would also like to thank my friends and colleagues with whom I have travelled this journey of research. A special thanks to my group of budding doctors, Mr. Nagendra Singh, Mr. Himanshu Anand, Mr. Rituraj Patwal, Mr. Anurag Verma, Mr. Saudagar Balasahab Dongre, Mr. Ajay Chilotra, Mr. Karanveer Dhingra, Mr. Ravi Teja, Ms. Supriya Kumari, Ms. Amritpal Kaur and Ms. Kritika Yadav. These people have made my research journey all the more memorable and pleasant.

As one cannot mention the names of all well-wishers, friends and beloved ones, I would like to pay my regards to one and all who supported me during this journey of knowledge. The financial help from the Department of Science and Technology, New Delhi under grant no. DST/TM/CERI/D(48)G is duly acknowledged which has provided me with the opportunity to work without worrying about the funds.

(Vinit Kumar)

ABSTRACT

In the current power demand situation, the participation of renewable energy sources (RESs) such as wind, solar, geothermal and hydro are increasing continuously. Amongst RESs, solar-based power generation is more adopted due to the source availability and numerous technological advancement. Especially, the grid connected or grid-interfaced photovoltaic (GIPV) system is being accepted widely due to the cost effectiveness and ease of maintenance, as they eliminate the need of installing batteries to store energy. Nevertheless, there are still many issues in the way to accept the GIPV system generally. In this respect, customers are facing some important issues such as the system size, surplus power and bounded use of the PV system. Moreover, it is also facing less effective maximum power point tracking (MPPT) techniques and control strategies to extract and exchange the power, respectively. Hence, to resolve these problems, such novel schemes are required which can reduce the size of the system, improves the MPPT and inverter control performances, utilized for the active power generation and reactive power compensation. Additionally, to expand the application of the PV system in other areas like electric vehicle (EV) based transportation system, a control scheme is also required. Hence, four different control schemes are proposed to resolve the aforementioned problems.

Firstly, a novel control approach for a GIPV system has been developed. This novel approach introduces a sensorless DC-link voltage control for a two-stage three-phase GIPV system, which reduces the system size and cost. The proposed two-stage system includes an intermediate boost converter (IBC) and pulse width modulation (PWM) strategy based voltage source inverter (VSI). In the first-stage control, the intermediate converter is incorporated with the MPPT technique. Amongst the various available MPPT techniques, due to ease of maintenance, the incremental conductance algorithm is implemented to enhance the voltage level of the PV array under variable irradiance condition. Further, the second-stage control of VSI deals with DC-link voltage regulation (outer-loop) and current control (inner-loop) matching with the conventional scheme. Distinctively, the proposed scheme avoids the outer-loop and controls the inner-loop. Hence, the reduction of DC-link high voltage sensor minimizes the cost as well as the size of the system. However, the DC-link voltage remains maintained through power bal-

ancing. Therefore, the removal of the outer-loop controller enhances the system stability and the dynamic response of the system under variable irradiance conditions.

In the second work, a GIPV system resolves the issue of surplus active power and inadequate performance of the existing MPPT techniques. Whereas, the surplus active power causes the overvoltage problem during peak hours of power generation at the point of common coupling in low or medium voltage level grid. Additionally, inadequate performance of the MPPT technique results in the power loss due to high settling time during the sudden change in irradiance. Therefore, to solve the surplus power problem and improve the MPPT algorithm performance in variable irradiance conditions a novel control strategy has been proposed. In this control strategy, a derated power generation mode (DPGM) control get activated to curtail the active power. Additionally, a drift-free (named as modified) perturb & observe (P&O) technique used to improve the performance of the MPPT algorithm. Consequently, the DPGM control scheme with the IBC shaves the surplus active power during the peak hours of power generation. Furthermore, the modified P&O (MP&O) algorithm deals with the fluctuation of irradiance during non-peak hours. Thus, the proposed control scheme appears more efficient for the system during the peak hours of power generation. Besides, it reduces power loss and settling time during the change in irradiance for non-peak hours.

In third work, the generated power is utilized from the connected local linear/non-linear loads and the rest of the power is transferred to the grid. Therefore, when the local load is present with the GIPV system, it demands reactive power compensation. The compensation is fulfilled either by the PV inverter or grid. However, the inverter transferring power with full capacity would have no margin to generate reactive power. Therefore, the reactive power demand is supplied from the grid, which causes an extra burden on the grid. Thus, to reduce the burden on the grid, a GIPV system with MP&O, MPPT technique has proposed in the third scheme. In third scheme, the proposed technique uses an IBC which extracts maximum power more efficiently as compared to the traditional MPPT technique. On the other hand, it curtails the generated active power and provides a margin for the PV inverters to generate reactive power. Further, the PV inverter generates active and reactive power to the local load and transfer power to the grid using inverter control. The inverter control comprises of instantaneous active and reactive power control. In this control scheme, it maintains voltage profile and provides more dynamically stable system under fluctuating weather conditions.

Lastly, in the fourth scheme, the PV system is implemented to support the new transportation option, i.e., for EV at remote locations and minimize the grid burdening in urban areas. The EV charger seeks energy from PV, however, it fluctuates due to change in irradiance and it can not generate constant energy. Therefore, an energy storage device is required to meet the energy demand and improve the sustainability of the charging station. Thereby, a system has been proposed, which consists of an energy storage system (ESS) along with the PV source and EV charger. The proposed system includes a PV array with a boost converter, two bi-directional converters (BDC) and ESS. The BDC is used for charging/discharging of the EV and ESS. However, the energy generated from PV is not sufficient to drive the demand during the absence or reduced sunlight, therefore, ESS is required to meet the energy demand. On the other hand, while generation is more than demand, the ESS utilizes the excess clean energy to make the system stable. This results, a reliable, cost-efficient, pollution-free EV charging station to support modern era transportation. All schemes proposed above for the GIPV systems are simulated in MATLAB/Simulink using simpower tools and the system performance is verified using the software-in-loop mode of Opal-RT 4510 in the real-time environment.

LIST OF PUBLICATIONS BASED ON THESIS

Journal Publications (SCI/SCIE)

1. Vinit Kumar, Mukesh Singh, "Sensorless DC-link control approach for three-phase grid integrated PV system", ***International Journal of Electrical Power and Energy Systems***, 112, 309-318. https://doi.org/10.1016/j.ijepes.2019.05.006
   (Impact factor: **3.588**)

2. Vinit Kumar, Mukesh Singh, "Derated mode of power generation in PV system using a modified perturb & observe MPPT algorithm", ***Journal of Modern Power Systems and Clean Energy***, (Early Access), DOI: 10.35833/MPCE.2019.000258
   (Impact factor: **3.090**)

3. Vinit Kumar, Mukesh Singh, "Reactive power Compensation Using MP&O, MPPT Technique in Grid-Interfaced PV System", (Under review)

Conference Publications

1. Vinit Kumar, Villuri Ravi Teja, Mukesh Singh and Sukumar Mishra, " PV Based Off-Grid Charging Station for Electric Vehicle", in ***IFAC-PapersOnline***, 52(4), 10-12 June, 2019, Jeju, Republic of South Korea, pp 276-281.

Contents

List of Tables

List of Figures

List of Abbreviations

ΔD	Step size of duty ratio
ΔP_{PV}	Change in PV power (W)
ΔT	Difference of the temperature at standard test condition (STC) and actual (K)
ΔV_{PV}	Change in PV voltage (V)
ω	Angular frequency of the grid voltage
C_{BDC}	Considered capacitor value of bi-directional converter
C_{boost}	Capacitor value of bi-directional converter in boost mode
C_{buck}	Capacitor value of bi-directional converter in buck mode
C_{DC}	Interfacing capacitor between intermediate boost converter and voltage source inverter
D	Duty ratio for boost converter
D_b	Uncontrolled switch of the intermediate boost converter
G	Operating solar irradiance ($\mathrm{W/m^2}$)
G_n	Reference solar irradiance ($\mathrm{W/m^2}$)
I_d^*, I_q^*	d-axis and q-axis reference current of the inverter (A)
I_d, I_q	d-axis and q-axis current of the inverter (A)
I_o	Reverse saturation current of diode (A)
I_a, I_b, I_c	Grid side currents of the grid intigrated PV system (A)
I_{DC}	Output current of boost converter (A)
I_{MPP}	Current at maximum power point (A)
I_{PV}	Current of PV array (A)
I_{scn}	Short circuit current of PV array at standard test condition (STC) (A)
I_{sc}	Short circuit current of PV array (A)
K'	Proportional gain of the feed-forward controller
k_i	Temperature co-efficient
L	Interfacing inductor at output of the inverter (mH)

L_b	Inductor of the intermediate boost converter
L_{BDC}	Considered inductor value of bi-directional converter
L_{boost}	Inductor value of bi-directional converter in boost mode
L_{buck}	Inductor value of bi-directional converter in buck mode
m_d, m_q	d-axis and q-axis modulation indexes for the inverter
N_p	Number of PV modules in parallel
N_s	Number of PV modules in series
$P(t_9 - t_{16})$	Power generated from PV source in particular hours of the day (W)
P_{DC}	Output power of boost converter (W)
P_{limit}	Power transfer limit (W)
P_{PV}	Power of PV array (W)
R	Resistance of each phase (Ω)
R_{in}	Input impedance of boost converter (Ω)
R_{out}	Output impedance of boost converter (Ω)
$S_1 - S_6$	Gate signals for the inverter
S_b	Controlled switch of the intermediate boost converter
$t_9 - t_{16}$	Particular hours of the day
V_d^*, V_q^*	d-axis and q-axis reference voltage of the inverter (V)
$V_{DC-link}^{ref}$	Reference DC-link voltage for the inverter (V)
V_d, V_q	d-axis and q-axis voltage of the inverter (V)
V_t	Thermal voltage of diode (V)
V_{batt}	Voltage level of the battery
$V_{DC-link}$	Measured DC-link voltage of the inverter (V)
V_{DC}	Output voltage of boost converter (V)
V_{MPP}	Voltage at maximum power point (V)
V_{PV}	Voltage of PV array (V)
V_{sa}, V_{sb}, V_{sc}	Grid side voltages of the grid intigrated PV system (V)
V_{sd}, V_{sq}	d-axis and q-axis voltage of the grid (V)

V_{ta}, V_{tb}, V_{tc}	Terminal voltage of the inverter (V)
BDC	Bi-directional converter
CC	Constant current
CS	Charging station
CSI	Current source inverter
CV	Constant voltage
DPGM	Derated power generation mode
ESS	Energy storage system
EV	Electric vehicle
G2V	Grid to vehiclee
GCBD	Grid-connected bi-directional
GIPV	Grid-interfaced PV system
HFT	High frequency transformer
IBC	Intermediate boost converter
IC	Incremental conductance
LFT	Low frequency transformer
MPP	Maximum power point
MPPT	Maximum power point tracking
NPC	Neutral point clamped
P-V	Power-voltage
P&O	Perturb and observe
PCC	Point of common coupling
PCU	Power conditioning unit
PI	Proportional integral
PLL	Phase lock loop
PV	Photovoltaic
PVBCS	PV based charging station
PWM	Pulse width modulation

RES	Renewable energy source
RESs	Renewable energy sources
SD	Standard deviation
THD	Total harmonic distortion
V2G	Vehicle to grid
VSI	Voltage source inverter

Chapter 1

INTRODUCTION AND THESIS OVERVIEW

1.1 Introduction

Electricity is a big concern for every one, not because it has becomes our basic need but also because of the increasing demand of electricity day by day. According to the data of international energy outlook 2019, world energy consumption increases nearly 50% between 2018 and 2050. According to the statistics [1], the energy consumption in 2012 was 549 quadrillion Btu which is increased to 629 quadrillion in 2020 and it is projected to near 910 quadrillion Btu by 2050. To match the electricity demand, we are mostly dependent on the conventional power generation systems whose fuels are coal, gas, oil and uranium (nuclear plant) which are non-renewable. Now a days some renewable energy sources (RESs) like hydro, solar, wind, biomass and tidal are becoming a part of power generation system to fulfil the raised electricity demand [2, 3]. The RESs based electric power production reached 26.2% of whole installed power generation capacity and according to the International Energy Agency (IEA) report, it is expected to reach upto 40% by 2040 [4]. Among these RESs, solar, wind and hydro have a major contribution towards the generation. Table 1.1 depicts the statical analysis of RES's participation in upcoming years [5]. Amongst all, the power generation through hydro is very much similar to the conventional approach i.e. thermal. However, the hydro energy based generation consists of a high installation cost and complex implementation strategy as compared to solar. Therefore, solar energy based power generation plant is more popular amongst all RESs [6]. According to the IEA report, the generation from wind source (8300 TWh) and solar PV (7200 TWh) expected to exceed from hydro (6950 TWh) by 2040 [4]. In another report from the International Renewable Energy Agency (IRENA), the growth of the solar PV capacity is increasing gigantically. The IRENA report presents that the PV generation participation

Table 1.1: The participation of RESs in power generation scenario

	2010	**2020**	**2035**
Electricity generation (TWh)	**4206**	**6999**	**11,324**
Bioenergy	331	696	1,487
Hydro	3431	4513	5,677
Wind	342	1272	2,681
Geothermal	68	131	315
Solar PV	32	332	846
Concentrating solar power	2	50	278
Marine	1	5	57
Share of total generation	**20%**	**25%**	**31%**

in global power production was 480 GW in 2018 and it is expected to reach upto 2840 GW in 2030 and 8519 GW by 2050 which is almost eighteen times of the generation of 2018^{th}.

The major reason of the adoption of the solar PV because of the sun light is plenty in nature and it is more than sufficient to fulfil the power demand of electricity. That is why the solar power is the main attraction of researchers these days. The growth of PV solar power generation has increased exponentially in recent times. Revolution in PV power converter technology has triggered the growth of power generation through solar PV system. This is due to increase in efficiency, power extraction capability from modules and reliability without impacting much cost [6–11].

PV system includes solar panels or modules which can be connected in a series and parallel combination for high power application and power converters that convert output of the module from DC to AC. These converters include semiconductor switches to get power from the system. Some systems also have storage devices and charging controllers, where energy absorbed by the module is stored in devices like batteries and super capacitors [12]. Energy extracted from PV system has to pass few stages to connect with utility grid. These stages include DC-DC converter and DC-AC converters with or without transformer which is shown in Fig. 1.1. On the basis variations in PV system, these are classified into stand alone [13, 14], grid connected and hybrid PV system that is shown in Fig. 1.2(a), 1.2(b), and 1.2(c) respectively. Due to the demand of electricity and less complexity of PV system structure, grid connected or grid interfaced PV (GIPV) system is more popular and beneficial. A GIPV system is cost

effective and requires less maintenance. A typical configuration of a GIPV system is mentioned in Fig. 1.1. It describes the components and stages of GIPV system. In this figure a PV system is connected with a filter, DC-DC converter, dc-link, DC-AC converter (Inverter), output filter, low frequency transformer (LFT) and grid. On the basis of stage, system is categorized into one stage GIPV system which consist of PV system with DC-AC converter connected to grid and two stage GIPV system which consist of PV system with DC-DC converter with DC-AC converter and grid. In [15], it has been discussed that a single stage configuration of GIPV is better suitable in the system because of its efficiency, less maintenance and size of the system. Among both configurations the main component of the system is inverter. It is the main processing unit of the system which converts input DC voltage into output high quality AC voltage. The utilization of the inverter depends on how it is going to handle into the system.

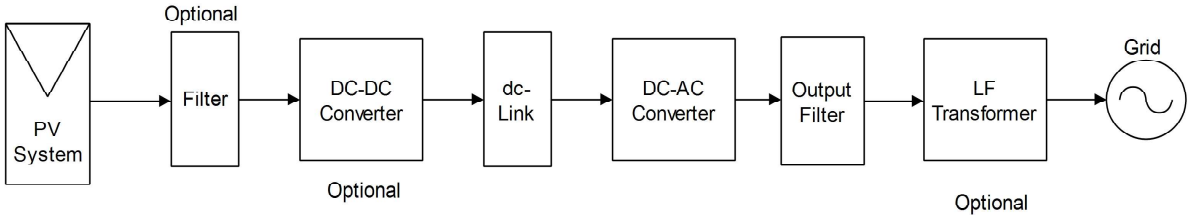

Figure 1.1: A typical configuration of grid interfaced PV system

1.2 Development in GIPV System Structure

Now, as per brief discussion about the grid interfaced PV system one thing is very clear that, the role of power inverters is very important. It is not only enabling the system to be more efficient and interconnected but also the use of more voltage level as well as complex power structure [11]. In papers [16–18], the authors have discussed about the various types of PV system structure based on the inverter technology which can be seen in Fig. 1.3. Technologies like centralized, string, multi-string, AC module and AC cell inverters, in the same order describe the development of inverters from the past to present. The other frame of structure is the use of single phase or three phase grid connected system. From the inverter point of view, for the high power application mostly three phase GIPV system is best applicable due to less loss per component, reduced size and decreased stress on switches [6, 19].

These structures are categorized on the basis of their capacity, size and where they used

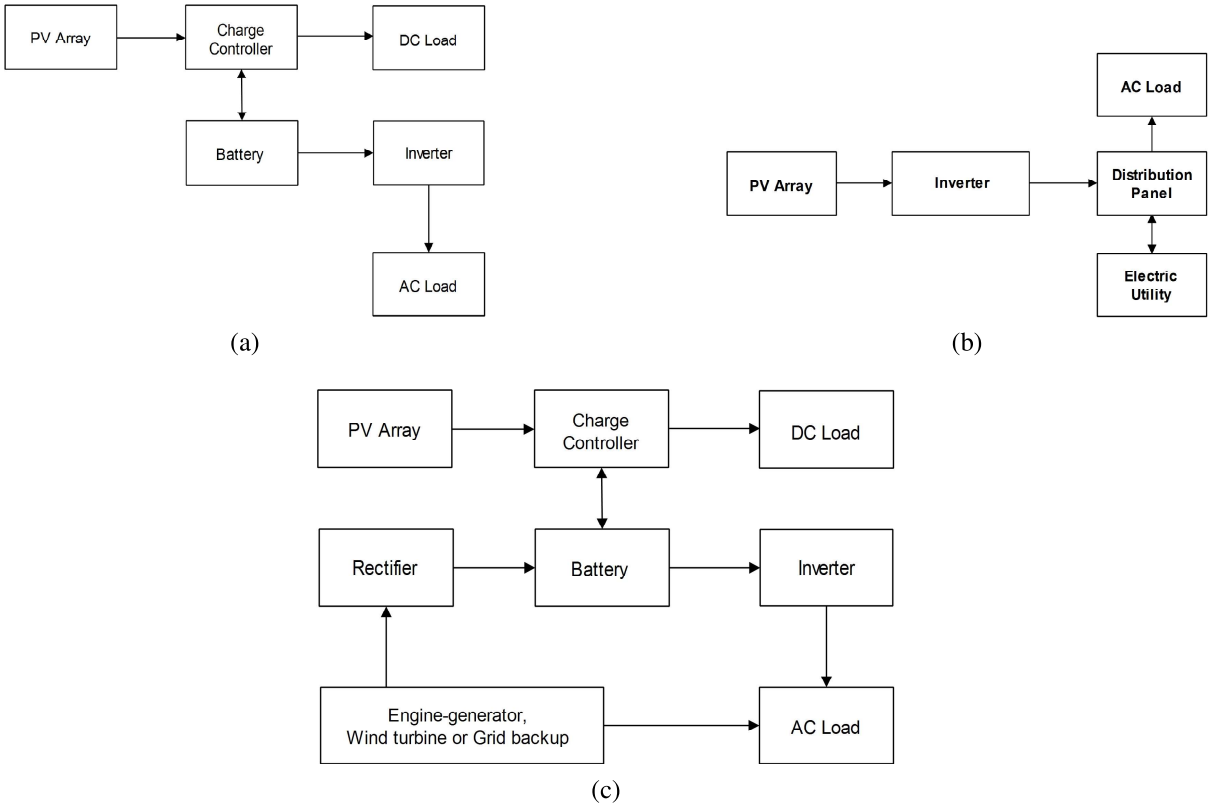

Figure 1.2: Block diagram of (a) stand alone (b) grid interfaced (c) hybrid PV system

(industrial, commercial or personal). A large scale generation system is used where there is requirement of high power and voltage level such as the utility grid. The central inverter technology is the part of this type of generation system. A medium scale generation system is less in capacity from the large scale but efficient to provide power for industrial use, so these are mostly use for medium applications. String and multi-string inverter technologies are the part of medium scale generation system. Last but not least, at a small level generation from PV system AC module inverter technology is mostly used to fulfill the requirement of customer directly. These categories are summarized in Table 1.2.

Table 1.2: Overview of grid interfaced PV inverters conversion capacity and connection

	Central	Multistring	String	AC module
Power Range	$<$ 850 kW	$<$ 500 kW	$<$ 10 kW	$<$ 350 W
Capacity to use	Large Scale	Medium Scale	Medium Scale	Small Scale
Grid Connections	3-Phase	1-Phase or 3-Phase	1-Phase	1-Phase

Systems discussed above can be called a good system when it operates efficiently as well as

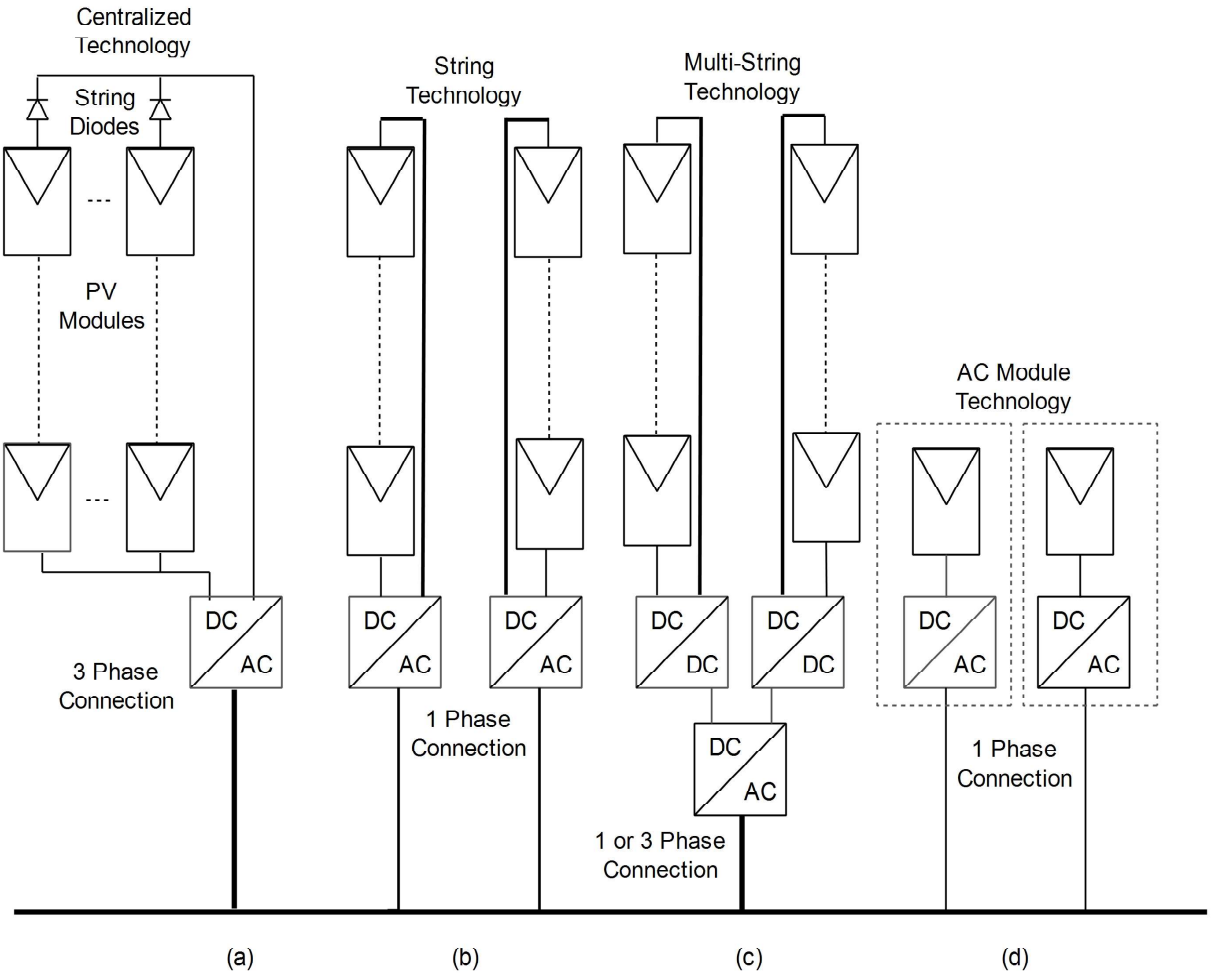

Figure 1.3: Overview of PV inverters: (a) centralized inverter (b) string inverter (c) multi-string inverter (d) AC module inverter

economically. Use of DC-DC converter, filters and LFT is optional since they are not essential for the system. This also reduce the number of stages. So, the GIPV system is further classified on the basis of there stages and components used in the system.

1.2.1 Classification of PV system

The available PV systems are majorly classified based on the components used in the system such as placement of the transformer and power processing steps [16].

Placement of transformer

Transformer in GCPVS provides galvanic isolation. This can be achieved with the placement of transformer at different places as shown in Fig. 1.4(a), 1.4(b) and 1.4(c). In Fig. 1.4(a),

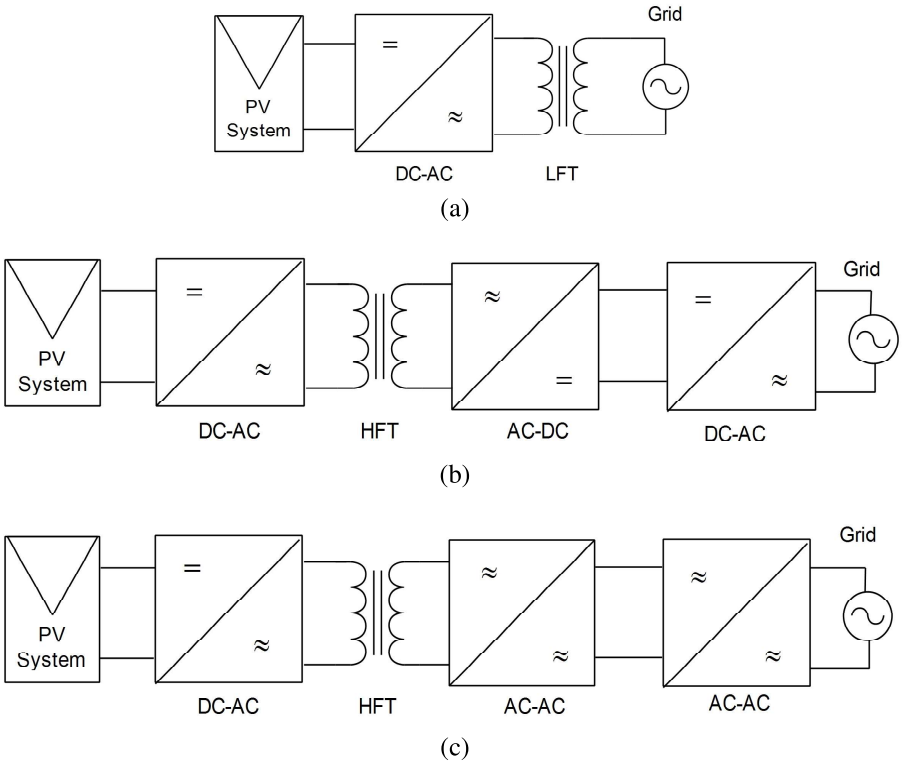

Figure 1.4: Basic structure of (a) LF transformer directly connected with grid (b) HFT with DC-DC converter (c) HFT between DC-AC and AC-AC converters.

a LFT is connected with the grid for the galvanic isolation which minimizes the presence of DC components in the system after DC-AC conversion . The presence of DC components in system, saturates the distributed transformer's core at the grid side. In modern PV systems, a high frequency transformer (HFT) with DC-DC converters or between DC-AC and AC-AC converters is used for isolation. The size of HFT is very light and implementation of HFT on printed circuit board is very convenient as compared to a bulky LFT in the system.

A single stage grid connected system fulfills all requirements as same as multi stage systems with higher efficiency and lower cost. Similarly, placement of transformer in GIPV system, not only affects the size and cost but also the overall efficiency of the system. "In case the transformer is omitted, the efficiency of the whole PV system can be increased with an extra 1%-2%" [20]. Therefore, a single stage transformerless grid connected system is more efficient, reliable and cost effective than other systems [21, 22].

Power processing steps

On the basis of power processing steps, PV systems are categorized as,

a) In a single stage GIPV system, PV module, maximum power point tracking (MPPT), DC-AC converter and grid handles all the tasks. This results in the reduction of installation cost and circuit complexity of the system as shown in Fig. 1.5(a). Less stages of system results in less power loss [23].

b) A two stage GIPV system as shown in Fig. 1.5(b) is a single stage system with intermediate DC-DC converter between PV module and DC-AC converter. This system provide high gain from the PV source to the dc link of DC-AC converter through intermediate DC-DC converter using MPPT [12, 24].

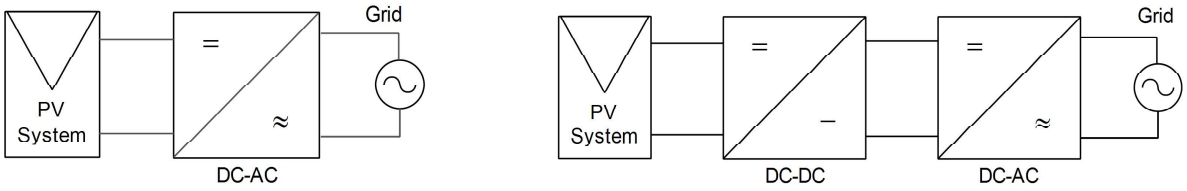

Figure 1.5: Block diagram of (a) single stage (b) two stage PV system

1.2.2 Topologies of inverter

In a grid connected PV market, various type of inverters or converters are present which is interfacing the PV system to the grid. This unit is called power conditioning unit (PCU). The selection of PCU is based on the purpose of utilization which helps in consideration of cost as well as efficiency of the overall system. This PCU is classified as follows.

- Voltage source inverter (VSI) and
- Current source inverter (CSI)

A standard VSI consist of a capacitor in the input side of inverter parallel with PV output. On the other hand a CSI consists of an inductor in the series with PV output at the input side of the inverter. Basic structure of a VSI and CSI can be seen in Fig. 1.6(a) and 1.6(b), respectively [25]. Generally, a GIPV system consist of two control loops. One is the inner control loop which control the output current of the inverter and other one is outer control loop which regulates the voltage at DC-link of the inverter according to the grid based on MPP

of the PV system. But in single stage PV system both function is performed by the inverter only [21]. VSI is the mostly used converter in grid connection application for higher power application, It provides fast dynamic response and high performance controller to meet grid standards [26, 27]. The requirement of conversion of DC side input into AC output is tried to achieve by some two or three or more voltage level transformerless VSI topologies [6, 28, 29]. These are full-bridge named as H-bridge and neutral point clamped (NPC) inverters, which are further derived in H5, HERIC (Highly efficient and reliable inverter concept), H6, REFU (by Refu solar), FB-ZVR (Full bridge zero voltage rectifier), coneargy NPC inverters and many more. These inverters are used in the system with their capability of solving the issues like efficiency, leakage current and electromagnetic interferences (EMI) [30, 31].

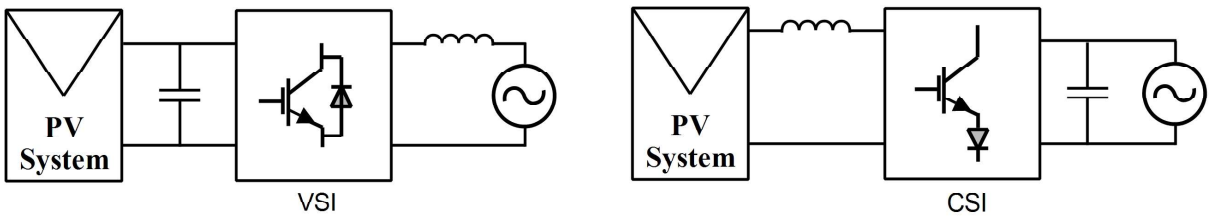

Figure 1.6: Block diagram of a standard (a) voltage source inverter (b) current source inverter.

According to the paper [32], the cost of the overall system is totally depends upon the inverter configuration and inverter component reliability, which shows that the system can be make more reliable and cost efficient by just managing design parameters of the simple H-bridge inverter. In [33–36], authors have discussed various inverter topologies and compared with other configuration to support the higher efficiency performances of the inverter. The issue of leakage current and common mode voltage is discussed in [20, 37–40]. They had also discussed about the way of handling this issue through various inverter configurations which have mentioned earlier. In [41], the author has discussed about the capability of the inverter to handle low voltage rid through condition.

1.3 Role of the GIPV System

In the present electricity demand scenario, PV, wind and hydro energies are being preferred over fossil fuels and nuclear for power production. As discussed above, PV has higher potential

to generate electricity and become an evident part of the main grid. Therefore, considering suitable control strategy, protection and power quality, the GIPV plant is generating power in hundreds of megawatt to support the grid. However, the GIPV system's prime objective is to generate the active power and transferring it to the grid. Simultaneously, the GIPV system may also acts as a reactive power compensator during the day as well as night time to reduce the burden of VAR compensators and the grid. In other applications, the GIPV systems are used to regulate the frequency and voltage in microgrid. Additionally, GIPV system act as a source for charging stations in the modern transportation system, especially when the primary grid is not present to charge the electric vehicles (EVs) in remote area.

1.4 Research Challenges

There are some challenges pointed out while implementing the GIPV system, which have been discussed below.

(a) **PV system configuration:** The installed GIPV system should be cost-effective for the customer's benefit, which can achieve by reducing the size of the system or by using an effective control strategy. These purposes can be fulfilled by minimizing power conversion stages of the system or reducing components such as sensors, LF transformers and filters which depend upon the application of the system.

(b) **Surplus power problem:** To increase the reliability on PV systems, an oversized GIPV system installation is done so that it fulfills the electricity demands even during low irradiance conditions. In case of the peak irradiance condition, the generated surplus power damages the equipment. Therefore, a system is required, which can handle all types of irradiances and generates the demanded power.

(c) **Increment in reactive power:** Generally, a grid interfaced PV system utilized to fulfil the active power demand. On the other hand, the owners of PV generation systems are levied on the basis of kilowatt-hour and not on their kilovolt-ampere hour yield. Hence, when inverter is transferring active power with full capacity, the inverter is unable to generate reactive power. Therefore, a control strategy is require which can handle the generated active power as well as the reactive power compensation from the GIPV

system.

(d) **Environmental challenges:** Generally, conventional power generation system pollutes the environment due to the use of fossil fuel. Therefore, a green energy based power generation system is required to support the grid which provides the non-polluted generating power plant and also participates to reduce the CO_2 emission. On the other hand, the fossil fuel based transportation system contributes to increase in the pollution level and increases CO_2 emission. Hence, in the modern era transportation system to reduce the CO_2 emission an electric vehicle should be charged using green energy (such as solar PV) based CSs instead of conventional energy based CSs.

1.5 Thesis Organization

This thesis has been strategies in six chapters to resolve the aforementioned problems.

1. In Chapter 2, the overview of the preliminary research work of various types of GIPV systems, MPPT techniques, active and reactive power control strategy has been presented. Based on this overview, some research objectives have been suggested to resolve previously acknowledged research challenges.

2. In Chapter 3, the overview of a three-phase GIPV system is presented. Along with the overview, the mathematical modelling of the single-stage and two-stage for the design purpose and related control is discussed in this chapter. Further, a 30 kW two-stage, three-phase GIPV system is developed using designed parameters and proposed control, where results verifies the potential vigour of the proposed system. Finally, the chapter is ended with the conclusion.

3. In Chapter 4, a novel MPPT control strategy is proposed for a GIPV system. The system framework and it's working strategy elaborates the need of the proposed control strategy for the GIPV system. Further, the simulation results are presented to support the proposed control strategy and performed work is concluded in the last.

4. In Chapter 5, an active and reactive power control strategy of a GIPV system is presented. Therefore, a brief introduction of the proposed GIPV and respective control for the active

and reactive power exchange is described. The results of the simulation where the comparison of traditional and proposed control technique simulated and tested in Opal-RT. Lastly, the chapter is devoted to the conclusion.

5. In Chapter 6, a framework of PV based charging station for EVs is proposed. Further, the modelling of the proposed system framework and results of the simulation work have been described in this chapter. Finally, the chapter is ended with the conclusion.

6. In Chapter 7, the highlights of the contributions towards the research is presented. Moreover, this chapter also highlights the direction of future research in present modern energy scenario.

Chapter 2

LITERATURE REVIEW

In this chapter, a literature review has been presented regarding the previous research works in the area power extraction techniques, role of inverter for active power transfer to the grid, reactive power compensation and other application of the photovoltaic (PV) system. Additionally, an analytical comparison is presented with advantages and disadvantages of various techniques used in previous research work. To specify the area of research, the literature review is focused on the following categories. In first category, the focus is on the various type of topologies related to the grid-interfaced PV (GIPV) system, role of the inverters and its applications. The second category presents the overview of various maximum power point tracking (MPPT) techniques to extract input power from the PV source. Further, the control schemes for the active and reactive power is discussed in third category. In fourth category, a derated mode operation of PV system is considered simultaneously, the application of PV to support charging stations is presented in fifth category. The preliminary research works of each categories are presented as follows.

2.1 Topologies of GIPV Systems

A topology of a grid interfaced PV system depends upon its application. These configurations consider inverter as a main component in GIPV system either it is single stage, two stage or multi stage. Its functionality and complexity depends upon the role of inverter and how that can be used is being discussed further in this literature review. A single stage grid interfaced PV system is self capable to handle the maximum power point tracking as well as the grid connection capability in the system. Mattos *et al.* [42] introduced a single stage single phase GIPV system based on integrated circuit which attending low distortion with high power factor output current. Freddy *et al.* [43] have presented the comparative analysis of transformerless

GIPV system. Jain and Agarwal [44] have introduced the comparative analysis of MPPT techniques in a single-stage, single-phase GIPV system and studied there merits and demerits using different kind of MPPT techniques. Singh *et al.* [45] have examined that the system not only feeding solar energy into the grid but also fulfils the requirement of MPPT which deals with the harmonic distortion and balancing the grid current. In this paper they have introduced improved linear sinusoidal tracer-based control algorithm with VSI for all proposed functions. In [46], Chinmay *et al.* have presented a single stage GIPV system functioning under abnormal grid condition (sag and swell) with wide range of input voltage variation. Zhou *et al.* [47] have discussed the performance of a single stage boost converter with coupled inductor for MPPT and feeding high quality of current into grid with improved reliability. Similarly Domenico *et al.* in [48], Francisco *et al.* in [49], Rahul *et al.* in [50], and Yang *et al.* in [51] takes about the ripple correlation control, ride through control in faulty grid, system using phase lock loop (PLL)-less fast character of triangle function control and cost effective system with reliability have performed using single-stage configuration of the GIPV system, respectively. When the requirement of high gain from the system is required, two-stage GIPV is more suitable to use. Chen *et al.* [52] have implemented a two-stage GIPV system for module integrated system to eliminate the chances of single point failure, high efficiency and low cost. Dipankar *et al.* [12] have proposed a two-stage stand alone system with high gain and the requirement of isolation using high frequency transformers at intermediate stage is fulfilled. As cited in [53], Wang *et al.* have applied sensorless DC-link scheme for the grid connected inverter with fixed DC voltage source. In this literature, authors have used the grid voltage and output current to estimate the DC-link voltage which turns out close to the actual value of DC-link voltage. Naidu and Singh [54] have presented this scheme for the control of doubly fed induction generator in wind energy conversion system. In their paper, they have presented a single VSI to reduce the power loss during power flow due to change in (less and more than) synchronous speed. As reported in [55], Mallik and Khaligh have presented a sensorless power factor correction control scheme for boost-type rectifier. This effort improves the transient response of the system by eliminating the voltage loop proportional integral (PI) controller. Zakzouk *et al.* [56] have presented a sensorless scheme for GIPV system which limits the system at single-phase. This scheme has a drawback of not transferring the bulk power and presence of the second order line frequency. Similarly, Taghizadeh *et al.* [57, 58] have presented a fast and robust scheme to

reduce the second order frequency by introducing notch filters. However, the introduced notch filters over sizes the proposed system. Therefore, to overcome the above mentioned problems, a sensorless two-stage, three-phase GIPV system is proposed.

2.2 Maximum Power Point Tracking Techniques

Maximum power point (MPP) in a module is a point at which, the product of voltage and current on the characteristics curve is maximum and the techniques used to track this point is called MPPT techniques. In a GIPV system, MPPT techniques are used with intermediate boost converter in dual stage or multi stage inverter system and with the inverter in the single stage inverter system [59]. Many researchers have classified various MPPT techniques on the basis of the properties such as tracking speed [60], complexity [44], MPP oscillation [61], accuracy and efficiency [62]. Jain and Agarwal [44] have compared many classical MPPT techniques based on array configuration, accuracy, cost of the system and tracking speed. However, the authors have presented the application based MPPTs which are not applicable for every system. Esram and Chapman [63] have presented the comparison of various MPPT algorithms according to the PV application. Similarly, Subudhi and Pradhan [64] have also presented a review of many MPPT algorithms. The review is based on the control strategy, circuitry and the cost of the application. There are many MPPT techniques are available to track the maximum power point, these are perturb & observe (P&O), incremental conductance (IC), parasitic capacitance, fuzzy logic based, artificial neural network based, particle swarm optimization based and some derived from these techniques. Among the MPPT techniques, P&O and IC are the oldest and classical. P&O is a widely used MPPT technique due to its easy implementation but it fails in the condition where irradiances changes rapidly. Asim *et al.* [65] have presented some modified classical numerical techniques for boost and buck converters but fails to achieve the higher range of operating voltages. Similarly, Kadri *et al.* [66] and Killi *et al.* [67] have presented a robust and modified P&O MPPT technique to handle variation in irradiances for a single-stage, three-phase GIPV system. As we know that the behaviour of sun is not regular, some disturbances called shading will occur time to time. This shading might be partial or full but it affect the PV generation and in this condition getting the MPP is very difficult. Lyden *et al.* [68], Wang *et al.* [69], Mohanty *et al.* [70] and Ghasemi *et al.* [71] have conducted

study to handle partial shading and get MPP providing different approaches, some have discussed Grey-wolf optimization some have derived P&O techniques to get MPP under partial shading condition. This review reflects that the P&O is less complex and having fast tracking capability amongst all presented. However, P&O is less accurate and consume more power in MPP tracking during variable irradiances. Therefore, many modified P&O, MPPT algorithms have been presented to overcome the MPPT problems. In this respect, Killi and Samanta [67] have proposed a modified P&O algorithm which resolves the drift problem during unpredicted irradiance change (erratic behaviour). As a result, this MPPT presents high efficiency and less power loss during tracking of the operating point. Yong and Huiqing [72] have presented an adaptive P&O algorithm with predictive current control. However, the authors have failed to consider the inductance change which influences the tracking accuracy of the algorithm. Similarly, Ahmed and Salam [61] proposed a modified P&O algorithm with dynamic perturbation step size and a boundary condition to enhance the efficiency of the algorithm. Although this directs the system towards the operating point, it fails to handle the irradiance changes. Further, Liu *et al.* [73] and Ghamrawi *et al.* [74] have proposed a dual-mode P&O algorithm with the variable step-size which contribute to resolve the problem of oscillation near MPP and MPP tracking speed. However, the employed algorithm has a slightly higher cost as compared to the traditional P&O and unable to identify the drift problem during variable irradiance condition.

2.3 Active and Reactive Power Control

In terms of stability and reliability, a power generation system should have connected in both conditions that is normal grid condition as well as abnormal grid condition. The inverter play a vital role to improve voltage profile when system is grid connected during abnormal condition [75]. The abnormal condition refers to the erratic behaviour of the irradiance. The erratic behaviour includes up and down condition of the solar irradiance and partial shading condition. According to Braun *et al.* [76], in a smart GIPV system, the inverter should have active and reactive control capability. Blaabjerg *et al.* [77] have conducted studies on the overview of control strategy of the inverter system under fault condition. The research is also focused on the power quality issues according to guidelines of the grid integration of distributed generators under different countries. Mishra *et al.* [78] have proposed a positive, negative and zero

sequence based control strategy for the voltage as well as reactive power compensation for PV connected unbalanced distribution network. However, while applying this proposed control strategy, authors required separate controllers for each sequences that make the system bulkier. Cagnano *et al.* [79] have examined that the Lyapunov theory is used to send massage to local controller to produce reactive power and for active power PV module is sufficient. Tsengenes *et al.* [80] have proposed a P-Q theory based control strategy to send active power into the grid and simultaneously, compensate the reactive power for the connected non-linear loads. However, this delivers reactive power during night time but fails during the peak time of PV power generation for the connected local non-linear loads. In [81–84], authors have discussed some other active and reactive power control strategy. Han *et al.* [85] reviewed various active and reactive power sharing techniques by considering cost analysis and system design for a microgrid application. However, the authors have failed to minimize the control complexity and effect of unknown environmental factors during high penetration of renewable energy sources. Jain *et al.* [86] introduced a single-stage GIPV system with predictive control. However, the proposed system is capable of harvesting maximum power and delivering reactive power independently but fails to achieve it during peak hours of PV power generation. Therefore, a system is required which can handle active as well as reactive power during all environmental conditions. In this respect, Weckx *et al.* [87] proposed a scheme for active and reactive power exchange using grid-interfaced inverter to minimize reverse power flow and overvoltage. In this approach, the authors have suggested a mathematical formulation i.e. first order spline. It curtails the active power as well as handles the reactive power compensation through grid-interfaced inverter.

2.4 Derated Mode Operation of GIPV System

Under derated mode of operation, the system work below the maximum available power. This mode of operation tries to fulfill the need of storage while surplus power is available [88]. During this mode of operation PV system behaves as a reserve. Many researchers contributed in solving the problems such as overvoltage and inadequate MPPT's performance in a GIPV system. Zarina *et al.* [89] have explored the role of PV system under derated mode of operation. They have used this concept to control the frequency of a hybrid PV rotating machine without storage system. Zhou and Bialek [90] presented a generation curtailment technique to

prevent the rise of voltage and reverse power flow in the lower network from high penetration of PV power. However, the authors did not recommend any control technique to minimize the switching losses and increases the utilization of the inverter. Further, Tonkoski *et al.* [91] have presented a droop based curtailment approach to protect the grid from overvoltage. Although this scheme increases the power loss as compared to normal active power curtailment, it affects the revenue of the system. Similarly, Omran *et al.* [92] suppresses the power fluctuation of GIPV system using various approaches such as battery storage, dump loads and software-based power curtailment. However, the above mentioned approaches have a high installation cost except power curtailment. Likewise, Ahmed *et al.* [60] proposed a reduced power mode control algorithm to suppress the output power of the system. It works in reduced power generation mode when generated power exceeds the system rating. Though the proposed control strategy fails to reduce the power losses during curtailment. Yang *et al.* [93] have proposed a constant power generation scheme to reduce thermal loading, improved the inverter utilization and reduced the switching losses of inverter during a rapid change in irradiance. However, the authors did not present an appropriate method to decide the power limit. In addition, Sangwongwanich *et al.* [94, 95] have presented a constant power generation scheme for the overshoot, power loss and active curtailment. The authors have used the power or current based scheme for fast dynamic response and MPPT for high robustness. Although the authors didn't use any other MPPT except perturb and observe (P&O) technique. Similarly, Tafti *et al.* [96] have also proposed a constant power generation scheme for the single and two-stage three-phase GIPV system. In this scheme, the authors have proposed a voltage based curtailment approach along with the flexibility of operating points. However, the main shortcoming of this scheme was that it didn't suggested any suitable approach to decide the voltage operating point during variable irradiance. Although they have only used conventional MPPT to find the operating point.

2.5 PV Based Charging Stations

Generally, PV source is utilized for the active and reactive power exchange. Nowadays, PV has incorporated in the modern transportation system as energy source for the charging stations to charge the EVs. In this direction, many researchers have presented some authenticated work. Singh *et al.* [97] have suggested that the source for CS will be the RESs. It can be used at

the remote locations where the reach of the grid is not possible. The RESs used for the CS are wind and photovoltaic (PV). However, the wind energy consists of more conversion stages to produce power as compared to the PV. Therefore, the feasibility of PV energy based off-grid charging station is more. Bhatti and Salam [98] have been presented a PV based EV charging stations. It developed due to the extensive presence of solar energy and the simple installation of PV power generation system. Several articles have been published to support the PV based charging station. Pinak *et al.* [99] have proposed a cost-effective PV based CS at the parking garage. The cost analysis of the system is considered using parking rate, installation cost and tax rebate. This benefits the garage as well as the vehicle owner. Apart from this benefit, the system also contributes to reducing the charging burden from the grid and the penetration of RES in transportation. However, the authors have not presented the economic analysis of this methodology for other locations in terms of per unit cost and installation cost. Moreover, the system is PV dependent which is not sustainable due to the intermittent nature of irradiance. As reported in [100], Goli and Shireen have presented a PV based charging station with the grid. The grid is supporting the CS when PV energy is not sufficient for the EVs. However, the grid is not available at every location which reduces the sustainability of the system. On a similar note, Hernandez and Sutil [101] have presented a PV based CS with regenerative braking and battery storage to support the system framework during peak-load. The aim of the author is to utilize the maximum amount of RES and reduce the charging cost. Similarly, Li *et al.* [102] have proposed a PV and wind-based CS with battery storage to handle the power generation fluctuations during variable environmental condition. In this paper, they have presented a SoC based control approach to overcome the issues occurred due to RES. However, they didn't determine the proper SoC estimation strategy for the EV battery.

2.6 Research Gap

The trend of integration of PV system into the grid is magnanimous and conjecture of development is hopeful. The development of a GIPV system includes all possibilities of improvement from PV panel to the grid. As a result, the interest of research in a GIPV system is increasing exponentially. In the current scenario, researchers face major potential challenges like configuration, topology of the converter, control strategy and MPPT capability of the system while

integrating the PV into the grid to provide voltage stability, reliability and high power quality in normal as well as weak grid condition. Configuration constitutes the presence of transformer and power stages (single or two stage) in the system. Topology of converter constitutes the capability of converter to deal with various issues like common mode voltage, input current ripple, shoot through, overvoltage , resonant and low voltage rid through problem. However, control strategy have to deal with the DC suppression loop, grid current controller and synchronization with the grid current. Configuration is very important factor to decide the existence of the GIPV system for any application. In [20], various transformerless approachs are discussed for GIPV system and authors have verified that, in case the transformer is omitted, the efficiency of the whole PV system can be increased with an extra 1%-2%. Similarly, [24] have presented the comparison of power loss between single stage and two stage GIPV system and found that the single stage configuration is more efficient than two stage system. However, the DC-link voltage fluctuation and reliability is less in the single stage system. Therefore, the selection of topology of the conversion system is the major challenge of the GIPV system to harvest maximum amount of energy from PV panel with higher efficiency and reliability. Different type of topologies of inverters are discussed in [30, 31] for various issues related to the grid interfaced PV system, which are mentioned in the starting of this chapter. As reported in [24, 39–41, 48, 49], the aforementioned issues have been studied and compared for single phase GIPV system. However, these is still need to investigate these issues for three phase single stage GIPV system. Selection of suitable converter topology will be justified only when the converter can effectively control flow of power from source to grid. The control strategy must be able to improve voltage and also support voltage stability as discussed in [77, 81]. There is still need of investigation to regulate the output of the converter according to the grid.

Some constructive studies were conducted on MPPT control techniques in [44, 63, 64] to present its handling capability with DC-DC and DC-AC converters. Allowing all possibility of change in GIPV system, there is a point of concern when system demand is less than the generation, there is an excess amount of power in the system. If the system is not equipped with storage facility, excess power get wasted. In such situations, system can be operated in derated mode. This also prevents the installation cost of storage. In [88, 89, 103], authors have discussed about the derated mode of operation to regulate frequency for a microgrid and prevent the overvoltage problem in a wind power generation system. In addition, the use of PV

as an energy source for EVs also can be a milestone in modern transportation era. Thus, the PV based charging stations may reduce the dependency on the conventional charging structure.

This literature review presents the current scenario of the grid interfaced PV system in terms of issues which is general at the point of common coupling (PCC) and behaviour of the inverter. The area of research on the basis of this literature review are listed below.

1. There is need to strategies a control technique, which is able to perform active and reactive power control to keep the power flowing efficiently from source to grid.

2. A single stage grid connected PV can't handle variation in insolation with simple MPPT techniques like P&O. Therefore, an effective MPPT technique is required which can handle the intermittent nature of insolation and enhance the maximum harvesting from the PV array.

Chapter 3

SENSORLESS DC-LINK CONTROL APPROACH FOR THREE-PHASE GRID-INTERFACED PV SYSTEM

3.1 Introduction

In the last few years, the dependence of the power sector is predominantly dependent on renewable energy source (RES). Recently, green energy has become the main concern for researchers to fulfill the increase in demand for electricity. That's why, the environmental organizations have been encouraging the use of these RESs such as wind energy, solar energy, and tidal energy as an alternative of fossil fuels for electricity generation [104]. Especially wind energy and solar energy have been reported to be more feasible in large scale implementation due to the recent research and development in power electronics [11]. Among the two, solar energy is more advantageous over wind due to its availability in nature. The solar energy could be further classified as thermal solar system and photovoltaic solar system. Among these solar energy systems, photovoltaic (PV) solar system is becoming more prominent because it is easy to install and requires low maintenance. Hence, PV system attracts researchers as an alternative source of power generation system at present and upcoming years [105]. Recently, the demand for electricity in public domain is being fulfilled by the implementation of PV system configurations like stand-alone, grid-connected and hybrid. Among these configurations, stand-alone and hybrid systems are of limited size and mainly used in the remote and rural areas. Whereas, the grid-connected system produces electricity to a large extent. It satisfies the electricity demand of a micro-grid as a distributed generation system [106]. Additionally, this supports the micro-grid as well as utility grid for voltage and frequency regulation. Hence, grid-interfaced PV (GIPV) system keeps an advantage over other configurations.

Further, the configuration of GIPV system depends upon the power processing stages of the system which includes PV array, filter (optional), intermediate converter (optional), DC-

link capacitor, DC-AC converter, output filter, low frequency transformer (optional) and grid as shown in Fig. 1.1 [7, 107]. Therefore, on the component basis, these are subdivided into single-stage and two-stage GIPV system. A single-stage GIPV system, includes only PV array, DC-link capacitor, inverter, output filter and grid thus reducing the size and weight of the system. Meanwhile, the complexity of this system increases due to the handling of many tasks (like maximum power point voltage handling, DC-link voltage regulation, current control and grid synchronization) by inverter only. Therefore, to reduce the complexity of the system, an intermediate boost converter (IBC) is introduced in the single-stage system. The IBC is placed between PV source and inverter, which is called a two-stage grid connected PV system.

In two-stage GIPV system, intermediate converter increases the voltage level of input side, which results in reduced number of PV panels [107–110] . Additionally, the intermediate converter with maximum power point tracking (MPPT) techniques extract the peak value of power from the PV array. An intermediate converter provides a regulated high voltage level with the same power to the system. It fulfils the voltage requirement at DC side and minimizes the requirement of low-frequency transformer at AC side of the inverter, which shows the impact on cost, volume and weight of GIPV system. The intermediate converter incorporated with the MPPT method provides source voltage and current from the PV array. It regulates the source voltage according to the desired output for the voltage source inverter (VSI) as an input DC source. The VSI functions as a conversion unit as well as a power conditioning unit for GIPV system. Power inverters perform various tasks such as DC-link voltage regulation, power conversion, grid synchronization, and control operation for the system. On the other hand, a situation such as variable irradiance at the input, sudden change in load at the output side and imbalance in grid voltage affects the performance of the system. Therefore, to maintain a smooth functioning of the system, the DC-link voltage regulation and synchronization of inverted sinusoidal current with utility grid is utilized. During these operations, the total harmonic distortion (THD) and power factor reach beyond the grid standards [26, 111]. Therefore, a pulse width modulation (PWM) based VSI is widely utilized in GIPV systems to minimize THD and improve power factor. Additionally, it produces fast dynamic response and high performance controllers to meet the grid standards as discussed in [26]. These standards are implemented by means of the control scheme. Therefore, the performance of the VSI extensively depends upon the control scheme implemented into the GIPV system.

The conventional control scheme of GIPV system adopts a voltage regulation as an outer-loop control and current control as an inner-loop control. For the outer-loop control, a pre-defined reference DC-link voltage is compared with a sensed voltage (sensed through a high voltage DC sensors) across DC-link capacitor at the input of the VSI. As a result, the DC-link voltage regulates according to the set value and provides the reference current for the current control loop. This is considered as the conventional scheme of voltage regulation where sensors are used at the DC-link position. Based on [96, 112–115], authors have presented this conventional approach for various applications. Apart from the conventional approach, many researchers have implemented the sensorless scheme at the DC side of VSI (DC-link position) for various applications.

In this proposed system, a two-stage control is presented. In the first stage, the intermediate boost converter is used with the MPPT algorithm and a VSI is used with current control in the second stage. Both stages are interfaced by a DC-link capacitor, which avoids the high voltage sensor in contrast to the conventional control scheme. This control is called a sensorless DC-link control. Since a high voltage sensor is not present for a DC-link capacitor, the outer control loop is not required further. As a result, it reduces the complexity of the VSI (handling of both inner as well as outer control loop) and improves the dynamic response of the system. In addition, this proposed system introduces a DC-link voltage control model by adding a loss factor. The loss factor term is defined as the combination of losses participating in the system due to the switches, interfacing inductors and variation in terminal voltage. Loss factor estimates the value of the reference DC-link voltage. Further the estimated DC-link voltage with proportional gain produces the active reference current to generate the switching pulses to the inverter. As a result, the system generates the appropriate amount of power for which it is designed. The generated power and corresponding output voltage and current are analyzed. The performance of the proposed system is verified and compared with the conventional system under variable irradiance conditions. The main significance of the proposed work is summarized as follows:

- Implementation of sensorless three-phase GIPV system.
- Inclusion of loss factor along with DC-link voltage control model is used to improve the dynamic response of the system

- Reduction in system's cost by neglecting the high voltage sensor.

3.2 Details of the Proposed System

Fig. 3.1(a) illustrates the detailed structure of the proposed two-stage, three-phase GIPV system. This system is widely adopted for residential as well as commercial purpose with rated power of 1-30 kW [116]. This system includes a PV array, an IBC, a DC-link capacitor, a VSI, filters (three interfacing inductors) and the grid. Further, these components are divided into two stages.

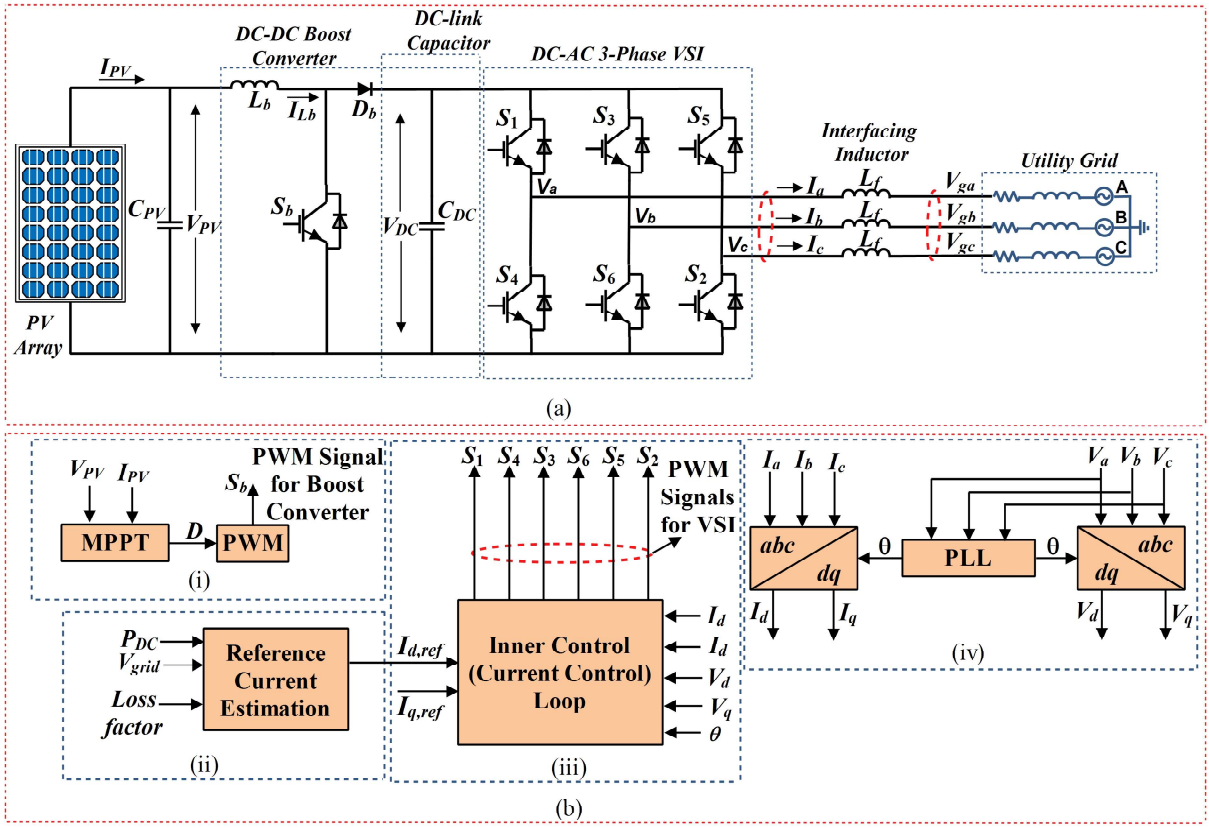

Figure 3.1: A two-stage, three-phase GIPV system (a) circuit diagram (b) control approach for (i) boost converter control block (ii) reference current estimation (iii) inner control loop producing PWM signals and (iv) grid synchronization unit

The first stage consists of a PV side boost converter and a VSI, which is used as a grid side converter. The solar PV array serves as an input of the IBC where the solar PV array is an arrangement of series and parallel combination of modules to achieve the desired input voltage V_{PV} and current I_{PV}. The IBC is implemented as an interfacing converter between PV array and VSI. It enhances the voltage level of the PV array so that VSI receives a sufficient voltage

for the GIPV system. The incremental conductance (IC) MPPT algorithm is used to decide the operating points *i.e.*, V_{MPP} (voltage at maximum power point) and I_{MPP} (current at maximum power point) at corresponding P_{MPP} (power at maximum power point). According to operating voltage and current, the IC MPPT algorithm generates the PWM pulse for the boost converter's switch as shown in Fig. 3.1(b)(i). In second stage, a PWM strategy based VSI is used. The use of PWM strategy with VSI results in minimum harmonic distortion. The VSI in this system performs various operations like (a) DC to AC power conversion (b) independent control of active and reactive power [117, 118] and (c) synchronization with grid [119]. Furthermore, these operations are executed with the use of proposed control. In Fig. 3.1(b)(ii), the proposed control block produces a reference current quantity for the inner control (current control) loop by controlling active power of the system. On the basis of active reference current (d-axis current), the current control loop is utilized to produce the switching pulses (PWM signals) for VSI as shown in Fig. 3.1(b)(iii). In this control loop, the reactive reference current (q-axis current) is set to be zero, to provide unity power factor current. The performance of the current control loop depends upon the synchronization of grid quantities (voltage, current and angle between both) with the output of VSI. The grid synchronization of the system is performed by means of phase lock loop technique as shown in Fig. 3.1(b)(iv). This monitors the grid quantities and provides support to control the active and reactive power of the system. The filters are used to smoothen the transferred power to the grid. In this system, the interfacing inductors are doing the task of the filter.

As aforementioned, the DC-link capacitor interfaces both stages of the system. It decouples the ac and dc power sources. Additionally, it maintains the input voltage level of the inverter during fluctuations in the presence of variable load and irradiance level (I_{rr}). The maintenance of DC-link capacitor voltage depends upon the power delivered and received by VSI. If the power received by the VSI is more than delivered, the energy stored in the capacitor will raise the voltage at the DC-link capacitor. On the other hand, if power received by the VSI is less than the delivered power, the capacitor will supply the remaining power to the inverter, which results in the reduction of DC-link capacitor voltage. If both of them are equal, the DC-link voltage will remain constant. Therefore, a novel control model is introduced, considering the loss factor, to maintain the DC-link capacitor voltage in a steady state condition. This is the main idea of this proposed scheme and will be further discussed in section IV.

3.3 Mathematical Modelling of Proposed GIPV System

3.3.1 Modelling of PV array

A PV array is a power generating unit, consisting of similar PV modules arranged either in series or parallel or combination of both. The basic characteristics of a PV module is well described with a single diode model as illustrated in Fig. 3.2. [120, 121]

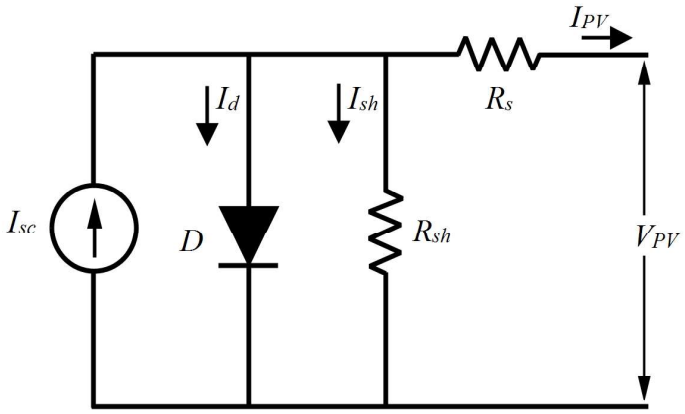

Figure 3.2: Single diode model of a PV module

The corresponding output current (I) of a single diode model is represented as follows:

$$I_{PV} = I_{sc} - I_d \left[\exp\left(\frac{qV_{PV} + qR_sI_{PV}}{N_sKTA} \right) - 1 \right] - \frac{V_{PV} + R_sI_{PV}}{R_{sh}} \tag{3.1}$$

where $I_{PV}, I_d, q, R_s, R_{sh}, N_s, K, T$ and A are the PV generated current, diode saturation current, electron charge, series resistance, parallel resistance, number of cells connected in series, Boltzmann constant, cell temperature and diode ideality factor of the module respectively. In practice, a PV array is an arrangement of several PV modules in series and parallel and the equivalent current I_{eqt} of a PV array is represented as follows:

$$I_{eqt} = N_{par}I_{sc} - N_{par}I_d \left[\exp\left(\frac{qV_{PV} + qR_sI_{PV}\frac{N_{ser}}{N_{par}}}{N_sKTAN_{ser}} \right) - 1 \right] - \frac{V_{PV} + R_sI_{PV}\frac{N_{ser}}{N_{par}}}{R_{sh}\frac{N_{ser}}{N_{par}}} \tag{3.2}$$

where N_{ser} and N_{par} is the number of series and parallel modules to configure a PV array. The maximum power of the PV array is defined as [122],

$$P_{MPP} = (N_{ser} \times V_{MPP}) \times (N_{par} \times I_{MPP}) \tag{3.3}$$

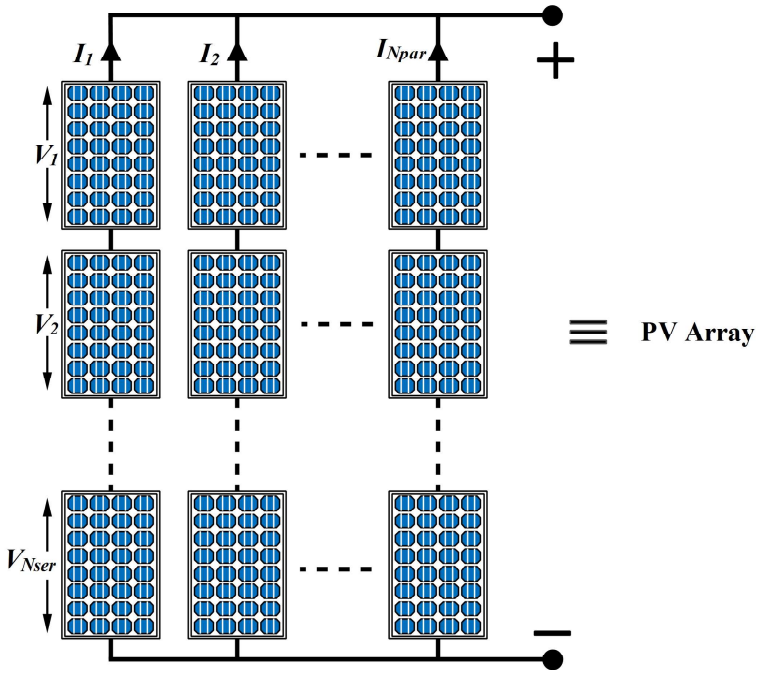

Figure 3.3: PV array using series and parallel arrangement of PV modules

where P_{MPP}, V_{MPP} and I_{MPP} are the power, voltage and current at the MPP respectively. Maximum power is defined as the product of the total number of modules connected in series and the total number of strings connected in parallel as shown in Fig. 3.3. The obtained V_{MPP} and I_{MPP} at particular P_{MPP} is provided to the boost converter. Further, the components (inductor and capacitor) of the converter are designed according to the rated value of the input voltage and current, which is obtained by the mathematical modelling of the intermediate boost converter.

3.3.2 Modelling of intermediate boost converter

The mathematical design of the intermediate boost converter estimates the parameters of the converter as displayed in Fig. 3.1(a) [123]. The state space representation of a IBC is defined as,

$$\dot{x_b} = Ax_b + Bu_b \tag{3.4}$$

$$\dot{y_b} = Cx_b + Du_b \tag{3.5}$$

where x_b, u_b, y_b, represent the state vector, input vector and output of the system respectively and A, B, C and D represents the parametric equations of the system. The parameter design and

performance of the system depends upon the storage elements and switches used in the system. The IBC section of Fig. 3.1(a) contains a controlled switch (S_b) and uncontrolled switch (D_b) and it's function for two switching instants. For the first infinitesimal time interval dT_s, S_b is ON and D_b is OFF. The following equations are obtained using Kirchhoff's law of voltage and current for first time interval.

$$\frac{di_{Lb}}{dt} = \frac{1}{L_b}v_{pv} \tag{3.6}$$

$$\frac{dv_{DC}}{dt} = -\frac{1}{R_{out}C_{DC}}v_{DC} \tag{3.7}$$

For second time interval of $(1-d)T_s$), S_b is OFF and D_b is ON and following equations are obtained,

$$\frac{di_{Lb}}{dt} = -\frac{1}{L_b}v_{DC} + \frac{1}{L_b}v_{pv} \tag{3.8}$$

$$\frac{dv_{DC}}{dt} = \frac{1}{C_{DC}}i_{Lb} - \frac{1}{R_{out}C_{DC}}v_{DC} \tag{3.9}$$

The parameters of the IBC used in following equations (3.6-3.9) are the inductor (L_b), capacitor (C_{DC}) and output load resistance (R_{out}) which depends upon the application of the system. The governing equations (3.6-3.9) presents the large signal model of the IBC for both time instants. The averaged large signal model of the system for both switching instants are obtained as,

$$\frac{di_{Lb}}{dt} = -(1-d)\frac{1}{L_b}v_{DC} + \frac{1}{L_b}v_{pv} \tag{3.10}$$

$$\frac{dv_{DC}}{dt} = (1-d)\frac{1}{C_{DC}}i_{Lb} - \frac{1}{R_{out}C_{DC}}v_{DC} \tag{3.11}$$

The averaged large signal model is the combination of steady state and small signal model (SSM) and the variables of the system can be written as [124],

$$\dot{x}_b = \dot{X}_b + \hat{\dot{x}}_b$$

$$\dot{u}_b = \dot{U}_b + \hat{\dot{u}}_b$$

$$\dot{y}_b = \dot{Y}_b + \hat{\dot{y}}_b$$

$$\dot{d} = \dot{D} + \hat{\dot{d}}$$

and after applying assumptions ($\dot{X} = 0$, d = D) of steady state condition, the following equation will be obtained as,

$$V_{DC} = \frac{1}{1-D} V_{PV} \tag{3.12}$$

The above equation presents the steady-state model of the system which helps in designing the converter. The SSM or linear model provides a control approach for the system. This linear model determines the dynamics and variations with respect to the operating point, which are mathematically obtained as,

$$\frac{d\hat{i}_{Lb}}{dt} = -\frac{(1-D)}{L_b}\hat{v}_{DC} + \frac{1}{L_b}\hat{v}_{PV} + \frac{V_{DC}}{L_b}\hat{d} \tag{3.13}$$

$$\frac{d\hat{v}_{DC}}{dt} = \frac{(1-D)}{C_{DC}}\hat{i}_{Lb} - \frac{1}{R_{out}C_{DC}}\hat{v}_{DC} - \frac{I_{Lb}}{C_{DC}}\hat{d} \tag{3.14}$$

where $\hat{i}_{Lb}$ and $\hat{v}_{DC}$, $\hat{v}_{PV}$ and $\hat{d}$, and D, L_b, C_{DC}, R_{out}, V_{DC} and I_{Lb} are the state variables, input variables, and constant parameters (of SSM) for the proposed IBC respectively. Equations (3.13) and (3.14) represent the small signal model of the IBC in the GIPV system. The subsystem (IBC) control depends upon the input variables and that is voltage (v_{PV}) and duty ratio (d). In this subsystem, v_{PV} keeps constant and d varies according to the desired output value V_{DC}, which is represented by (3.12) in steady-state condition. V_{DC} is the input DC voltage for the DC-AC VSI. The performance of the VSI for grid integration depends upon the appropriate component (rating of switches and interfacing inductors) selection and good control strategy for the operation. The component selection depends upon the rating of the power transfer and the control approach depends upon the mathematical modeling of the structure in a selected environment (natural reference frame or synchronous reference frame).

3.3.3 Modelling of grid interfaced VSI

The mathematical representation of the grid interfaced VSI is shown in Fig. 3.1(a), where V_a, V_b and V_c represent the terminal voltages of the inverter, $V_{g,a}, V_{g,b}$ and $V_{g,c}$ are the grid voltages and L_f considered as the equivalent interfacing inductors for all three phases [125]. The equivalent circuit of a single phase is presented in Fig. 3.4.

In this figure, KVL is applied and the mathematical equations of all three phases are ob-

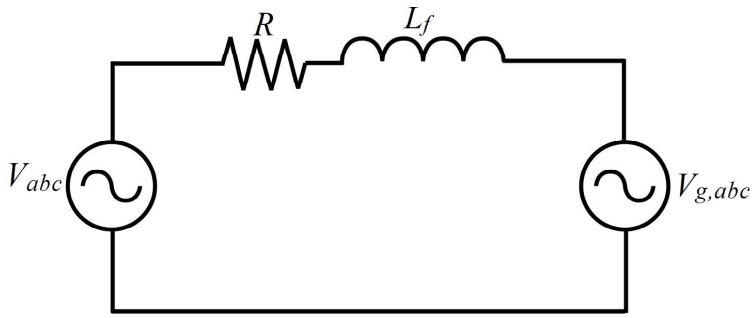

Figure 3.4: Equivalent circuit diagram for three phase

tained as follows:

$$V_a = RI_a + L_f \frac{dI_a}{dt} + V_{g,a} \tag{3.15}$$

$$V_b = RI_b + L_f \frac{dI_b}{dt} + V_{g,b} \tag{3.16}$$

$$V_c = RI_c + L_f \frac{dI_c}{dt} + V_{g,c} \tag{3.17}$$

equations (3.15-3.17) could be further rewritten as,

$$\frac{d}{dt}\begin{bmatrix} I_a \\ I_b \\ I_c \end{bmatrix} = \begin{bmatrix} -\frac{R}{L_f} & 0 & 0 \\ 0 & -\frac{R}{L_f} & 0 \\ 0 & 0 & -\frac{R}{L_f} \end{bmatrix} \begin{bmatrix} I_a \\ I_b \\ I_c \end{bmatrix} + \frac{1}{L_f} \begin{bmatrix} \Delta V_a \\ \Delta V_b \\ \Delta V_c \end{bmatrix}$$

In the above representation, $\Delta V_{abc} = V_{abc} - V_{g,abc}$ and ΔV_{abc} is presented as the differences of inverter output voltage and grid voltage of all three phases. The above equation is further transformed to synchronously rotating reference frame (SRF). In this reference frame, the active and reactive power become decoupled, which allows the controller to be controlled separately. The system represented in SRF is obtained as,

$$\frac{d}{dt}\begin{bmatrix} I_d \\ I_q \end{bmatrix} = \begin{bmatrix} -\frac{R}{L_f} & \omega \\ -\omega & -\frac{R}{L_f} \end{bmatrix} \begin{bmatrix} I_d \\ I_q \end{bmatrix} + \frac{1}{L_f} \begin{bmatrix} \Delta V_d \\ \Delta V_q \end{bmatrix}$$

From the above representation, we have to maintain the voltage at the input side of the VSI and at the PCC. This can be effectively achieved by controlling the active and reactive power flow

into the system. The representation of voltage in the synchronous reference frame is obtained as,

$$V_d = V_{g,d} + RI_d + L_f \frac{dI_d}{dt} - \omega L_f I_q \tag{3.18}$$

$$V_q = V_{g,q} + RI_q + L_f \frac{dI_q}{dt} + \omega L_f I_d \tag{3.19}$$

The current control of the GIPV system in SRF depends upon the equations (3.18) and (3.19).

3.3.4 Synchronization of VSI with grid

Grid synchronization of the power converter is the instantaneous monitoring of the present status of the grid to which the power converter is to be added. In grid synchronization, the synchronized power converter and grid works in harmony. Additionally, it is a adaptive process of minimizing the error which is the difference of internal reference signal generated by power converter and the grid variable mainly grid voltage. To deal with the transformation of the three phase quantity (natural reference frame) to two phase (synchronous reference frame) quantity, the information of the phase angle (θ) is required. In the way of the search, there are mainly two type of synchronization techniques are discussed i.e. frequency and time domain detection method which are implemented by Fourier analysis and phase lock loop (PLL), respectively. Amongst both techniques, PLL is being used more for the engineering application due to use of feedback and repetitive tuning of the signal. The basic structure of the PLL is shown in Fig. 3.5.

Figure 3.5: Basic structure of the PLL

where PD compares the two input signals and generates error signal which is filtered out by the LP and then used by the VCO to generate output signal. This process continues until ε_{PD} is not zero. Once the error is zero the output phase will be locked.

This section decides all control parameters on the basis of mathematical modelling of PV

array, IBC and grid-interfaced VSI. The decided control parameters like input voltage and current from PV array, simultaneously, duty ratio (d) for IBC and control structure for grid-interfaced VSI are further executed from the MPPT control and VSI control, respectively are discussed in the next section.

3.4 Control Approach for GIPV System

3.4.1 Proposed incremental conductance MPPT algorithm

Firstly, MPPT algorithm extracts MPP from the PV array using IC technique. In conventional IC technique, the output power is the derivative of voltage which is obtained as,

$$\begin{aligned} D_{VPV} \times P_{PV} &= D_{VPV} \times (I_{PV} V_{PV}) \\ &= I_{PV} + V_{PV} \times D_{VPV} \times I_{PV} \\ D_{VPV} \times P_{PV} &= I_{PV} + V_{PV} \frac{\Delta I}{\Delta V} \end{aligned} \tag{3.20}$$

$$at \quad MPP, \quad D_{VPV} \times P_{PV} = 0$$

$$\frac{\Delta I}{\Delta V} = -\frac{I_{PV}}{V_{PV}} \tag{3.21}$$

$$so, \quad \frac{\Delta I}{\Delta V} \quad is \quad \begin{cases} = -\frac{I_{PV}}{V_{PV}} & \text{at MPP} \\ > -\frac{I_{PV}}{V_{PV}} & \text{below MPP} \\ < -\frac{I_{PV}}{V_{PV}} & \text{above MPP} \end{cases} \tag{3.22}$$

where D_{VPV} is $\frac{d}{dV_{PV}}$, P_{PV}, V_{PV} and I_{PV} are the input PV power, input PV voltage and input PV current respectively. The proposed algorithm is developed as a conventional IC technique and voltage perturbation is considered as a step change to track the MPP from the system as mentioned in flowchart which is shown in Fig. 3.6. Further the obtained duty cycle on the basis of perturbation is regulated with integral regulator. The integral regulated IC MPPT algorithm implemented for the MPP is decided by (3.22) as mentioned. This decides the operating point for IBC at corresponding P_{MPP} and is known as V_{MPP} and I_{MPP}.

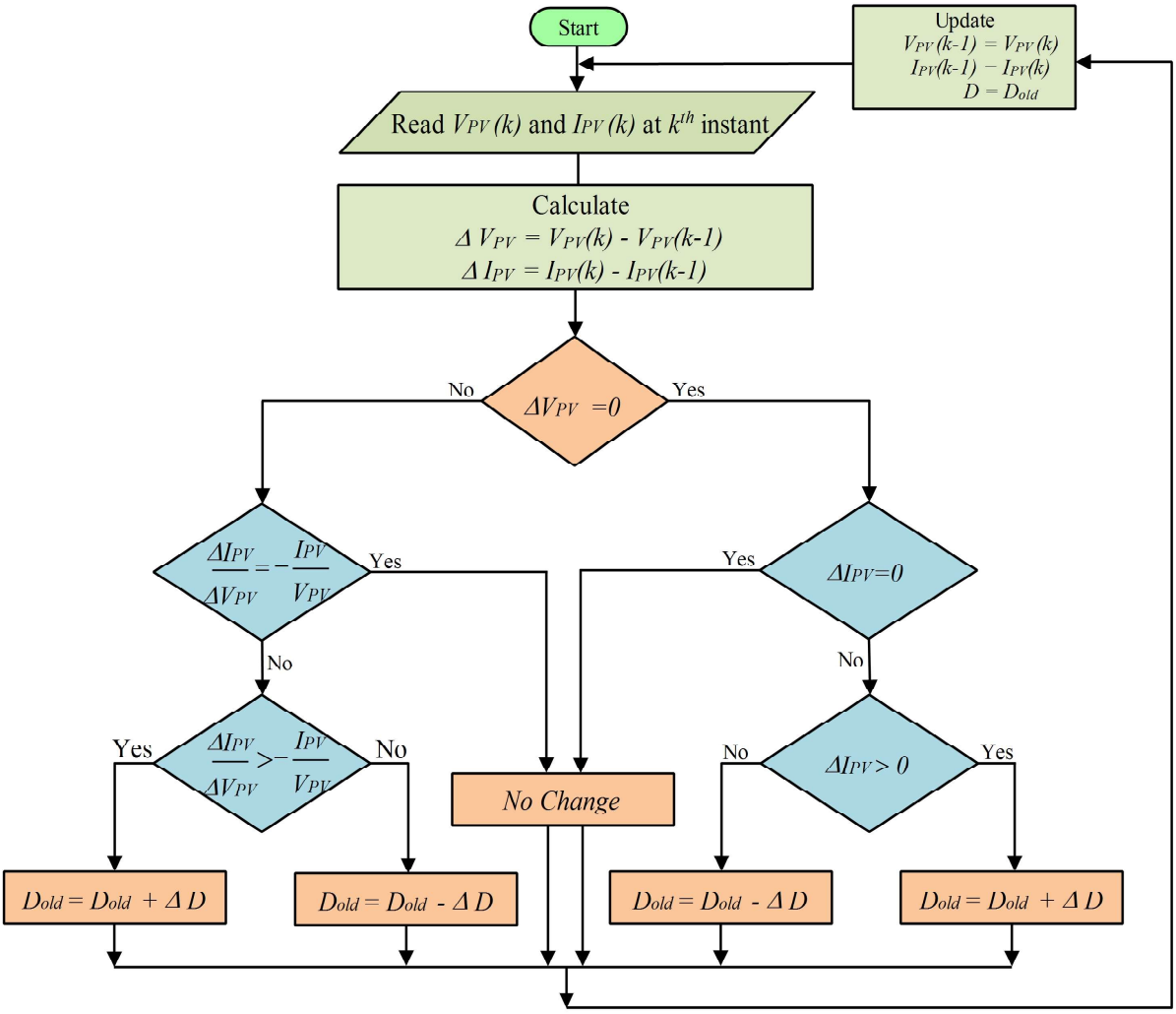

Figure 3.6: Flowchart of the incremental conductance (IC) MPPT algorithm

3.4.2 Control of IBC with MPPT algorithm

The sensed voltage (V_{MPP}) and current (I_{MPP}) of the PV array for the use of IC MPPT algorithm gives the maximum operating power (P_{MPP}) at which the derivative of power with respect to voltage will be zero. This IBC gives the required input voltage for the VSI. The control of IBC is regulated with the integral regulator as shown in Fig. 3.7

where V_{PV} and I_{PV} is the voltage extracted from the PV array during operation and $\frac{\Delta I}{\Delta V}$ is the generated reference point using (3.21) from the MPPT algorithm. The generated reference value is further regulated with the sensed value (V_{PV} and I_{PV}) to control the duty ratio of the boost converter, which results in the desired output voltage. After this stage, the IBC output is used as a DC input source for the VSI and for further participation in the grid integration control.

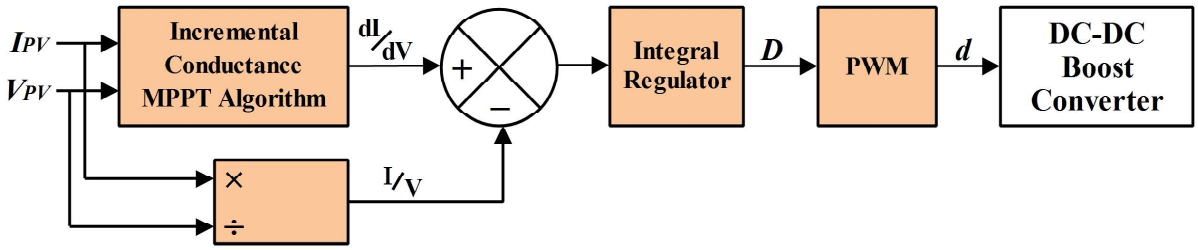

Figure 3.7: Block diagram control loop of IBC with MPPT

3.4.3 Proposed control scheme for two-stage grid interfaced VSI

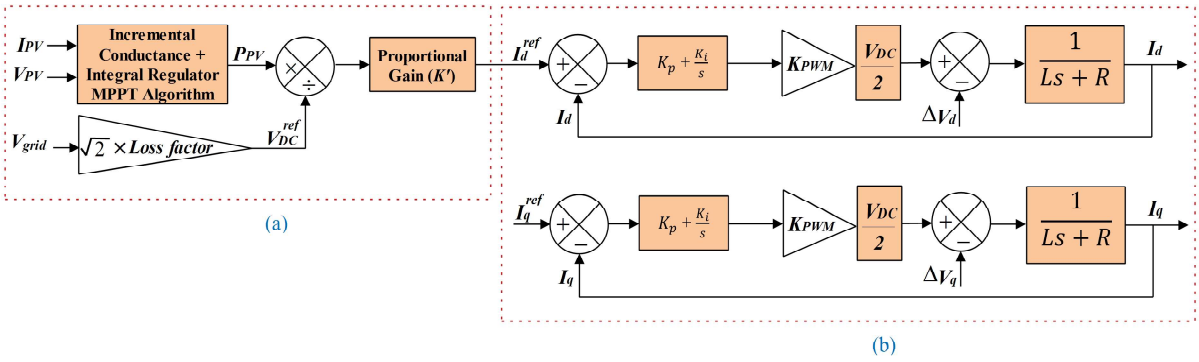

Figure 3.8: The proposed control scheme of a two-stage GIPV system contains (a) a feed-forward control to generate reference current and (b) current control loop

The conventional control scheme of a grid interfaced inverter consists an outer loop and an inner loop or in other words voltage regulation loop and current control loop, respectively. The outer loop of the system is generally responsible for the generation of reference current, for the active power flow in the system on the basis of fixed DC-link voltage, called as reference DC-link voltage. The controller regulates the voltage according to this value and gives a reference current for d-axis in SRF controlled system. The system reference current is generated according to the available power coming PV source of the system and the voltage of grid as shown in Fig. 3.8. The loss factor, which is mentioned in (3.23), is calculated by considering the losses of switches (5%), interfacing inductor (10%) and the variation in nominal grid voltage (10%). This approximated reference DC-link voltage is mathematically obtained as [114],

$$V_{DC,e}^{ref} = \sqrt{2} \times V_{grid} \times Loss\ factor \tag{3.23}$$

The DC-link voltage varies with respect to the variation in the irradiance level. The novelty of this proposed system is of not requiring a voltage sensor to measure the DC-link capacitor

voltage to track any reference DC-link voltage value as it's done in conventional technique to generate the reference current. This current is primarily responsible for the generation of active power into the GIPV system. The net amplitude of the current is estimated as,

$$I_{g,e} = \frac{P_{PV}}{V_{DC,e}^{ref}} \tag{3.24}$$

By the above mentioned technique, the generated current further introduces a proportional gain (K'). As K' increases, the transient time increases and filter performance of the system decreases. Therefore, the gain is tuned in such a way that it enhances the d-axis current of the system in SRF which ultimately achieves the active power flow and generates switching pulses for the VSI.

3.4.4 Proposed control scheme for single-stage grid interfaced VSI

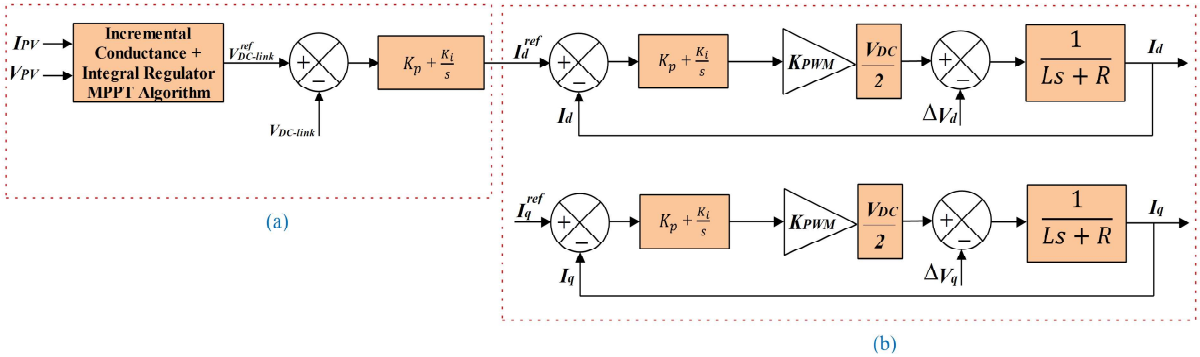

Figure 3.9: The proposed control scheme for a single-stage GIPV system contains (a) IBC free control loop to generate reference current and (b) current control loop

In a conventional single-stage GIPV system, instead of the outer control loop, the incremental conductance MPPT algorithm with an integral regulator generates the reference current directly as shown in Fig. 3.9(a). Further, generated reference currents for active power and predefined value for reactive power generation are compared with the grid currents and passes through the PI controller in $dq-$reference frame. The generated signal from the PI-controller follows the decoupled current control scheme to generate the gate pulses for VSI as shown in Fig. 3.9(b).

This subsection intends to discuss the control approach of each converter used in GIPV system. The performance of control scheme used in this system at different stages is analysed

Table 3.1: Design parameters of PV array using PV module 'KC200GT'

PV Module	
Power at MPP (P_{MPP})	200.143 W
Maximum power point voltage (V_{MPP})	26.3 V
Maximum power point current (I_{MPP})	7.61 A
Open circuit voltage (V_{oc})	32.9 V
Short circuit current (I_{sc})	8.21 A
PV Array	
Power at MPP (P_{MPP})	30 kW
Maximum power point voltage (V_{MPP})	394.5 V
Maximum power point current (I_{MPP})	30000/394.5 $\approx$ 76.1 A
Number of series module (N_{ser})	394.5/26.3 = 15
Number of parallel modules (N_{par})	76.1/7.61 = 10

by varying the input source parameters. The variation in the performance of the system is discussed in next section.

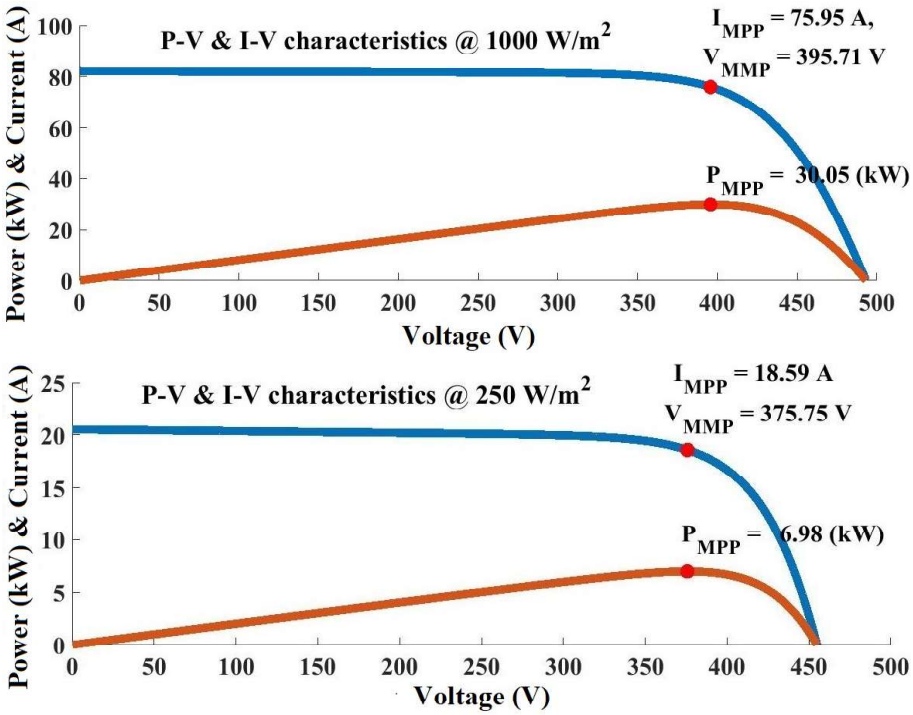

Figure 3.10: PV array I-V and P-V characteristics curve at 1000 W/m^2 and 250 W/m^2

3.5 Results and Discussions

A 30 kW system is considered and simulated with MATLAB/Simulink by using sim power system tool box. It has been tested at different irradiance levels for both conventional as well as proposed control scheme.

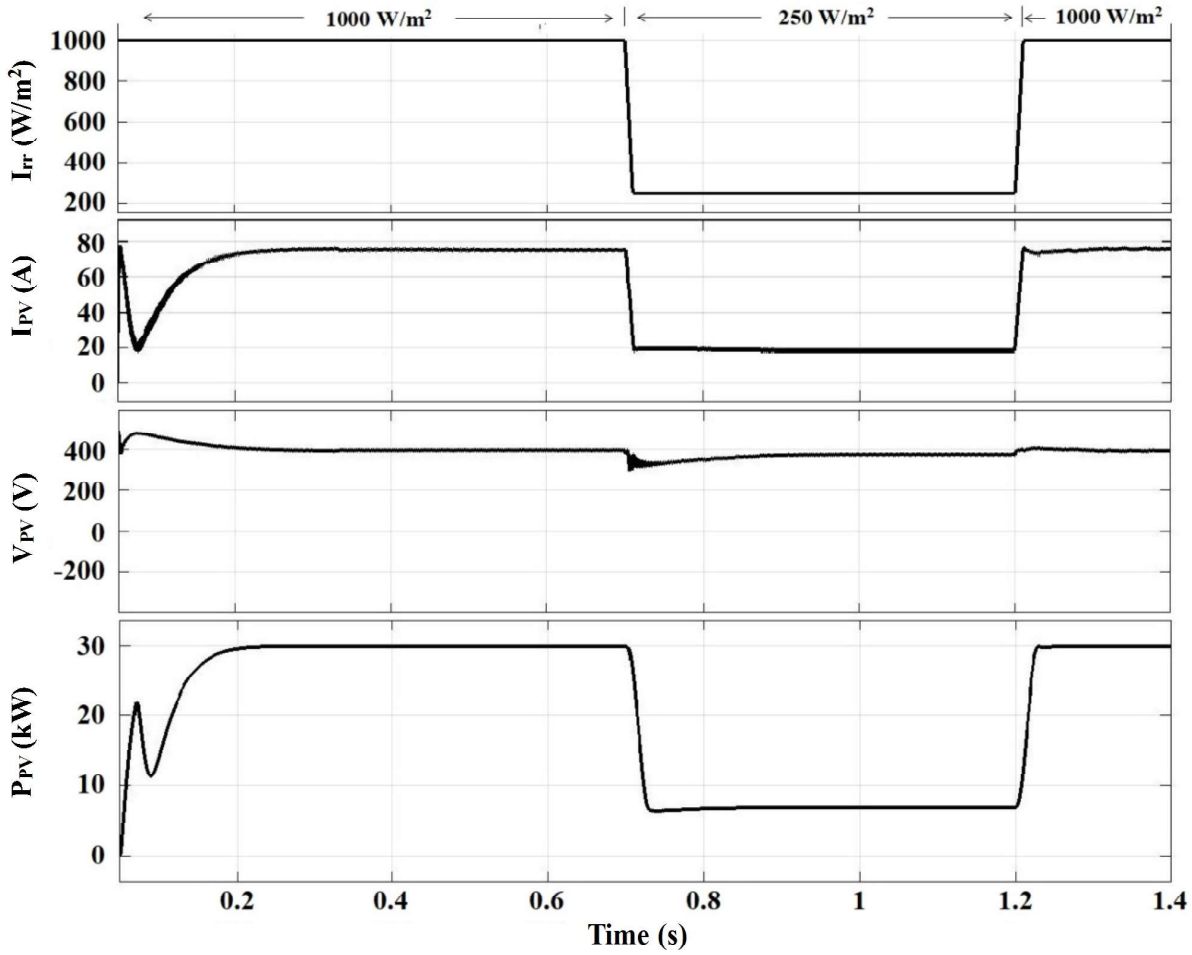

Figure 3.11: Simulated Steady state performance of the PV array at variable irradiances level (I_{rr}) i.e. 1000 W/m^2 and 250 W/m^2

3.5.1 Analysis of PV array at variable irradiance level

A 30 kW PV input source is considered for proposed system. A single diode model of PV modules (KC200GT) are arranged in series and parallel combination for PV array. The parameters of PV array corresponding to PV module is shown in Table 3.1. The combined characteristics curve i.e. power vs voltage and current vs voltage of solar PV array at variable irradiance condition i.e. 1000 W/m^2 and 250 W/m^2 is shown in Figure 3.10, respectively. Fig. 3.11 shows

that the PV array at 1000 W/m^2 irradiance level produces 30.05 kW P_{MPP}. The value of I_{MPP} and V_{MPP} with respect to the P_{MPP} is 75.95 A and 395.71 V respectively. Similarly, for 250 W/m^2 irradiance level the value of P_{MPP} is 6.98 kW and the operating I_{MPP} and V_{MPP} is 18.59 A and 375.75 V, respectively. The above mentioned data shows a variation in irradiance level which leads to a drastic change in current and power but the change in voltage level is very marginal. The dynamic response of the PV array is analysed in terms of change in irradiance. The PV array parameters such as I_{rr}, I_{PV}, V_{PV} and P_{PV} are analysed by changing irradiance level from 1000 W/m^2 to 250 W/m^2 at t=0.7 s to t=1.2 s and attaining the previous position i.e. 1000 W/m^2 at t=1.2 s. In the given time interval, the change in the irradiance level produces a change in the input current so the input power is shown in Fig. 3.11. Further, for variable irradiance condition the performance of the overall system with conventional control scheme and proposed control scheme is discussed in the following subsections.

3.5.2 Case I: Conventional control scheme in variable irradiance condition

The performance of the conventional control scheme is tested on variable irradiance level. It is verified at the irradiance levels of 1000 W/m^2 and 250 W/m^2. Fig. 3.12 shows that, the irradiance level is changing from 1000 W/m^2 to 250 W/m^2 at 0.7 s till 1.2 s and attaining the previous position i.e. 1000 W/m^2 at 1.2 s. During this condition, all variations in voltage level, power level, change in direct current and DC-link voltage are shown in Fig. 3.12. The MPPT voltage for the proposed 30 kW system is 395.71 V which is achieved by the system during the power flow from source to the grid. The system voltage changes while changing the irradiance level from 395.71 V to 382 V and corresponding power flow during this condition is 6.17 kW. During all variations observed in Fig. 3.12 shows that the voltage level at the point of common coupling (PCC) is almost constant but the variation in current level is due to the change in irradiance level. In the conventional control scheme, the reference value for DC-link voltage is fixed at 700 V and system always tracks this value for desired PCC voltage. This reference

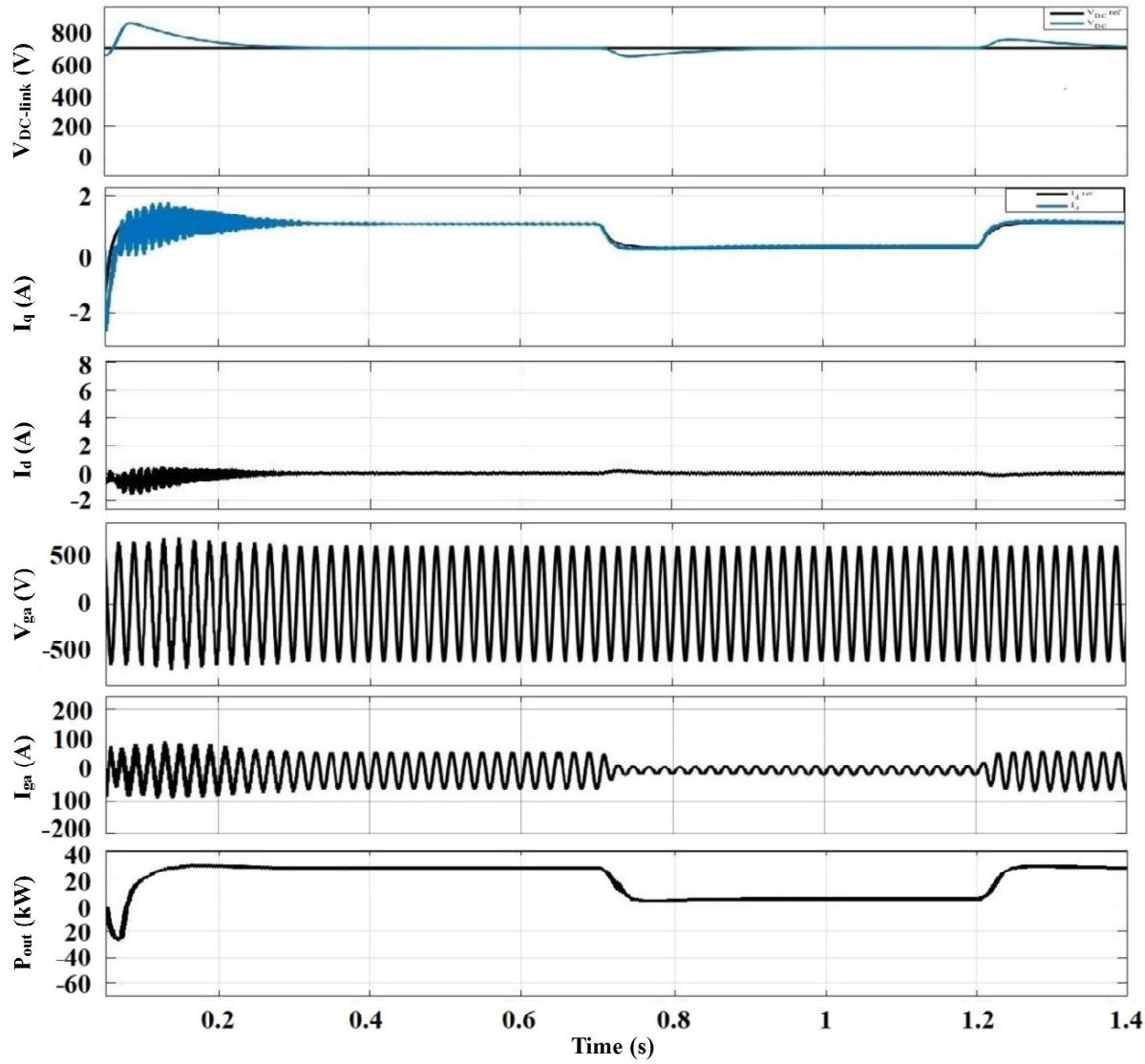

Figure 3.12: *CaseI*- Behaviour of conventional control scheme for DC-link voltage, d-axis current, q-axis current, grid voltage of phase A, grid current of phase A and output power fed into the grid with respect to change in irradiance level

value is calculated as in [122],

$$V_{DC} = \frac{2\sqrt{2} \times V_{LL}}{\sqrt{3}m} \tag{3.25}$$
$$= \frac{2\sqrt{2} \times 415}{\sqrt{3} \times 0.96} = 705.92 \approx 700 \text{ V}$$

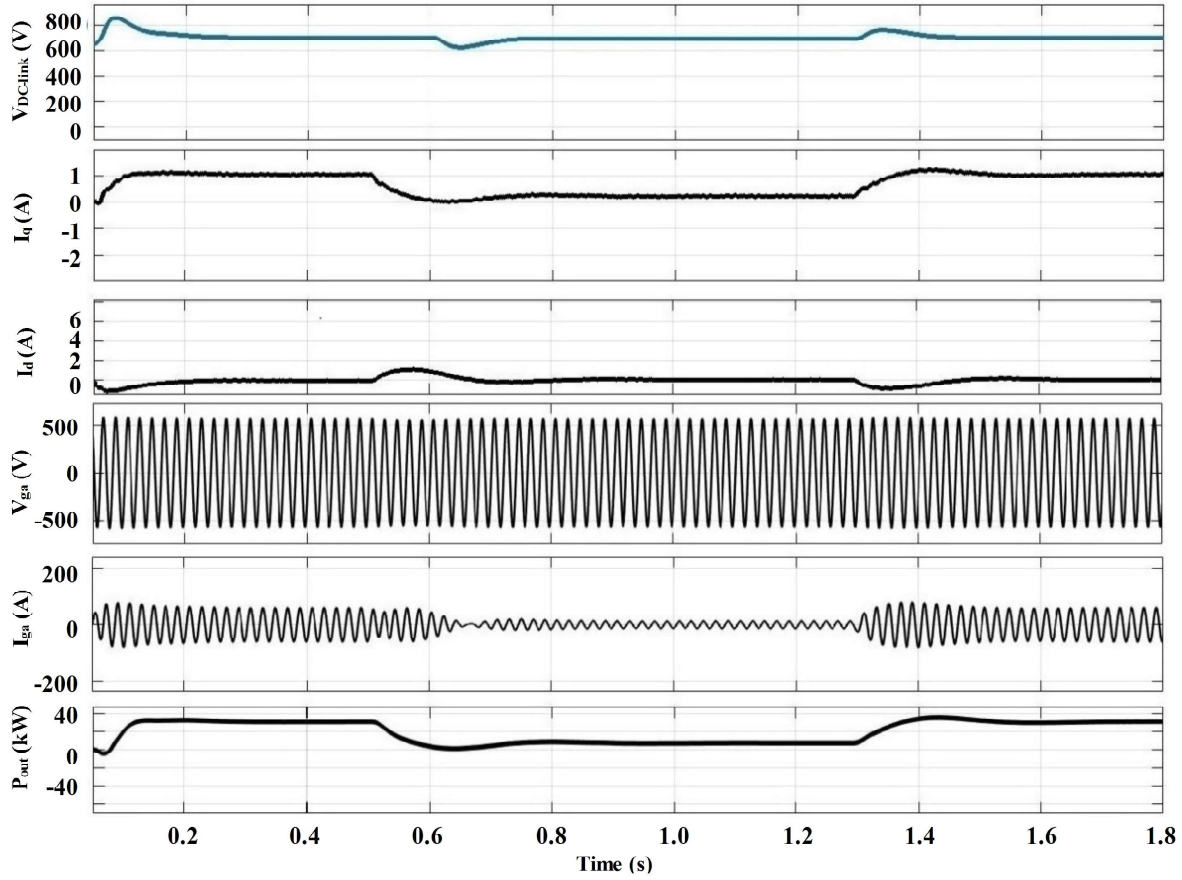

Figure 3.13: *CaseII*- Behavior of proposed control scheme for DC link voltage, *d*-axis current, *q*-axis current, grid voltage of phase A, grid current of phase A and output power fed into the grid with respect to change in irradiance level

3.5.3 Case II: Proposed control scheme at variable irradiance level

Fig. 3.13 illustrates the dynamic behavior of the proposed sensorless control approach of GIPV system. This system is tested at different irradiance level to investigates the dynamic behavior of the system. The system starts working at 1000 W/m^2 irradiance level. At t = 0.5 s, the irradiance changes from 1000 W/m^2 to 250 W/m^2 which leads the current and power of the system to decline. This situation is observed till t = 1.3 s, further it reaches to its previous value 1000 W/m^2. The dynamic behavior of the system shows that the same amount of irradiance change takes lesser time in contrast to the conventional control scheme of the system. The DC-link voltage estimated in this condition is calculated by (3.23). In this approach, the system has selected the value of loss factor (includes the 5% swithcing loss, 5% interfacing inductors and

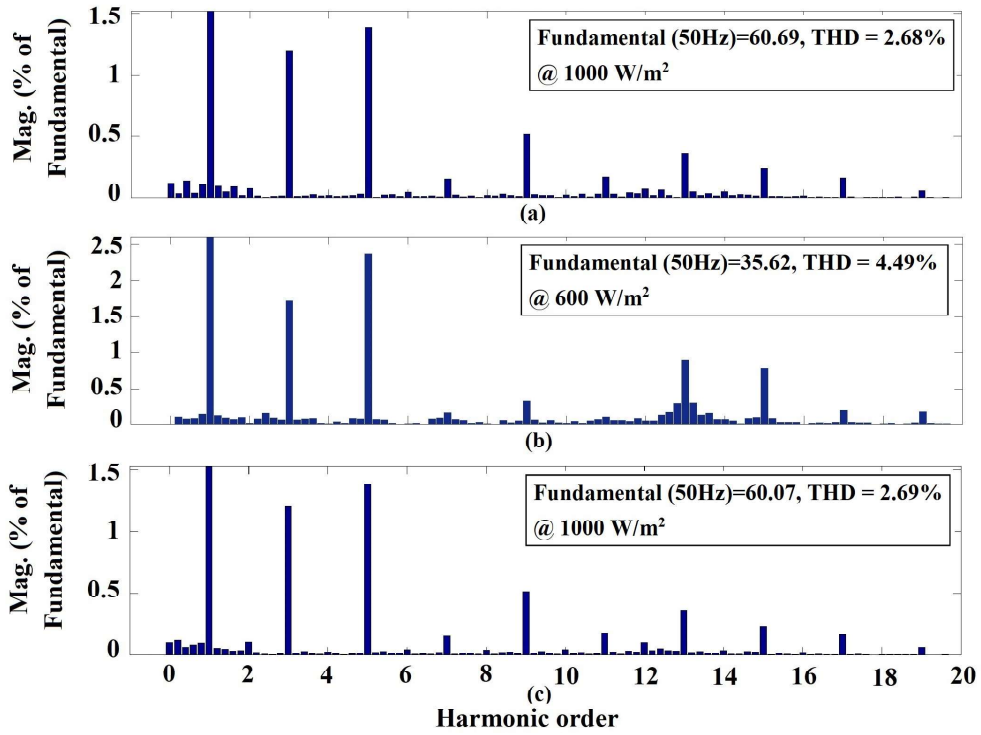

Figure 3.14: THD present in output current (a) at the starting of 1000 W/m^2 (b) from 1000 W/m^2 to 600 W/m^2 (c) from 600 W/m^2 to 1000 W/m^2

10% voltage variation i.e. loss factor = 1.05×1.05×1.1 = 1.21) to be 1.2.

$$V_{DC,e}^{ref} = \sqrt{2} \times V_{grid} \times Loss\ factor$$
$$= \sqrt{2} \times 415 \times 1.2 = 704.27 \text{ V}$$

The input voltage of the system changes from 395.71 V to 382 V during change in irradiance level and power of the system is 6.98 kW. The change in irradiance level leads the DC-link voltage to oscillate a bit but it again achieves the estimated DC-link voltage quickly as demonstrated in Figure 3.13.

3.5.4 Analysis of transient response and harmonics

The transient response [126, 127] at DC-link has been studied for the proposed control scheme. The effect of transient and voltage ripple at DC side have been explored in terms of THD [128, 129] present in output current at AC side under variable irradiance condition. In the proposed control scheme, when the system starts performing at 1000 W/m^2, the system provides DC-link voltage of approximately 704 V under steady state condition with initial overshoot of 21.18%

Table 3.2: Transient analysis of the conventional and proposed control scheme

Irradiance (I_{rr})		Transient parameters	
		Overshoot/Undershoot	Settling time (t_s)
Starts from 1000 W/m^2	Proposed Scheme	+21.18%	0.35s
	Conventional Scheme	+21.57%	0.41s
From 1000 to 600 W/m^2	Proposed Scheme	-5.81%	0.175s
	Conventional Scheme	-3.91%	0.367s
From 600 to 1000 W/m^2	Proposed Scheme	+5.26%	0.15s
	Conventional Scheme	+3.75%	0.35s

and it's settling time (t_s) is 0.35s as shown in the V_{DC} performance curve of Fig. 3.13. During this time, the THD present in the output current is within limit i.e., 2.68% as shown in Fig. 3.14(a). Further, at first step change, the irradiance is stepping down from 1000 W/m^2 to 600 W/m^2 whereas, the DC-link voltage is approximately 697 V with undershoot of 5.81% and it's t_s is 0.175s which is observed in the V_{DC} performance curve of Fig. 3.13. Simultaneously, the THD present in the output current is 4.49% which is also within the limit is shown in Fig. 3.14(b). Likewise, during second step change, the irradiance is stepping up from 600 W/m^2 to 1000 W/m^2 whereas, the DC-link voltage is increasing to approximately 704 V with overshoot of 5.26% and t_s is 0.15s that is also observed from the performance curve of V_{DC} in Fig. 3.13. In addition to this, THD in the output current is maintained at 2.69% which is well within the limit as illustrated in Fig. 3.14(c). Finally, the THD condition of output current due to the DC-link voltage ripple under variable irradiance condition is presented in Fig. 3.14. In addition, the transient response of the proposed scheme with respect to the conventional has been compared in Table 3.2 and it gives very close results which proves the validity and feasibility of the proposed system.

3.6 Conclusion

A novel sensorless DC-link voltage technique for two-stage three-phase GIPV system has been introduced and implemented in this chapter. This technique avoids the outer control loop and proposes a new DC-link voltage control model to produces an active reference current for PV power generation. Thus, the power balancing and constant voltage at DC-link are achieved

through the estimated value. As a result, the complexity of the system and control schemes are reduced, which increase the dynamic response of the system during variable irradiance condition. Besides, the elimination of the sensor minimize the system design as well as cost. The validness and robustness of the proposed system have been demonstrated on 30 kW two-stage, three-phase GIPV system in MATLAB/Simulink environment using sim power tools. The performance of the system is analyzed under variable irradiance conditions for the proposed as well as the conventional control technique. It exhibits a fast dynamic response under variable irradiance condition. In the steady state condition, both the control techniques show similar results which exhibit the feasibility of the proposed control technique.

Chapter 4

DERATED MODE OF POWER GENERATION IN PV SYSTEM USING A MODIFIED PERTURB & OBSERVE MPPT ALGORITHM

4.1 Introduction

In today's scenario of power generation, the acceptance of renewable energy sources (RESs) are increasing due to the shortcoming of fossil fuels. Therefore, the RESs are supporting the power generation. The RESs include wind energy, solar energy, hydro energy, fuel cell and tidal energy. Among these RESs, installation of photovoltaic (PV) solar system is advantageous due to low-cost maintenance. Therefore, the acceptance of the PV systems for grid support is booming in the renewable energy market. However, the PV power generation depends upon the irradiance. It affects the power generation but can be improved by forecasting of the power as discussed in [130, 131]. Additionally, the use of PV systems has exponentially increased due to advancement in power electronics research [11]. These are utilized in various forms which are classified as stand-alone PV, grid-interfaced PV (GIPV) and hybrid PV system. Among these, the GIPV system has an advantage over others due to its bulk power transfer capability. However, the GIPV system has some disadvantages due to surplus power generation such as overvoltage at various points at the feeder level and especially at the point of common coupling (PCC). Additionally, the maximum power point tracking (MPPT) algorithm takes more settling time which causes power loss during variable irradiance conditions.

The aforementioned issues affect the smooth functioning of the GIPV system. The most affecting factor to the system is the high amount of power generation during peak hours, it causes overvoltage in the grid. It also affects the safety of grid-connected network's equipment such as transformers, circuit breakers, relays or contactors (for low or high voltage application

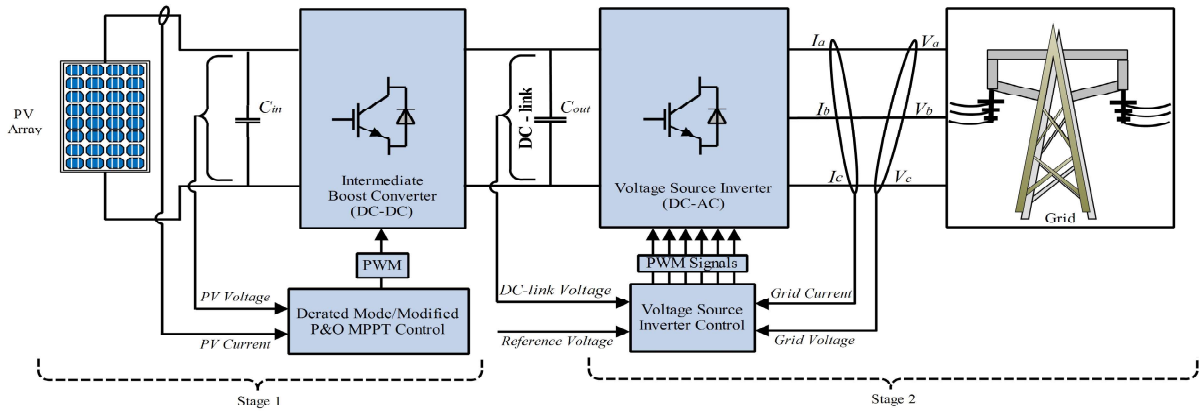

Figure 4.1: Block diagram of the proposed two-stage, three-phase grid interfaced PV system

respectively) [132] and conductors. In addition, the tracking capability of MPPT algorithms get affected due to the random change in irradiance condition. Above mentioned issues affect the performance of the system and impose an extra cost when equipment gets damaged. Therefore, a suitable control approach and the MPPT algorithm is required.

As aforementioned, the control schemes which have been applied for the derated mode of operation during peak hours of power generation, lag to do the following:

1. Most of the existing technologies are based on conventional MPPT techniques.
2. Implemented systems are mostly a single phase GIPV system.
3. A proper tracking strategy has not been proposed which can reduce the power loss during the search of maximum power point (MPP).

The above-mentioned limitations can be resolved through a proposed derated power generation scheme with a modified MPPT. The proposed scheme will perform in peak as well as in non-peak hours of power generation and improves the tracking capability of the MPPT algorithm. It will resolve the problem of overvoltage and the others such as drifting, oscillation near MPP and tracking speed. As a result, the power loss during the search of operating point will be reduced under variable irradiance level. Hence, a suitable MPPT algorithm is required.

4.1.1 Motivation

The aforementioned issue of excess power generation during peak hours affect the distribution network. Therefore, limiting of power transfer is required during peak hours generation.

The power transfer is limited by introducing the tap-changing transformer, voltage regulator, increasing the conductor size, storage and curtailment approach [91, 133]. Among all methods of power limiting, the curtailment of surplus power is the most suitable method [90]. In this respect, Omran *et al.* [92] have proposed a derated mode approach for curtailment of the surplus power. Likewise, various methods of derated mode operation are addressed in the literature. They have implemented a current, voltage, power and perturb & observe (P&O), MPPT based derated mode generation. In comparison to all, the selection of P&O based derated mode generation is most suitable due to less complexity. However, system efficiency and accuracy is less. Additionally, the algorithm oscillates near the operating point (i.e., drifting from the operating point in the random direction). Therefore, a novel MPPT technique is required to keep the system in derated mode generation with higher efficiency, accuracy, less drift and minimum power loss.

4.1.2 Contribution

The significant contributions of this chapter are summarized as follows.

1. A derated mode GIPV system has been proposed to limit the power transfer and resolve the overvoltage problem at PCC during peak power generation.
2. The proposed scheme introduces a modified MPPT which limit the power transfer.
3. This MPPT algorithm results in improved tracking speed and efficiency which reduces the power loss during variable irradiance condition.

4.2 System Framwork and Working Strategy

This section briefs the system structure and proposed control strategy of the GIPV system. The proposed system consists of two-stages as shown in Fig. 4.1. The stage one includes a PV array, intermediate boost converter (IBC) and MPPT control. In the proposed system, a modified MPPT algorithm has been implemented which work in derated power generation mode (DPGM) and modified MPPT mode. The DPGM gets activated when generation exceeds the pre-defined power limit (P_{limit}), otherwise it works in modified MPPT mode [93]. Further, the modified MPPT generates a pulse width modulation (PWM) signal for the IBC to get desired

DC-link voltage level. On the other hand, in the second stage, the system is consist of an IGBT based voltage source inverter (VSI) and integrated with the grid. The interfacing inductors are used between the inverter and the grid to inject the current as well as generated power with the help of inverter control. The inverter control of the proposed system consist of a dual control loop and the grid synchronization technique. The control of the system is obtained in synchronously rotating or *dq* reference frame [134]. This consist of a direct (d) and quadrature (q) axis which deals with the active and reactive power control respectively. Furthermore, the controller generates the PWM signals to trigger the VSI and transfer power. Finally, the complete system is developed and simulated for a 30 kW, two-stage, three-phase, grid interfaced PV system.

4.3 Proposed Control Technique

In this section, the control approach of each converter used for the first and second stage of the system has been presented. In the first stage of control, the functionality of MPPT with the IBC is illustrated in the upcoming subsections.

4.3.1 Conventional P&O MPPT algorithm

In the MPPT technique, the extracted voltage and current from the PV source is provided to the MPPT controller as shown in Fig. 4.2. This controller reaches to the operating point using direct duty ratio, three-step strategy on the power-voltage (P-V) characteristic curve as shown in Fig. 4.3.

In Fig. 4.3, the region of the operating point depends upon the slope of the power (change in PV power i.e., ΔP_{PV}). The three-step approach is considered for the left and right region of the P-V characteristic curve. In the left region, the slope of the power is positive with respect to the voltage so it moves forward towards the operating point. On the right side, power slope is negative with respect to the voltage, therefore it moves back towards the operating point as expressed in (4.1).

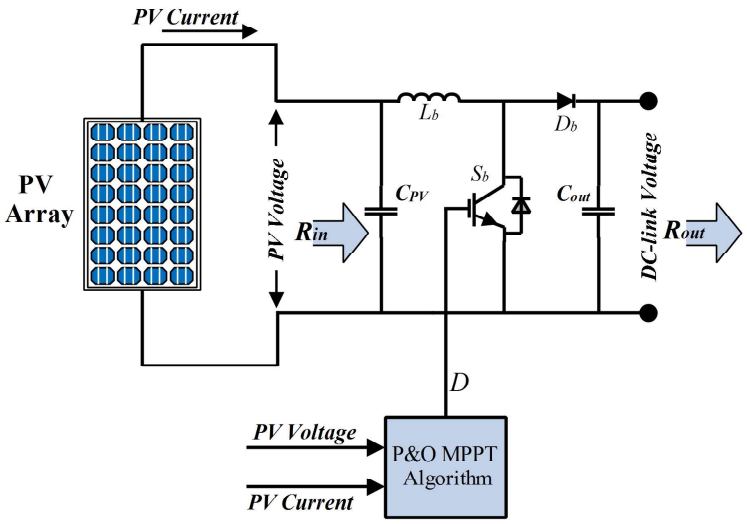

Figure 4.2: Circuit diagram of DC-DC IBC with MPPT control

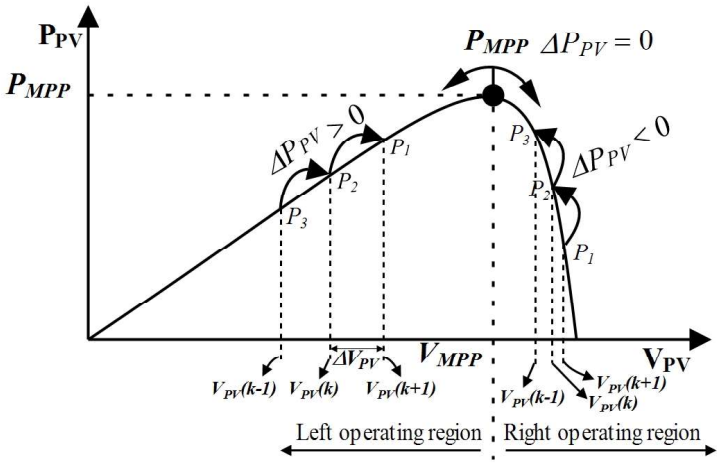

Figure 4.3: Conventional P&O MPPT algorithm searching strategy

$$if \quad \frac{dP_{PV}}{dV_{PV}} \quad is \begin{cases} > 0, & \text{Move forward towards MPP} \\ < 0, & \text{Move back towards MPP} \\ = 0, & \text{At MPP} \end{cases} \tag{4.1}$$

The corresponding increment and decrement in the duty ratio are due to the change in input power w.r.t. voltage. Consequently, the impact of the change in duty ratio on output voltage

V_{DC} and current I_{DC} of IBC can be illustrated as

$$V_{DC} = \frac{1}{(1-D)} V_{PV} \tag{4.2}$$

$$I_{DC} = I_{PV}(1-D) \tag{4.3}$$

and the ratio of V_{DC} and I_{DC} is the output impedance R_{out} of the boost converter which is calculated as follows.

$$R_{out} = \frac{V_{DC}}{I_{DC}} = \frac{R_{in}}{(1-D)^2} \tag{4.4}$$

where R_{in} and D is the input impedance and duty ratio respectively. At constant R_{in}, the value of R_{out} is inversely proportional to the duty ratio. Therefore, to achieve the maximum power, voltage and current at a particular duty ratio, the value of R_{out} is depicted as

$$R_{out} = \frac{V_{MPP}}{I_{MPP}} \tag{4.5}$$

Moreover, the performance of P&O depends upon the increment or decrement in step size (ΔD) of duty ratio [135]. Whenever, the value of ΔD is small, the time response to achieve the MPP is more which results in power loss. On the other hand, with a large step, the time response is fast, but the drift problem occurs during the variable irradiance condition as explained in [67]. It occurs due to the lack of direction knowledge (i.e., an increase in ΔP_{PV} is due to variable irradiance or perturbation of ΔD). Therefore, the operating point gets confused about the situation that whether it should move towards the MPP or away from the MPP. Moreover, the conventional P&O only tracks the MPP during peak or non-peak hours of power generation. However, it does not participate in limiting the excess power generated during peak hours.

4.3.2 Modified P&O MPPT algorithm

The proposed modified algorithm reduces the power loss as well as improves the time response. It also keeps the system drift-free during variable irradiance condition. In addition, the proposed MPPT limit the excess power generation during peak hours. The proposed algorithm operates in two modes such as modified MPPT mode and derated power generation mode (DPGM) as illustrated in Fig. 4.4. Whenever, the generated PV power is within the

power transfer limit (P_{limit}), the system works in modified MPPT mode. Otherwise, the system works in DPGM is expressed as followes.

$$P_{DC}(t) = \begin{cases} P_{PV}(t); & \text{Modified MPPT mode for} < P_{limit} \\ P_{limit}(t); & \text{DPGM for} \geq P_{limit} \end{cases}$$

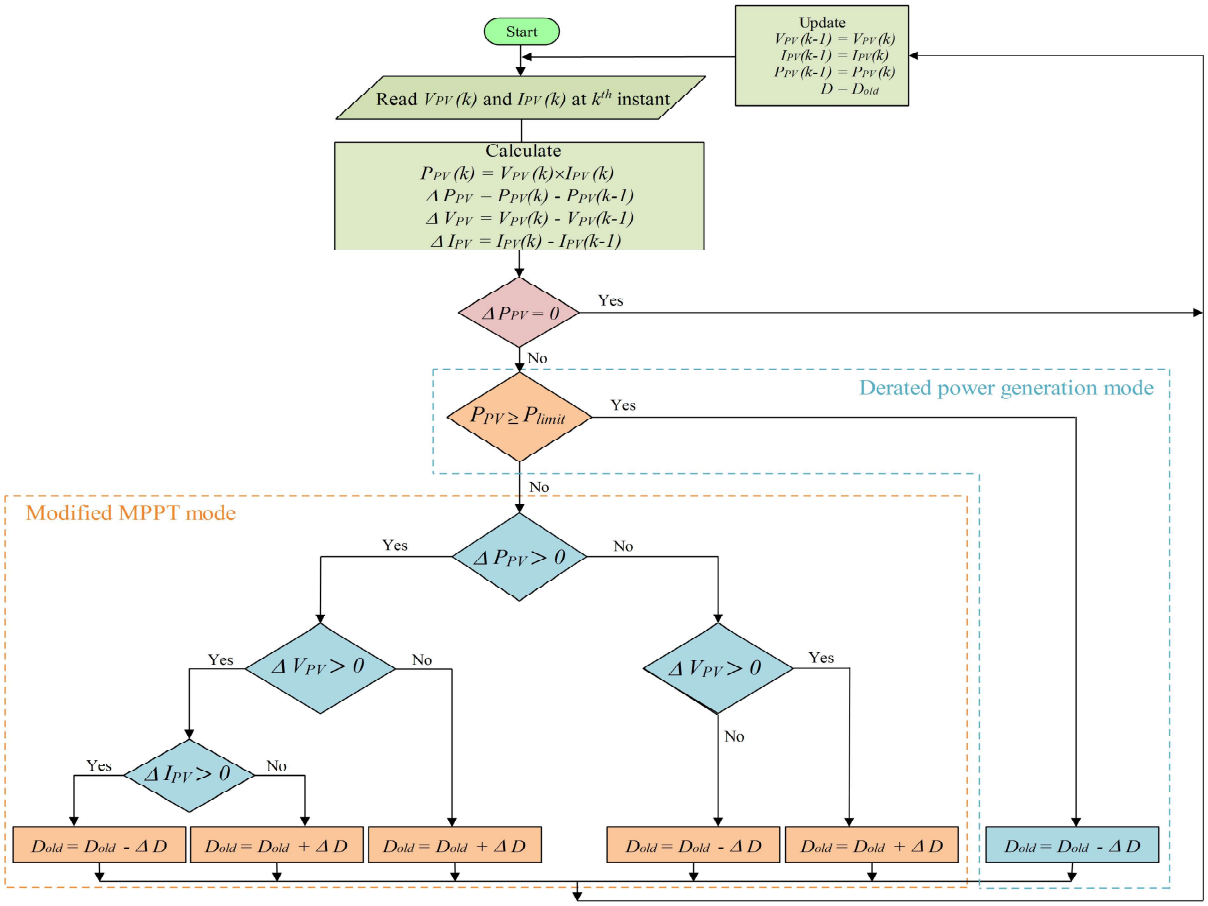

Figure 4.4: Flowchart of the modified P&O MPPT algorithm

Modified MPPT mode

The modified MPPT mode of the proposed algorithm follows the direct duty ratio (D), three-step strategy as mentioned in Section 4.3.1. In this strategy, a large value of ΔD is considered for the better time response. However, the large value of ΔD creates the problem of drift during irradiance change. As discussed in [67], the current level depends upon the irradiance level, which can be explained for a single diode model PV array and related equations are depicted

as follows [136, 137].

$$I_{PV} = N_p \left[I_{sc} - I_o \left\{ \exp\left(\frac{V_{PV}}{N_s V_t} \right) - 1 \right\} \right] \tag{4.6}$$

$$I_{sc} = N_p \left[I_{scn} + k_i \left(\Delta T \right) \right] \frac{G}{G_n} \tag{4.7}$$

where I_{sc}, I_o and V_t are the short circuit current, reverse saturation current and thermal voltage of the cell respectively. N_s and N_p present the series and parallel arrangement of modules respectively. I_{scn}, G_n, G, k_i and ΔT are the short circuit current at STC, reference irradiance, operating irradiance, temperature coefficient and difference of the temperature at actual and STC respectively. The MPP value of the PV array is delivered at particular R_{out} is depicted as

$$I_{MPP} = N_p \left[I_{sc} - I_o \left\{ \exp\left(\frac{V_{MPP}}{N_s V_t} \right) - 1 \right\} \right] \tag{4.8}$$

By putting Taylor's expansion on (4.8) till first order and substituting (4.4) and (4.5), the (4.8) can be obtained as

$$V_{MPP} = \frac{N_p I_{sc}}{\left[\frac{(1-D)^2}{R_{in}} + \frac{I_o N_p}{N_s V_t} \right]} \tag{4.9}$$

$$I_{MPP} = \frac{(1-D)^2 N_p I_{sc}}{R_{in} \left[\frac{(1-D)^2}{R_{in}} + \frac{I_o N_p}{N_s V_t} \right]} \tag{4.10}$$

By substituting (4.7) in (4.9) and (4.10), the V_{MPP} and I_{MPP} can be expressed as follows.

$$V_{MPP} = \frac{N_p^2 \left[I_{scn} + k_i \Delta T \right] \frac{G}{G_n}}{\left[\frac{(1-D)^2}{R_{in}} + \frac{I_o N_p}{N_s V_t} \right]} \tag{4.11}$$

$$I_{MPP} = \frac{(1-D)^2 N_p^2 \left[I_{scn} + k_i \Delta T \right] \frac{G}{G_n}}{R_{in} \left[\frac{(1-D)^2}{R_{in}} + \frac{I_o N_p}{N_s V_t} \right]} \tag{4.12}$$

where G and T are the variable parameters in (4.11) and (4.12). Therefore, the maximum value of V_{MPP} and I_{MPP} w.r.t. G is expressed as

$$\frac{dV_{MPP}}{dG} = \frac{N_p^2\left[(I_{scn}+k_i\Delta T)\frac{1}{G_n}+\frac{G}{G_n}k_i\frac{dT}{dG}\right]}{\left[\frac{(1-D)^2}{R_{in}}+\frac{I_oN_p}{N_sV_t}\right]} \tag{4.13}$$

$$\frac{dI_{MPP}}{dG} = \frac{(1-D)^2N_p^2\left[(I_{scn}+k_i\Delta T)\frac{1}{G_n}+\frac{G}{G_n}k_i\frac{dT}{dG}\right]}{R_{in}\left[\frac{(1-D)^2}{R_{in}}+\frac{I_oN_p}{N_sV_t}\right]} \tag{4.14}$$

Since G is increasing, I_{scn}, I_o, k_i, N_p, N_s, V_t and G_n are constant at STC and G, D and R_{in} are positive. Simultaneously, temperature also increases w.r.t. irradiance. Therefore, in (4.13) and (4.14) all the terms are positive as irradiance increases which means voltage and current are positive w.r.t. irradiance which is expressed as follows.

$$\frac{dV_{MPP}}{dG} > 0 \;\; and \;\; \frac{dI_{MPP}}{dG} > 0$$

Similarly,

$$\frac{dV_{PV}}{dG} > 0 \;\; and \;\; \frac{dI_{PV}}{dG} > 0$$

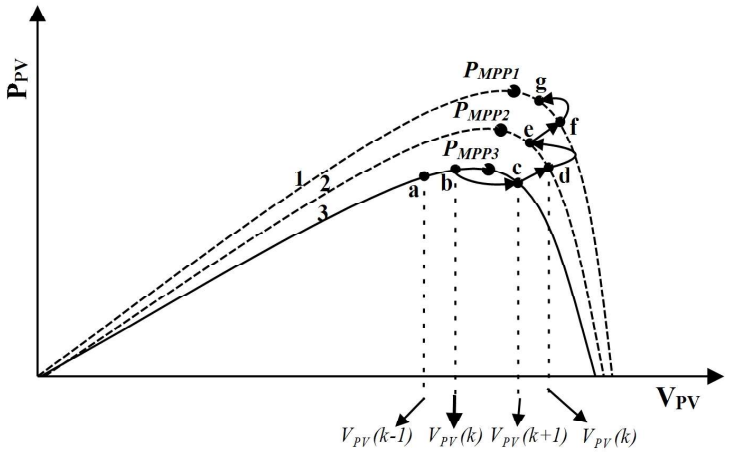

Figure 4.5: Drift analysis of operating point during variable irradiance condition

As mentioned above, the voltage and current increase w.r.t. irradiance. Thus, based on cur-

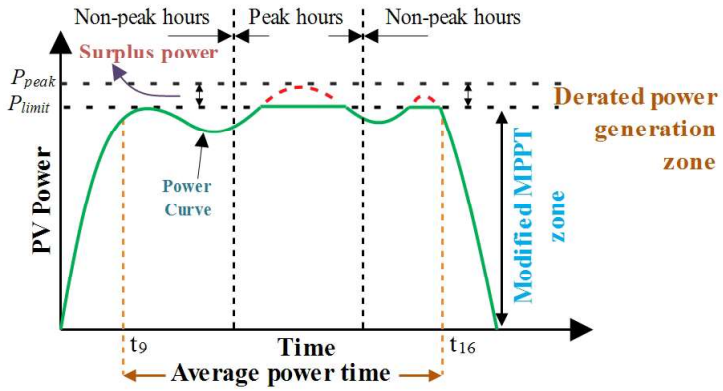

Figure 4.6: Day time power profile of a PV array

rent, voltage and power information, the drift problem can be avoided and analysed as follows.

When irradiance is increasing, the point ⓑ shifted to point ⓒ and then shifted to ⓓ on a new P-V curve as shown in Fig. 4.5. In this curve, the difference between point ⓑ and ⓓ for P, V and I is positive. It can be observed that the ΔV and ΔI are positive only when irradiance is increasing. This shows that the current's information during MPP tracking is essential. Further, based on these observations, ΔV and ΔI are positive which leads to the reduction in duty ratio. Consequently, the corresponding voltage decreases as compared to the conventional P&O where the voltage used to be increased. This depicts that the operating point which is used to move away from the MPP started moving towards the MPP because of the information of current. It means that the operating point is not deviating from MPP during variable irradiance condition or in other words, not drifting away from the MPP.

Derated power generation mode

In derated power generation mode, the modified P&O MPPT algorithm gets activated during available surplus power. As it is known that the peak power rating of the installed PV array is always more than the average power generated during the whole day. Thus, the PV array generates surplus power during peak hours. Therefore, to remove the surplus power, a power limit is required within which the power can be transferred without affecting the distribution network equipment. For this system, a power limit P_{limit} has been considered which is the

average of power generated during 9 to 16 hours of the day and is presented as follows.

$$P_{limit}(t) = \frac{P(t_9) + P(t_{10}) + ... + P(t_{16})}{t_9 + t_{10} + ... + t_{16}} \tag{4.15}$$

where $P(t_9), P(t_{10}), ..., P(t_{16})$ are the peak powers generated during $t_9, t_{10}, ..., t_{16}$ respectively. When the generated power exceeds the P_{limit}, the derated mode turns on and shaves the surplus power. In Fig. 4.6, the power curve is within the limit at every time instant which shows the active participation of DPGM.

Based on the above discussions in subsection 4.3.1 and 4.3.2, the conventional and proposed MPPT algorithms with IBC generates the DC power in first stage control. Further, in second stage control, the generated DC power is provided to the VSI for power conversion with inverter control which has been discussed in the next subsection.

4.3.3 Inverter control for grid integration

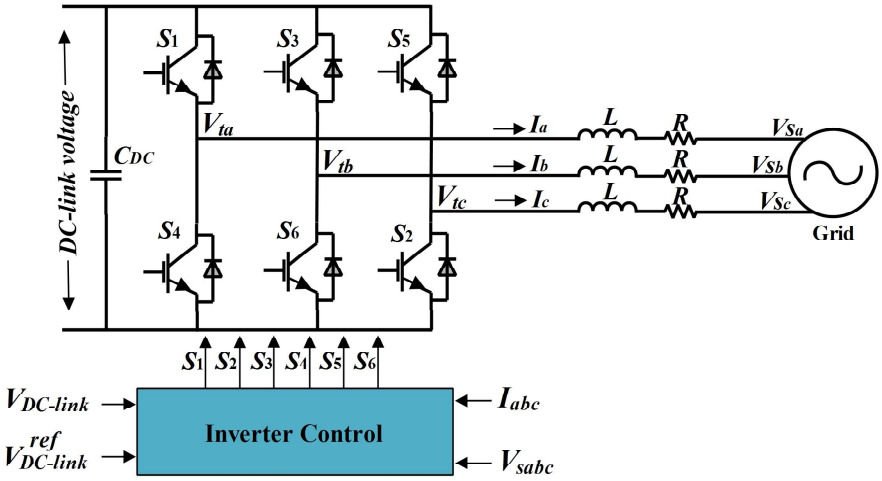

Figure 4.7: Circuit diagram of grid interfaced VSI

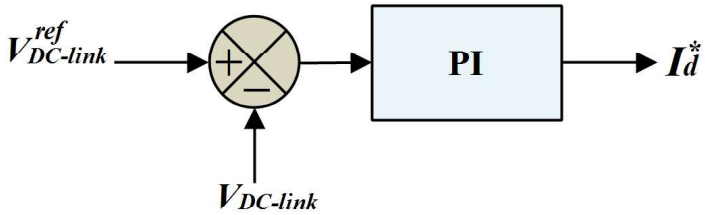

Figure 4.8: Voltage regulation/outer loop of inverter control

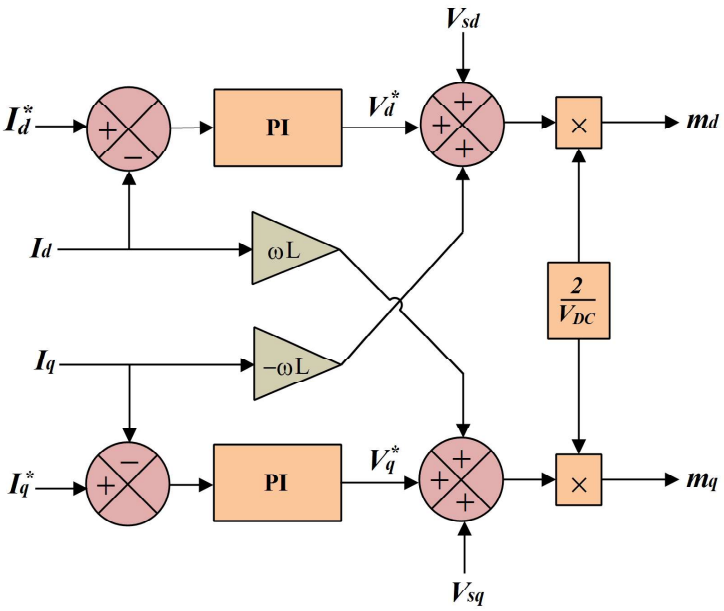

Figure 4.9: Current control/inner loop of the inverter control

The generated DC power is converted into AC power using VSI. The obtained AC power is further injected into the grid with the help of inverter control as shown in Fig. 4.7. In this process, the inverter control performs voltage regulation, current control and grid synchronization in synchronous (dq) reference frame. The voltage regulation or outer loop produces the reference current I_d^*. In this loop, the DC-link voltage is compared with a pre-defined reference voltage using a proportional-integral (PI) controller which produces I_d^* as shown in Fig. 4.8. On the other hand, in the inner loop, the decoupled current control scheme is used to generate the gate pulses for the VSI. In this technique, I_d^* is taken as the reference current for the active power control. Similarly, I_q^* is the reference current for reactive power control which is set as zero to transfer the power at unity power factor. Furthermore, both active and reactive power controllers generate the modulating signals as shown in Fig. 4.9. The respective mathematical modelling of the system as per Fig. 4.7 is depicted below [138].

$$\frac{dI_{abc}}{dt} = -\frac{R}{L}I_{abc} + \frac{1}{L}(V_{tabc} - V_{sabc}) \tag{4.16}$$

where R, L, V_{tabc}, V_{sabc} and I_{abc} are the resistance, interfacing inductance, inverter terminal voltage, grid voltage and the current respectively.The mathematical expressions of the system are of a higher degree in the natural reference frame (abc). Therefore, to use a simple controller

(i.e., PI) and less mathematical complexity, the present reference frame (abc) is transformed into rotating reference frame (dq) using Park's transform [113] and the resultant equations are illustrated as follows.

$$\frac{dI_{dq}}{dt} = -\frac{R}{L}I_{dq} \pm \omega I_{qd} + \frac{1}{L}(V_{tdq} - V_{sdq}) \tag{4.17}$$

or,

$$L\frac{dI_{dq}}{dt} = -RI_{dq} + V^*_{dq} \tag{4.18}$$

where

$$V^*_{dq} = V_{tdq} - V_{sdq} \pm \omega L I_{qd} \tag{4.19}$$

and ω is the angular frequency of the grid voltage. As mentioned in [139], the terminal voltage of inverter requires input DC-link voltage and modulation index. Hence, in dq-reference frame, the modulation index is presented as follows.

$$V_{tdq} = m_{dq}\frac{V_{DC}}{2} \tag{4.20}$$

Now, substituting (4.20) in (4.19) to get the modulating signals which is depicted as follows.

$$m_{dq} = \frac{2}{V_{DC}}(V^*_{dq} \mp \omega L I_{qd} + V_{sdq}) \tag{4.21}$$

These modulating signals m_d and m_q have been transformed from $dq \rightarrow abc$ to provide the gate signals ($S_1 - S_6$) to the VSI which generates voltage and current. Since the power has to be transferred in the grid, the generated voltage and current should be in phase. Therefore, a phase-locked loop technique has been added in the system which synchronize the VSI's generated voltage and current with the grid.

Finally, in the next subsection, the performance of the control approaches are evaluated and verified in the MATLAB/ Simulink environment.

4.4 Results and Discussions

A 30 kW, two-stage, three-phase, grid-integrated PV system using modified P&O MPPT algorithm is simulated in MATLAB/Simulink environment with Simpower tools. The modified MPPT performs derated power generation which restricts the power generation when it reaches to or beyond the P_{limit}. Simultaneously, the conventional P&O algorithm is also examined to select a suitable ΔD for the modified P&O algorithm under variable irradiance condition. Thereafter, the performance of the conventional and modified P&O algorithm are analysed in terms of PV power, PV voltage, duty ratio, DC-link and output power as follows.

4.4.1 Conventional P&O MPPT algorithm

For the evaluation of input voltage deviation and time response, the conventional P&O algorithm is tested for different values of ΔD. Simultaneously, to test the robustness of the system, the algorithm is evaluated under variable irradiance condition. For the sake of evaluation, a small step size $\Delta D = 3e^{-7}$ and a big step size $\Delta D = 3e^{-4}$ is considered. Now, it can be observed from Fig. 4.10(a) and 4.10(b) that due to the large step size, the oscillation in input voltage is significant. Furthermore, it is evident that the duty ratio achieves a steady state condition in less time under variable irradiance condition which is shown in Fig. 4.10. Hence, it can be concluded that the fast dynamic response can be achieved through a large step size. However, the operating point oscillates near the MPP due to large step size. In order to remove the oscillation near MPP, a modified P&O algorithm is adopted.

4.4.2 Modified P&O MPPT algorithm

The performance of the modified P&O algorithm is evaluated in two modes. One is a modified MPPT mode and another is derated power generation mode.

Modified MPPT mode

In this mode, the modified MPPT works like the conventional P&O until power generation does not reach to the power limit. Besides, the modified algorithm provides the right direction and less variation in voltage of the operating point towards MPP. Fig. 4.11 depicts that the variation in V_{PV} which is less as compared to the conventional P&O. Simultaneously, the change in the

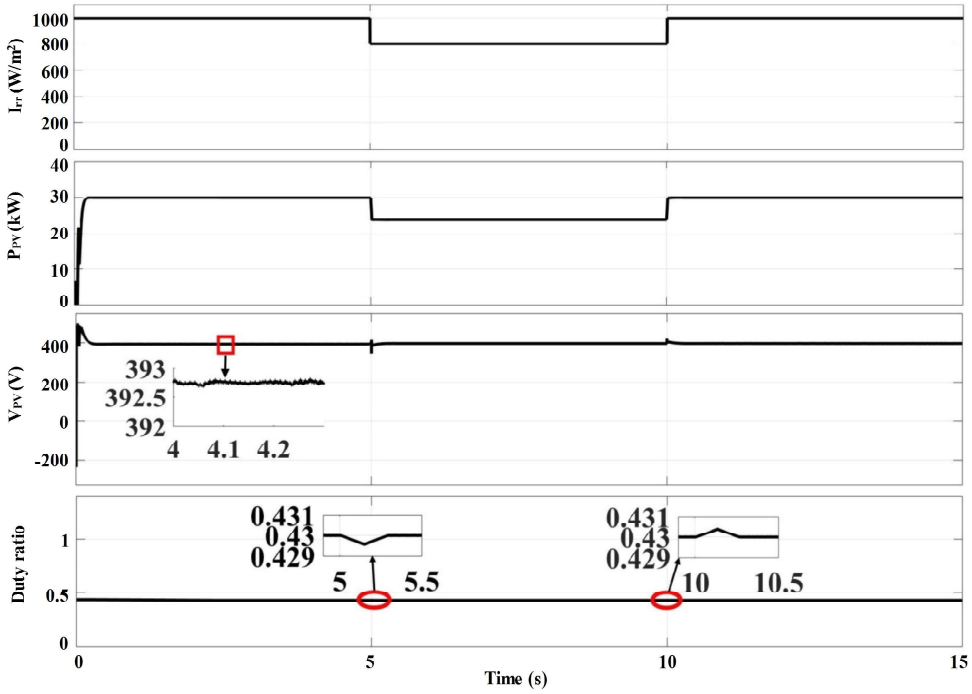

(a)

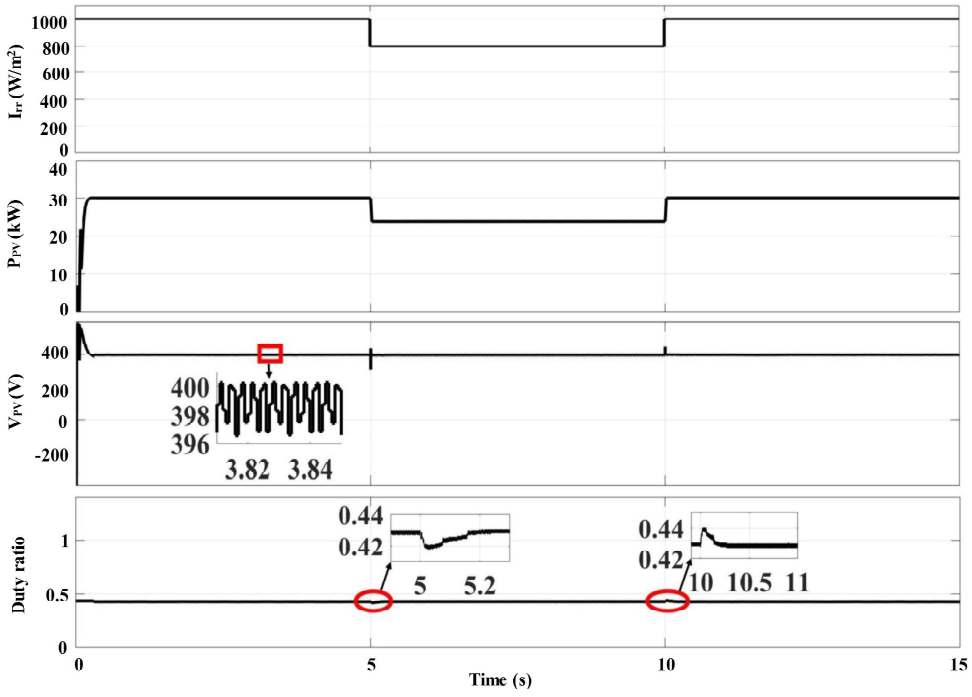

(b)

Figure 4.10: Dynamic performance of conventional P&O algorithm (a) at $\Delta D = 3e^{-7}$ (b) at $\Delta D = 3e^{-4}$

duty ratio is positive when irradiance is increasing as discussed in modified MPPT mode of Section 3. On the other hand, when irradiance is decreasing, the current decreases so the input voltage and corresponding duty ratio increases. Thus, the V_{PV} does not deviate and reaches

to the operating point. In addition, the effect of irradiance change in DC-link voltage, phase voltage (V_a) and current (I_a) is shown in Fig. 4.11.

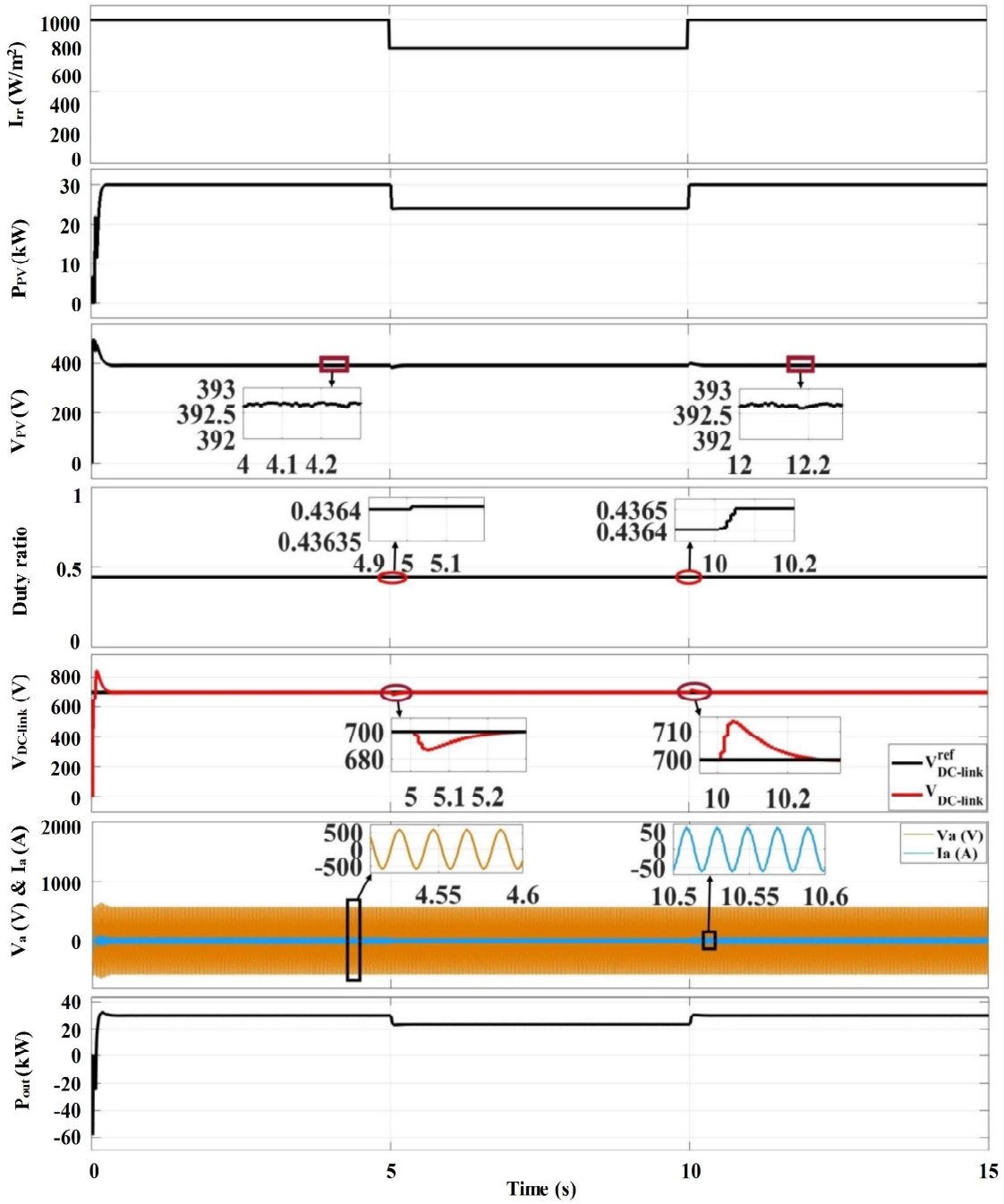

Figure 4.11: Steady state performance of MP&O algorithm in modified MPPT mode

Derated power generation mode

The system enters in derated power generation mode when the net power generation exceeds the power limit. During this mode, the modified P&O MPPT algorithm curtails the excess power.

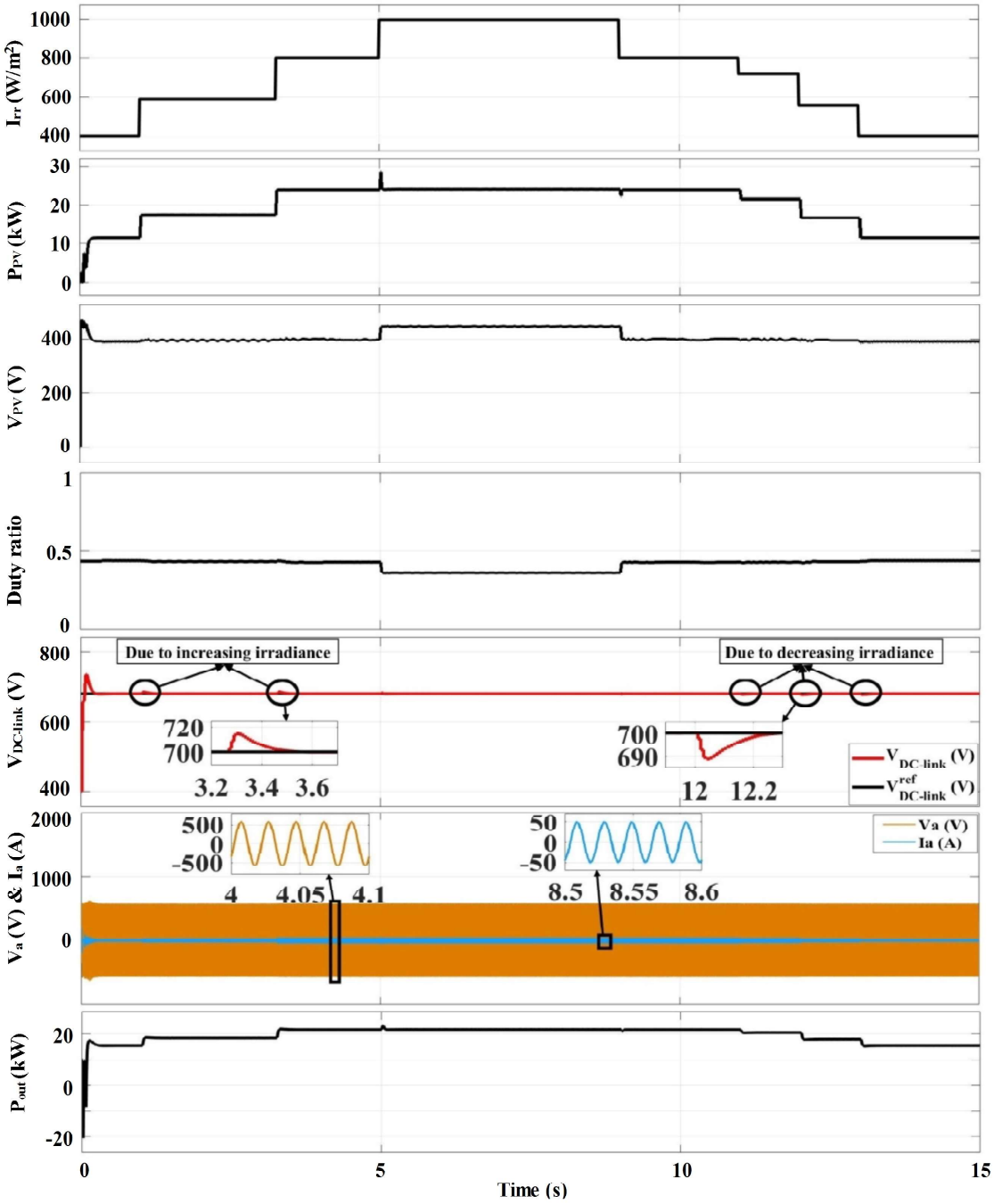

Figure 4.12: Steady state performance of modified P&O algorithm in derated power generation mode

A power profile is presented in Fig. 4.6 which is based on the irradiance change between morning to evening time. In this chapter, the system is simulated for t=15s where one second scaled as one hour of the day to replicate the peak and non-peak hours of the power profile. Now, Fig. 4.12 depicts that the system starts generating power from t=0 and it enters into the peak-hours zone after t=5s. In this zone, the excess power is shaved using modified MPPT and

it remains in this mode till t=9s. In this time, the system generates P_{limit} of 24 kW, which is the average power during 9 to 16 hours. During this time, the system performs in a derated power generation mode. Furthermore, the performance of V_{PV}, duty ratio, DC-link voltage, grid voltage and current are presented in Fig. 4.12.

4.4.3 Statistical analysis

Table 4.1: Performance analysis of the conventional and modified P&O MPPT algorithm

Sr. no.	Irradiance condition	Evaluation parameter		Conventional P&O	Modified P&O
1	At constant irradiance condition (600 W/m^2)	$t_{s,V_{MPP}}$	Mean	0.768	0.61
			SD	2.2781e^{-16}	1.1391e^{-16}
		$t_{s,V^{ref}_{DC-link}}$	Mean	0.6312	0.57
			SD	0.000410391	1.13906e^{-16}
2	At variable irradiance condition (600 to 400 W/m^2)	$t_{s,V_{MPP}}$	Mean	1.9365	1.768
			SD	0.03437793	0.00615587
		$t_{s,V^{ref}_{DC-link}}$	Mean	2.066	2.049
			SD	0	0.003077935
3	At variable irradiance condition (400 to 600 W/m^2)	$t_{s,V_{MPP}}$	Mean	3.265	3.237
			SD	4.55626e^{-16}	0.03785012
		$t_{s,V^{ref}_{DC-link}}$	Mean	3.5319	3.39
			SD	0.004278465	4.55626e^{-16}

Abbreviations: SD - standard deviation; $t_{s,V_{MPP}}$- Settling time to meet V_{MPP}; $t_{s,V^{ref}_{DC-link}}$ - Settling time to meet $V^{ref}_{DC-link}$

Further, to analyse the performance of proposed modified P&O and conventional P&O algorithm, a statical analysis has been presented in Table 4.1. The statical analysis is presented in terms of mean and standard deviation (SD) of the settling time to meet V_{MPP} and $V^{ref}_{DC-link}$ of the system. In this respect, 30 trial runs are carried out to analyse the performance of both the algorithms at constant and variable irradiance conditions. The trial runs are performed at constant irradiance condition i.e. 600 W/m^2 for t=6s. Whereas, in variable irradiance condition at t=1.5s, it changes from 600 W/m^2 to 400 W/m^2 and back from 400 W/m^2 to 600 W/m^2 at t=3s. Table 4.1 is evident of the trial's outcome in the form of mean and SD of the settling time. The mean result of the proposed algorithm is better than the conventional algorithm. Simultaneously, the SD result's of the proposed algorithm appear almost zero for constant as well as variable irradiance condition. The above mentioned results indicate the high robustness and search capability of the proposed modified P&O algorithm.

4.5 Conclusion

A two-stage, three-phase, grid interfaced PV system works in derated power generation mode to curtail the extra feed-in power during the peak hours is presented. In addition, it avoids the drift phenomena which exists in traditional P&O algorithm. Furthermore, the proposed algorithm works in a modified MPPT mode during the non-peak hour. In this mode, the MPPT holds the information of current to distinguish irradiance change. Thus, it can estimate the direction of search towards MPP during irradiance change. Thereby, the operating point does not diverge from the shortest path of MPPT. Moreover, to enhance the tracking capability of the modified MPPT, it is examined on different step size (ΔD). In this chapter, a large step size has been chosen which increases the time response and reduces the oscillation using the proposed algorithm. The system is implemented for 30 kW, two-stage, three-phase, GIPV system and simulated in MATLAB/Simulink environment using Simpower tools. The system's performances present that the proposed algorithm actively participates in power curtailment during the peak hours of power generation. Additionally, the performances show that the modified algorithm gives a faster response than the traditional P&O algorithm under variable irradiance condition.

Chapter 5

REACTIVE POWER COMPENSATION USING MP&O MPPT TECHNIQUE IN GRID INTERFACED PV SYSTEM

5.1 Introduction

A photovoltaic (PV) based power generation system produces electricity to the utility grid for the public utilization. Nowadays, the exhaustion of fossil fuels and the production of PV power at lower price encourages customers to use it in day to day life. However, the variations in PV power generation is acknowledged as less reliable power source due to intermittent nature of sunlight. Additionally, the drawbacks such as installation cost and lower power conversion efficiency of the PV systems fails to attract the electricity consumers. Therefore, the advancements in power electronics technologies improves the system efficiency and provides opportunities to utilize the PV source in various applications [11, 140].

The development in power electronics technologies improves the efficiency and reliability of the grid-interfaced PV (GIPV) system. Additionally, the advancement in technologies allow systems to implement various control schemes for converters. Furthermore, these converters perform functions such as voltage regulation, active, reactive power generation and extraction of maximum power from the PV module or array. The extraction of available peak power from the PV source is known as maximum power point tracking (MPPT). Whereas, the MPPT participate directly with inverter and boost converter in a single and two stage PV system, respectively. The single stage PV system has an advantage over two stage system due to the absence of boost converter. However, intermittency of irradiance creates more variation in DC-link voltage at the input of the inverter which increases the complexity of the system. Therefore, a two stage system was introduced, in which a boost converter with MPPT control provides a stable DC input for the grid-interfaced inverter. For MPP control, various MPPT

techniques have been suggested in [44, 63, 64]. The suggested MPPT techniques pursuit the maximum power point (MPP) and at this point system provides power to the loads such as end users, energy storing devices and other PV applications. In [44, 59, 63, 64, 141], various MPPT techniques are suggested, among these, perturb & observe (P&O) and incremental conductance (IC) are the traditional approaches. However, they are very efficient at standard test condition but fails to track the MPP and oscillates around it during change in irradiances. Therefore, to handle the variations during change in irradiance, a modified P&O (MP&O) technique is found more reliable and efficient.

M. Killi and S. Samanta [67] have proposed a drift free MP&O technique which minimizes the oscillations of operating point during variable irradiance condition. In this scheme, a current based mathematical justification is presented to provide right direction to the operating point towards MPP. However, current is the deciding parameter but it is irradiance dependent and variable in nature. Therefore, the operating point oscillate near the MPP increases during fast changing irradiance condition. J. Ahmad and J. Salam [142] have proposed an adaptive P&O MPPT technique which minimizes the drifting, oscillation near MPP and selection of global peak during partial shading condition. In this scheme, authors have implemented condition check such as large and small power deviation, boundary conditions, recording of perturbation direction and minimization of perturbation size. However, more condition check increases the complexity hence results in reduced tracking efficiency. Similarly, Ali *et al.* [135] have also introduced a MP&O algorithm which minimizes the steady state oscillations and improves the efficiency. However, authors have restricted the applications of the proposed scheme. Therefore, from the above discussed literature, it is clear that the MP&O technique minimizes oscillations and improves the efficiency during variable environmental conditions. Furthermore, the obtained maximum power from the boost converter using MP&O technique is provided to the grid interfaced inverter.

A grid interfaced inverter performs various functions which are highlighted previously in this section. Simultaneously, it maintains the voltage at junction point of inverter and grid. The junction point or point of common coupling (PCC) parameters such as voltage, frequency and phase angle gets synchronized using inverter control scheme. In this respect, several schemes have been have been discussed in the literature review for a three-phase GIPV inverters. On the other hand, the GIPV system is used to compensate the reactive power using MP&O algorithm

in derated mode to reduce the grid burden.

5.1.1 Motivation

In the modern power scenario, a GIPV system participate to support the grid by transferring real power. Additionally, the voltage source inverter (VSI) used in GIPV system is capable of generating the reactive power. This ability of VSI is an added benefit which reduces the grid burden and provide stability during the sudden change in generation as well as local loads. Therefore, various control schemes are suggested in [80, 85–87] for the exchange of active and reactive power through a GIPV system. However, as per author's knowledge, very few have achieved the independent compensation. The independent compensation means that the reactive power demand from the local loads are only fulfilled by the inverter. Thus, the burden i.e. the reactive power compensation through the grid can be reduced to zero. This can be achieved by derating of PV power generation so that, the inverter transfers real power less than its capacity. Therefore, the inverter gets margin to generate required reactive power. To derate power generation, various traditional and modified MPPT techniques are suggested in [67, 135, 142] which harvest the maximum power as well. However, amongst the suggested techniques, the MP&O is suitable in the context of simplicity, implementation and efficiency.

5.1.2 Contribution

The significant contributions of this scheme are summarized as follows.

1 A grid independent reactive power compensation approach has been introduced without increasing the solar PV inverter size.

2 A MP&O, MPPT technique is operated in derated mode for independent reactive power compensation through a GIPV system.

3 The MP&O technique used to curtails the active power when reactive power compensation is required and harvest maximum power otherwise.

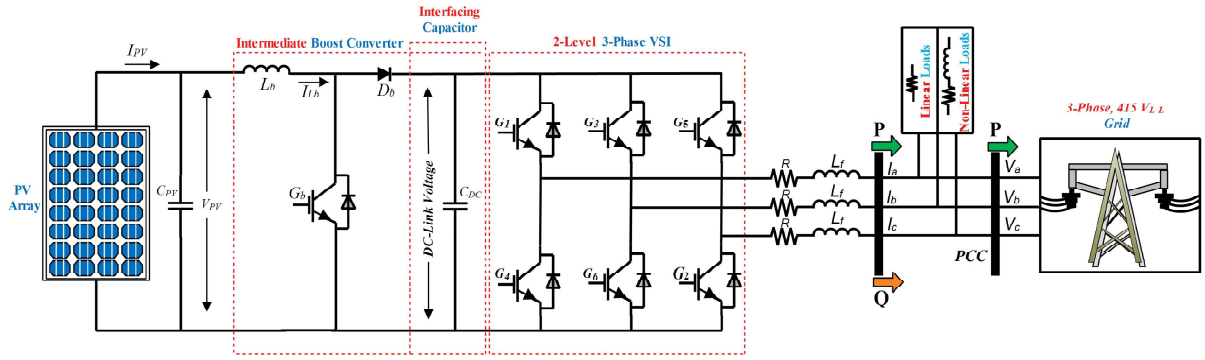

Figure 5.1: A proposed two-stage three-phase GIPV systems structure

5.2 System Framework

Fig. 5.1 represents a two-stage, three-phase GIPV system for active and reactive power control. In this system, first stage includes the PV source, intermediate boost converter (IBC) and MP&O, MPPT control. The MP&O, MPPT algorithm extracts the maximum available peak power from the source. Additionally, it works in derated mode of operation when system moves beyond the allowable generation limit. The allowed generation limit (P_{limit}) depends upon the reactive power demand from the local loads. Since the reactive power is the phenomena of inverter, it deals with the inverter control that is carried out in the second stage. In this stage, an IGBT based VSI is connected with the grid as well as local linear and non-linear loads at PCC. The grid interfaced VSI control is carried out in decoupled synchronously rotating reference frame using instantaneously active and reactive power control scheme. The active power generation depends upon the source of the system. Moreover, the reactive power generation from the inverter is decided on the basis of demand from the local load. Accordingly, the MP&O adjust the active power curtailment and derates the generation level. Therefore, the inverter can generate the required reactive power without any support of the grid.

5.3 System and Proposed Control

As mentioned in Section II, the PV source, IBC and VSI are the main operational devices of the proposed system. In this Section, the device's working strategy and proposed control strategies such as MPPT and inverter control have been discussed and are presented as follows.

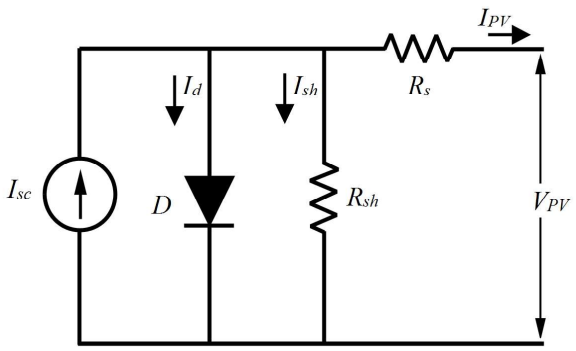

Figure 5.2: Single diode model of a PV cell

5.3.1 PV source

PV power, voltage and current varies with respect to change in irradiance. The impact of change in irradiance is presented from a single diode model of a PV cell as shown in Fig. 5.2. In this figure, the short circuit current I_{sc} of PV cell is irradiance dependent quantity which is presented as follows [143].

$$I_{sc} = \{I_{sc,n} + K_i(T - T_n)\}\frac{G}{G_n} \tag{5.1}$$

where K_i is the temperature coefficient of the current as per data-sheet of PV module and $I_{sc,n}$ is the short circuit current at standard test condition (STC). T_n and G_n are temperature and irradiance, respectively at STC while T and G are their operating values. The resultant PV current I_{PV} obtained from each PV cell is illustrated as follows [120].

$$I_{PV} = I_{sc} - I_o\left[\exp\left(\frac{qV_{eqt}}{\alpha KT}\right) - 1\right] - \frac{V_{eqt}}{R_{sh}} \tag{5.2}$$

$$V_{eqt} = V_{PV} + I_{PV}R_s \tag{5.3}$$

where V_{eqt} is equivalent voltage across diode while I_o, V_{PV}, R_s and R_{sh} are the reverse saturation current, PV voltage, series and parallel resistance, respectively. Whereas, the constant quantities such as q, K and α are the electron charge, number of PV cells, Boltzmann constant and ideality factor, respectively. The series and parallel arrangement of PV cell produces a module,

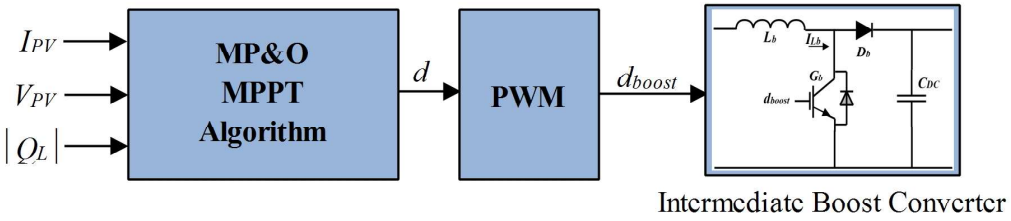

Figure 5.3: Intermediate boost converter control using MP&O algorithm

similarly, it forms an array of desired voltage and current, as an input source of the IBC.

5.3.2 IBC with proposed MPPT control

An IBC interfaces with the PV source and VSI. Since IBC is of boost nature, it enhances the PV voltage level by keeping power constant. The output voltage $V_{DC-link}$ of the IBC is illustrated as follows.

$$V_{DC-link} = \frac{1}{1-d_{boost}} V_{PV} \tag{5.4}$$

where d_{boost} is the duty ratio for the IBC. In this scheme, the output voltage $V_{DC-link}$ or V_{MPPT} of the converter is achieved by varying the duty ratio which is controlled by the proposed MPPT technique as shown in Fig. 5.3. Simultaneously, the MPPT controller achieves the active power curtailment. Here, a modified perturb & observe (MP&O), MPPT control technique has been introduced. The introduced technique works on three steps direct duty ratio based method [144] to reach at peak power point as shown in Fig. 5.4. In this method, the direction of operating point depends upon the nature of dP/dV which is illustrated as follows.

$$\frac{dP}{dV} \; is \begin{cases} > 0; & V \uparrow; \; then \; d \uparrow \\ < 0; & V \uparrow; \; then \; d \downarrow \\ = 0; & V = V_{MPPT}, \; d = d_{boost} \end{cases} \tag{5.5}$$

where dP/dV indicates the slope of power with respect to voltage, $V \uparrow$ indicates the increasing PV voltage. Similarly, $d \uparrow$ and $d \downarrow$ indicates the increasing and decreasing duty ratios of

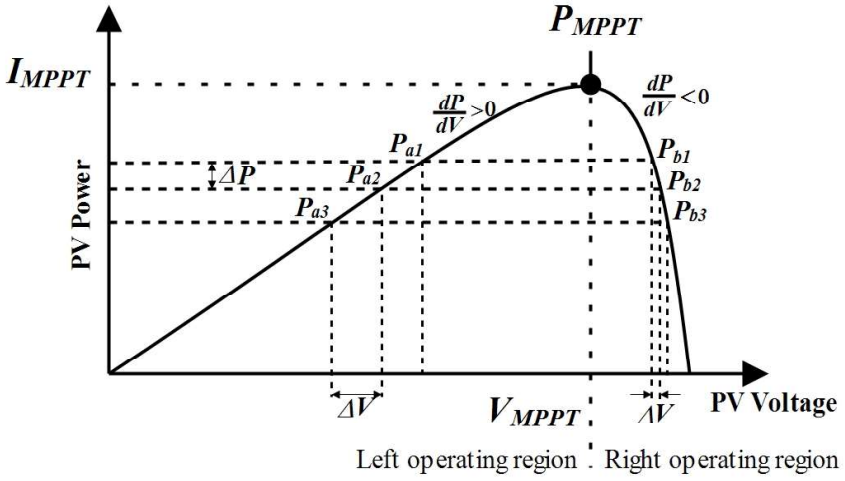

Figure 5.4: Characteristic behaviour of power-voltage curve

the IBC, respectively. Additionally, MPPT curtails the active power generation when the peak power generation is available and simultaneously, a local load demands reactive power compensation. In this case, the inverter transfers less power then its rated capacity and created margin is used to generate the reactive power. The derated power generation (*i.e.* P_{limit}) value depends upon the demanded reactive power from the local loads. Further, as per P_{limit}, the IBC extracts power from the PV source by adjusting the duty ratio which is presented mathematically as follows.

$$|Q_{load}| \; is \begin{cases} = 0; & P_{limit} = P_{PV}; d = d_{boost} \\ \neq 0; & P_{limit} = P_{PV} - |Q_{load}|; d \downarrow \end{cases} \tag{5.6}$$

where $|Q_{load}|$ is the reactive power demand from the local non-linear loads. Along with this, the working of the proposed algorithm has been presented in Fig. 5.5. Further, due to the coordinated control of MP&O algorithm, the inverter can transfer the active power lesser than its capacity. In consequences, it could fulfil the reactive power demand required from the local non-linear loads which is explained in the next subsection.

5.3.3 Grid interfaced inverter with active and reactive power control

A voltage source inverter (VSI) acts as a DC to AC converter when it transfer power to the grid. The active power (P_{PV}) transfer capability of the VSI is variable in nature. Whereas, the

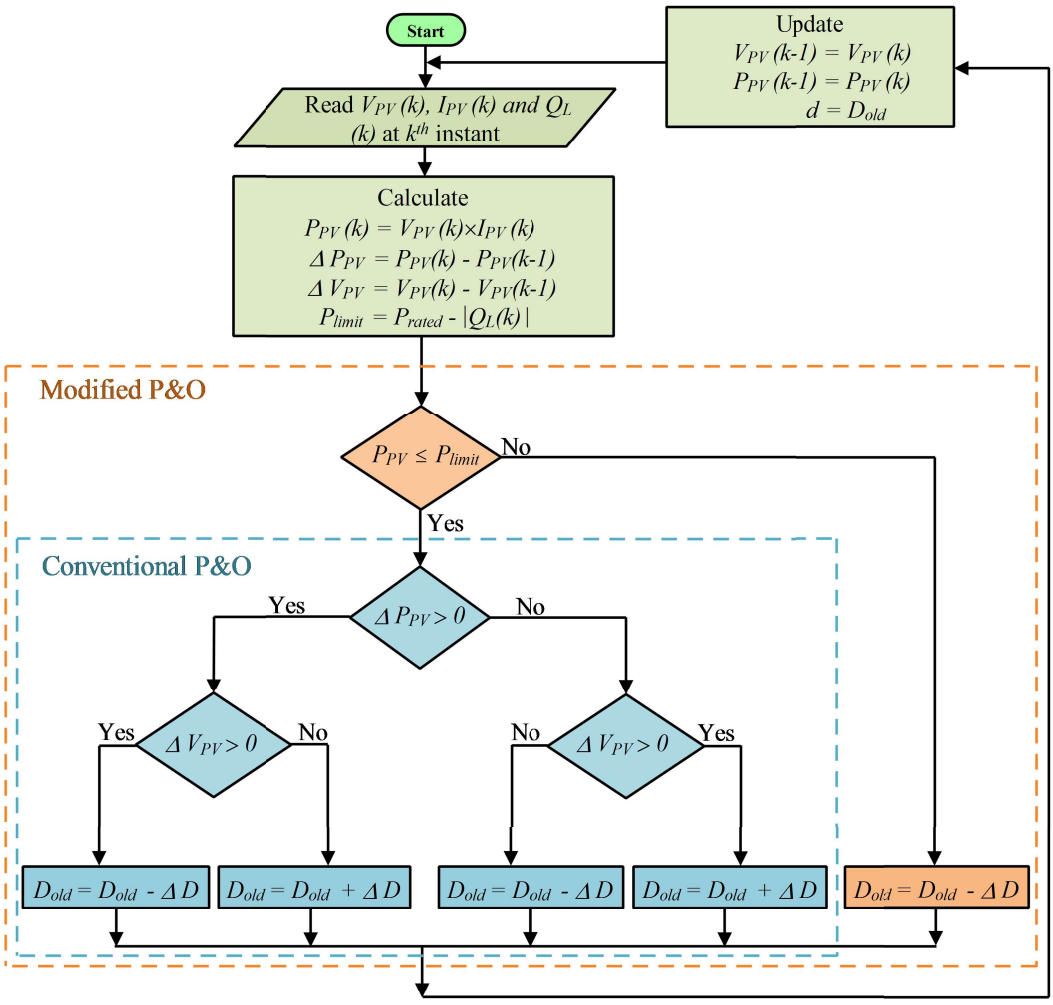

Figure 5.5: Flowchart of modified perturb and observe (MP&O) algorithm

instantaneous reactive power (Q_{inv}) capability of the VSI is limited within its fixed apparent power (S_{inv}) capability which is presented as follows [145].

$$S_{inv} = \sqrt{P_{PV}^2 + Q_{inv}^2} \tag{5.7}$$

$$S_{inv,max} = \sqrt{P_{MPP}^2 + Q_{max}^2} \tag{5.8}$$

$$Q_{max} = \sqrt{S_{inv,max}^2 - P_{MPP}^2} \tag{5.9}$$

where $S_{inv,max}$ and Q_{max} are the maximum apparent power capability and reactive power capability of the PV inverter, respectively. Whenever, the inverter reduces its real power transfer capability, it's reactive power consumption or delivery limit increases as shown in Fig. 5.6 and illustrated as follows.

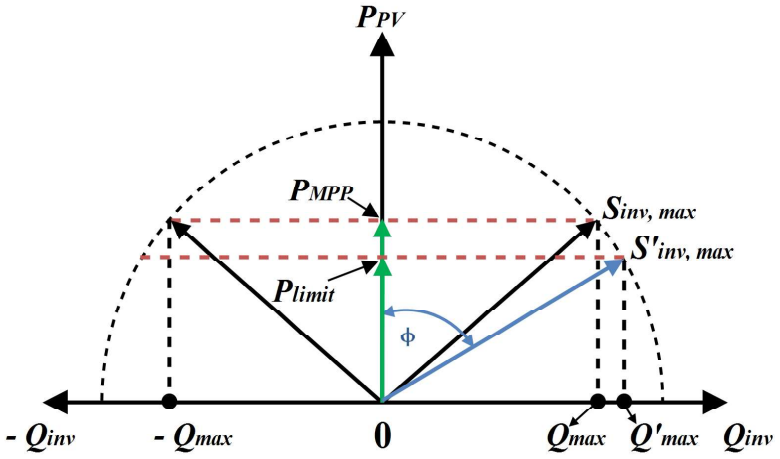

Figure 5.6: Phasor diagram representation of the inverter capability

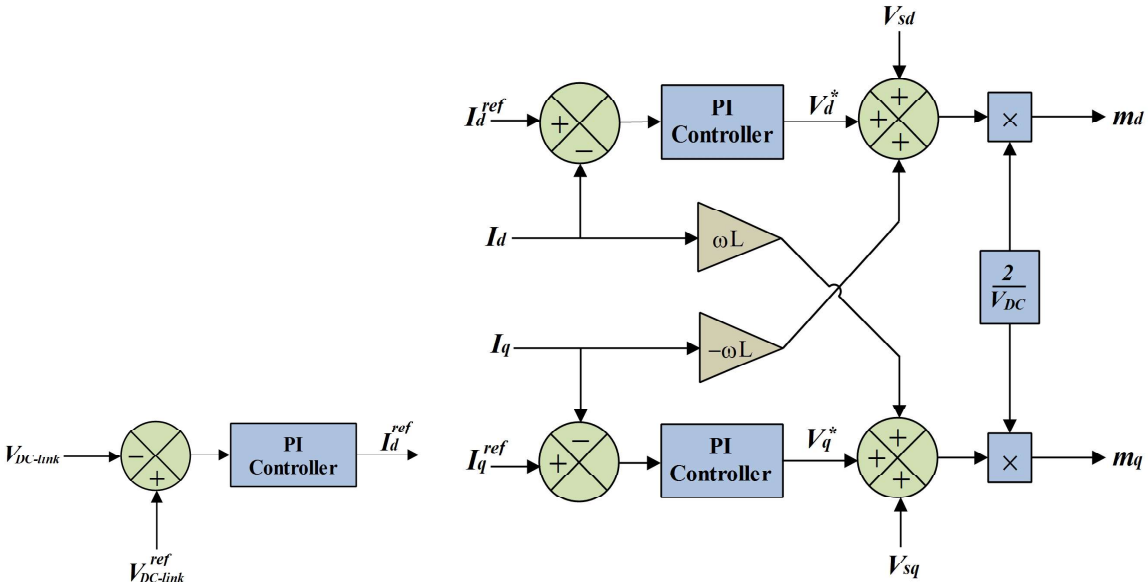

Figure 5.7: Inverter control for active and reactive power (a) outer loop control (b) inner loop control

$$Q'_{max} = \sqrt{(S'_{inv,max})^2 - P^2_{limit}} \tag{5.10}$$

where Q'_{max} and $S'_{inv,max}$ are the allowed reactive power and apparent power when the real power transfer capability of the inverter is decreased by reducing the active power generation using MP&O algorithm. In this case, the power transfer (P_{out}) from the system is presented as

follows.

$$P_{out} \leq P_{limit} = min\{P_{limit}, P_{PV}\} \tag{5.11}$$

Further, to achieve the various active power conditions and variable reactive control in synchronously rotating (dq) reference frame is calculated as follows [146].

$$P_{out} = \frac{3}{2}(V_d I_d + V_q I_d) \tag{5.12}$$

$$Q_{load} = \frac{3}{2}(V_q I_d - V_d I_q) \tag{5.13}$$

where V_d, I_d and V_q, I_q are voltage and current components of direct (d) and quadrature (q) axis in dq-reference frame respectively. Simultaneously, the phase lock loop (PLL) is assigned to synchronize the inverter and grid voltages which makes $V_q = 0$ in dq-reference frame. Therefore, assuming $V_q = 0$, the desired active and demanded reactive power is calculated as follows.

$$P_{out} = \frac{3}{2} V_d I_d \tag{5.14}$$

$$Q_{load} = -\frac{3}{2} V_d I_q \tag{5.15}$$

In the proposed GIPV system, the active power control is executed by the DC-link voltage ($V_{DC-link}$) regulation in outer control loop. In outer control loop, the measured and pre defined reference $V_{DC-link}$ ($V^{ref}_{DC-link}$) is compared. Thereafter, the compared signal passes through the proportional integral (PI) controller which results in a $d-$ axis reference current (I^{ref}_d) as shown in Fig. 5.7(a). Similarly, the $q-$ axis reference current (I^{ref}_q) is obtained by (5.15). Further, pulse width modulation (PWM) signals are produced using I^{ref}_d and I^{ref}_q as shown in Fig. 5.7(b). Moreover, I^{ref}_d and I^{ref}_q are decision-makers for the control of active and reactive power, respectively. Although, the nature of the reactive power (either positive and negative) is depends upon the type of connected load i.e. inductive or capacitive type. If the nature of load is inductive, the reactive power is positive and lagging in nature. On the other hand, if nature of load is capacitive, the reactive power is negative and leading in nature. Hereafter, the performance of the VSI for active and reactive power control during variable irradiance conditions are evaluated using simulation and real-time analysis.

5.4 Results and Discussions

To evaluate the performance of the proposed control strategy, a 30 kW two-stage, three-phase GIPV system has been considered. In this system, a PV array of 30 kW is considered as input source which is structured by the series and parallel arrangement of PV modules. A Kyocera Corporation made "KC200GT" PV module's parameters are considered and respective specification of the PV array followed by the PV module are summarized in Table 3.1. Further, at first stage, the PV source generates voltage (V_{PV}) of 394.5 V at MPP using IBC and MPPT under normal as well as fluctuating irradiance condition (G). The IBC with the help of MPPT produces desired DC output voltage ($V_{DC-link}$) i.e. 700 V as an input of the grid interfaced inverter. Furthermore, the grid interfaced inverter converts DC to AC power and transfer it to the grid. In between, the system consider the local linear and non-linear loads to test the reactive power generation capability of the inverter and performance of proposed MPPT technique. The entire system is analysed under various irradiance condition in MATLAB and the performances are validated in real-time environment using Opal-RT 4510.

5.4.1 System performance in simulation mode

In MATLAB/Simulink environment, the system is simulated using simpower blocksets to test the performance of traditional as well as proposed MP&O, MPPT techniques under various irradiance condition. Additionally, it evaluates the effectiveness of proposed over the traditional technique in terms of reactive power compensation under various irradiance conditions. Therefore, three irradiance conditions have been considered i.e. G_1=600 W/m^2; G_2=800 W/m^2 and G_3=1000 W/m^2 and system is simulated for t=10s. The first irradiance condition G_1 at t=0s, system starts generating PV power and it increases when irradiance changes from G_1 to G_2 at t=2s and G_2 to G_3 at t=4s. Simultaneously, the PV power decreases when irradiance condition changes from G_3 to G_2 at t=6s and G_2 to G_1 at t=8s. At these time instants, the system generates P_{PV}=17.72, 23.8 and 30.02 kW at G_1, G_2 and G_3, respectively. Further, the obtained source voltage and current under fluctuating irradiance conditions are utilized by IBC and VSI using traditional as well as the proposed control approach. Simultaneously, a local load of 5 kW resistive and 5 kVA inductive has been considered for t=2s to t=7s to test the system performance of traditional and proposed control scheme.

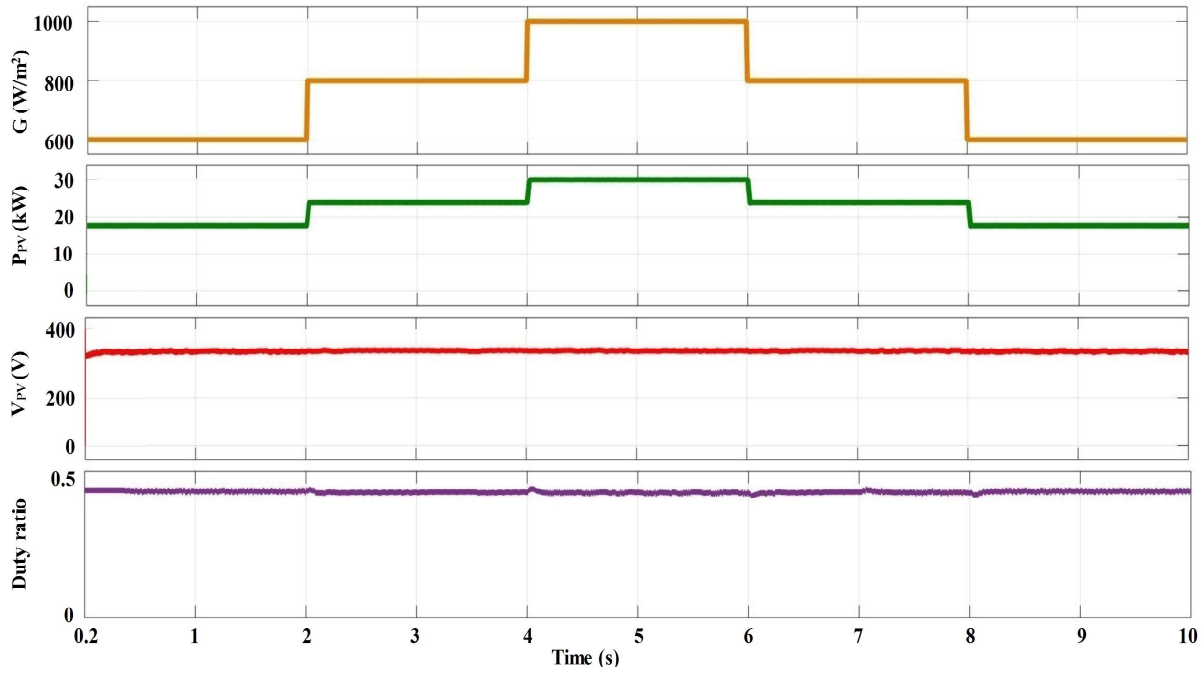

Figure 5.8: The performance of P_{PV}, V_{PV} and duty ratio *w.r.t*. G for conventional approach

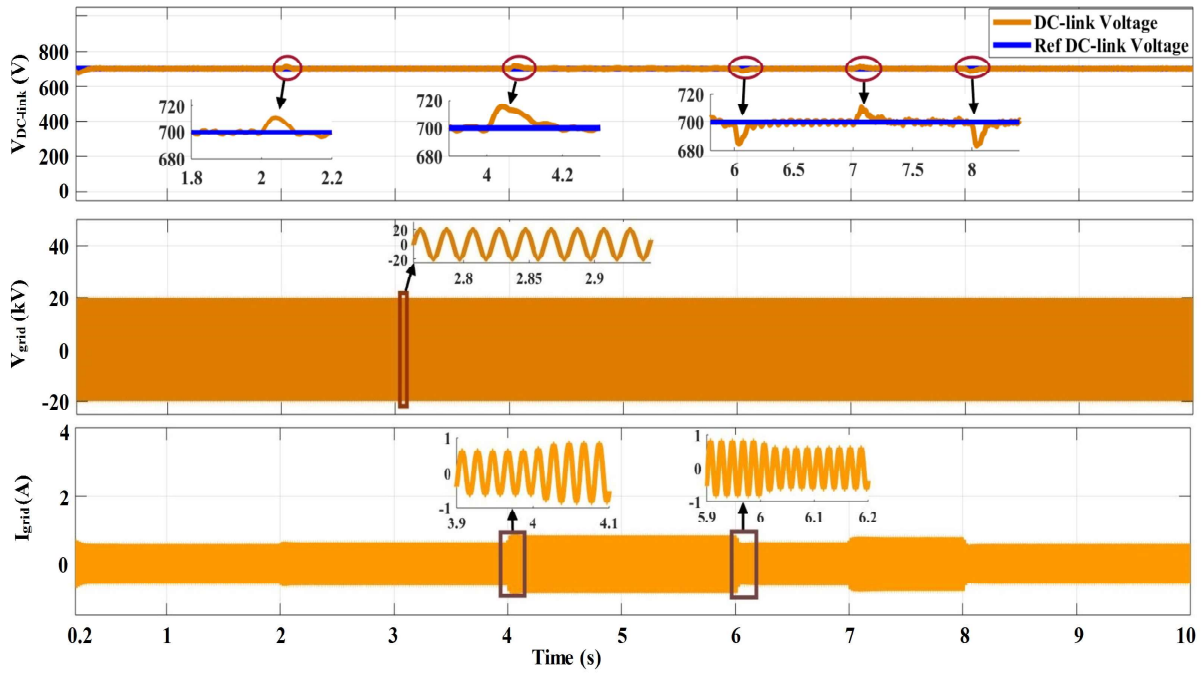

Figure 5.9: Dynamic behaviour of the conventional approach in terms of $V_{DC-link}^{ref}$, $V_{DC-link}$, V_{grid} and I_{grid}

Traditional control approach

In traditional control approach, the obtained voltage and current is utilized through IBC using P&O, MPPT algorithm to achieve the maximum power from the source. The voltage and cor-

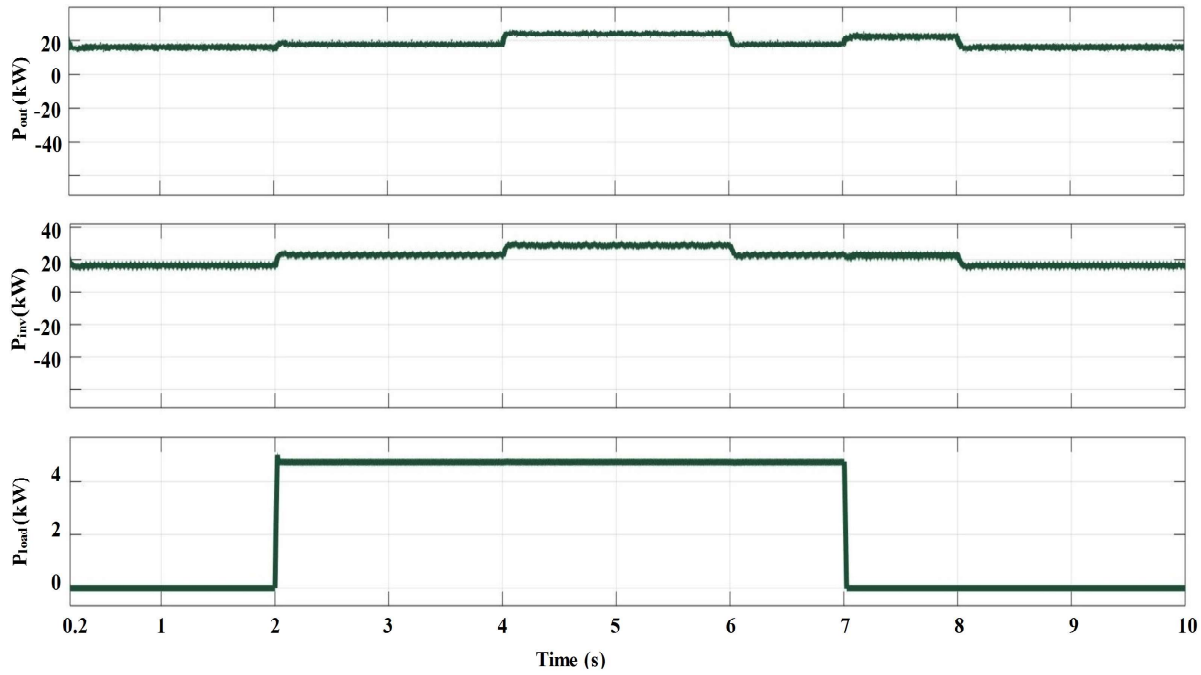

Figure 5.10: Dynamic behaviour of the conventional approach in terms of P_{out}, P_{inv} and P_{load}

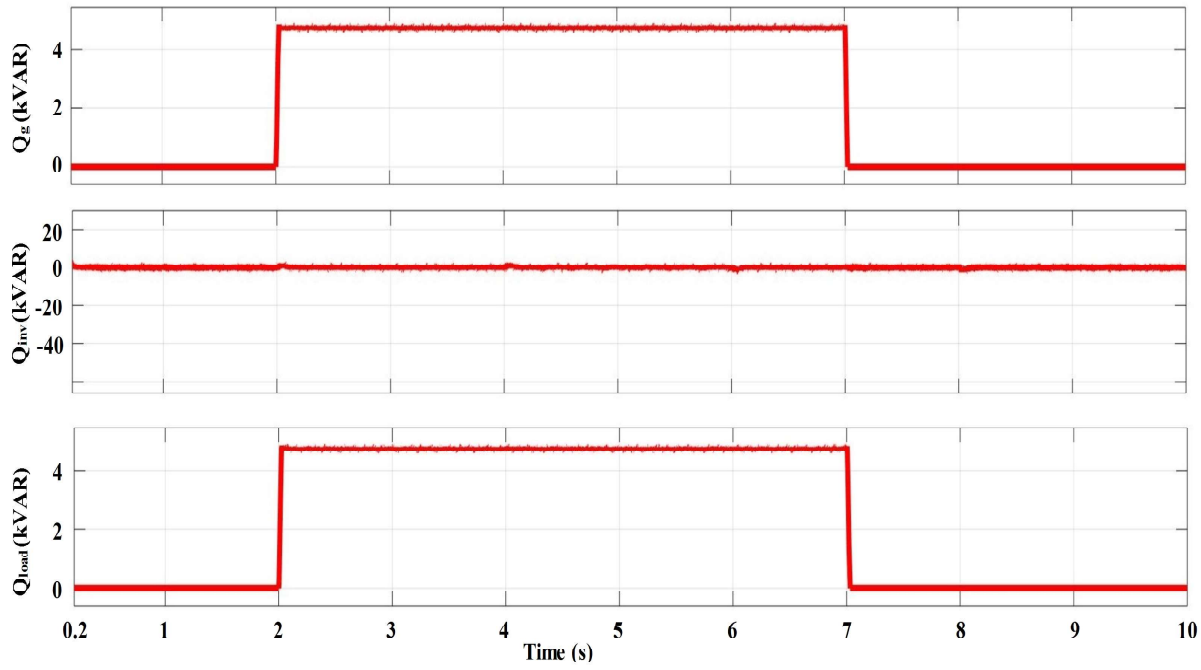

Figure 5.11: Dynamic behaviour of the conventional approach in terms of Q_{load}, Q_{inv} and Q_g

responding duty ratio of the IBC is approximately constant due to minimum effect of irradiance on the PV array voltage (P_{PV}). The performance of PV array in terms of PV power, PV voltage and duty ratio of the IBC w.r.t. changing irradiance conditions are shown in Fig. 5.8. The output voltage and current of the IBC is utilized as an input for the VSI. Further, VSI using

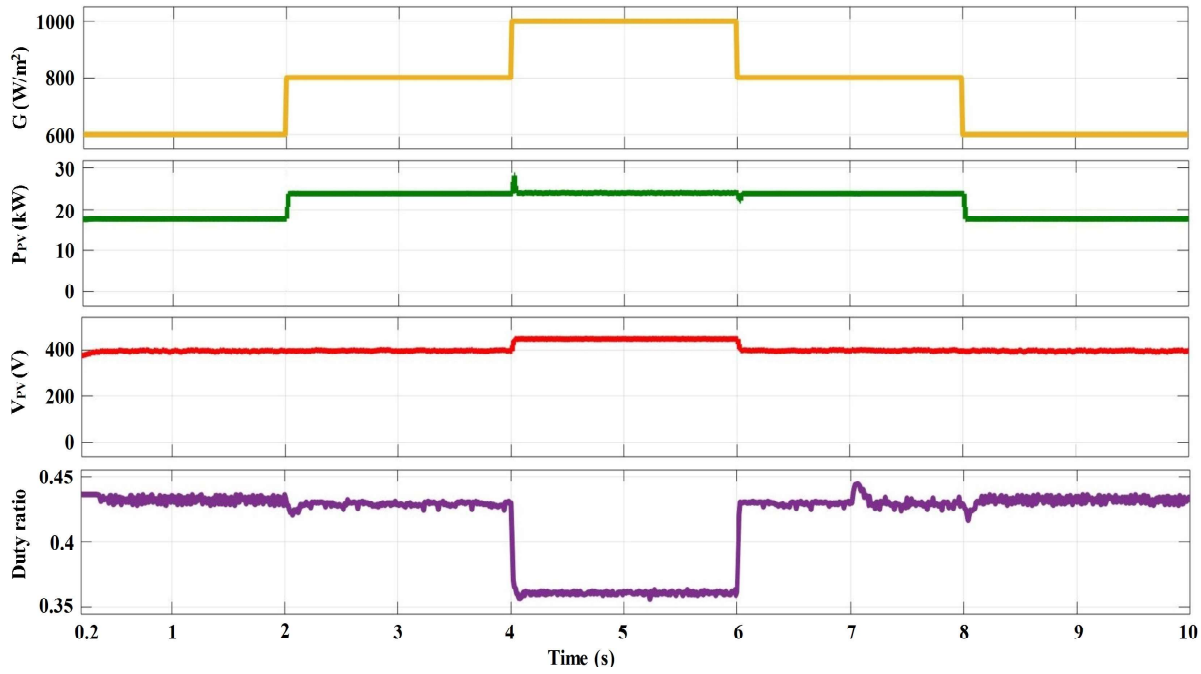

Figure 5.12: The performance of P_{PV}, V_{PV} and duty ratio *w.r.t*. G for proposed MPPT control

input voltage ($V_{DC-link}$) converts DC to AC power using inverter control. During inverter control, the outer loop regulates and maintains the DC-link voltage. Simultaneously, the inner loop generates the injected current and voltages to the grid using current control. The performance of the inverter control is presented in terms of DC-link voltages, grid voltages and injected grid current which is shown in Fig. 5.9. Moreover, the inverter control is used to generate the active and reactive power. The obtained active power is consumed by the connected local linear (5 kW resistive) load and the remaining active power is transferred to the grid. The load is connected during t=2s to t=7s and at this time the inverter is generating P_{inv}=23.8 kW at G_2 irradiance condition, thus the transferred power to the grid is P_{out}=18.8 kW. Similarly, P_{out} for the grid at other irradiance conditions such as for G_1 and G_2 are shown in Fig. 5.10. On the other hand, the non-linear local load consists of 5 kVA inductive load, which demands reactive power compensation. The compensation of the reactive power demanded from the non-linear load is fulfilled by the grid or inverter. As discussed in Section III, when inverter is transferring power with full capacity, the reactive power generation from the inverter will be zero which can be seen from Fig. 5.11. Therefore, to reduce the burden of the grid, the reactive power is supplied from the inverter only. In consequence, a proposed control approach has been used in the system.

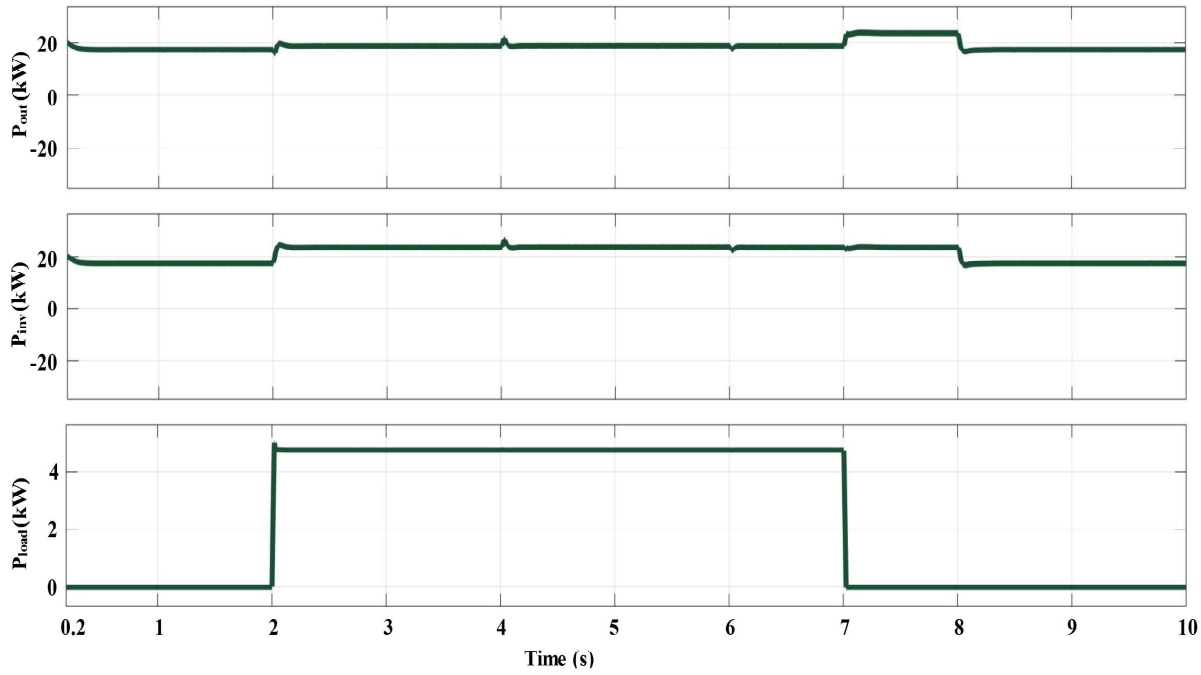

Figure 5.13: Dynamic behaviour of the proposed control scheme in terms of P_{out}, P_{inv} and P_{load}

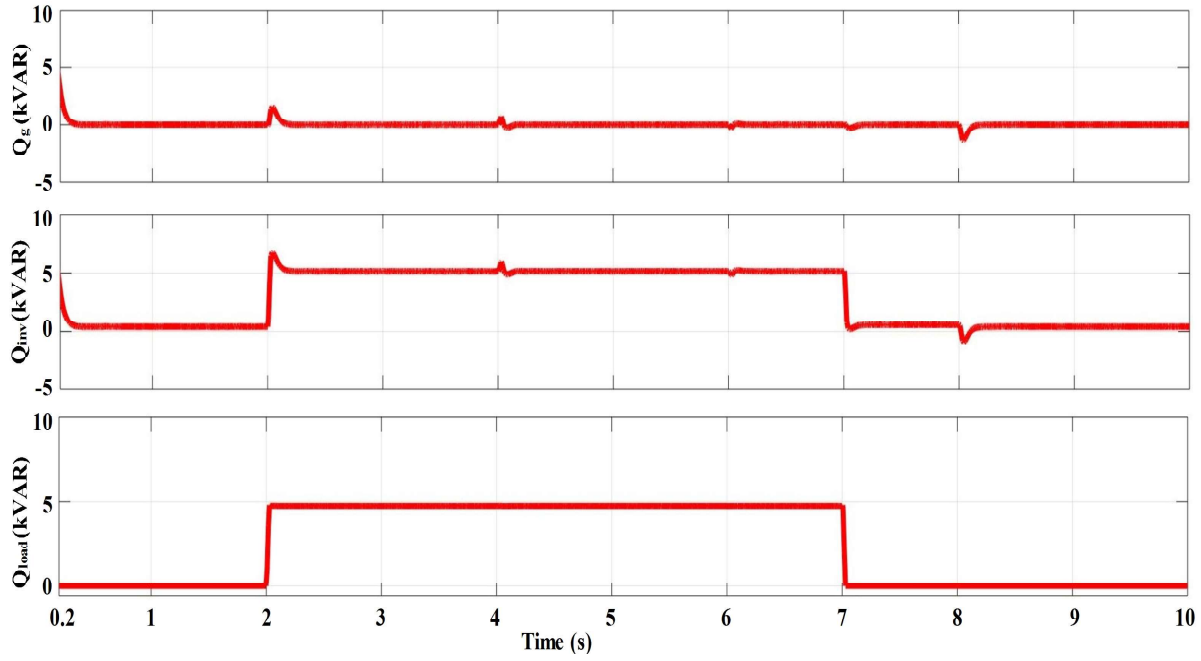

Figure 5.14: Dynamic behaviour of the proposed control scheme in terms of Q_{load}, Q_{inv} and Q_g

Proposed control approach

In proposed control, Its behaviour is similar to the conventional approach until the derated mode is not activated. The derated mode gets activated when the reactive power demand is available.

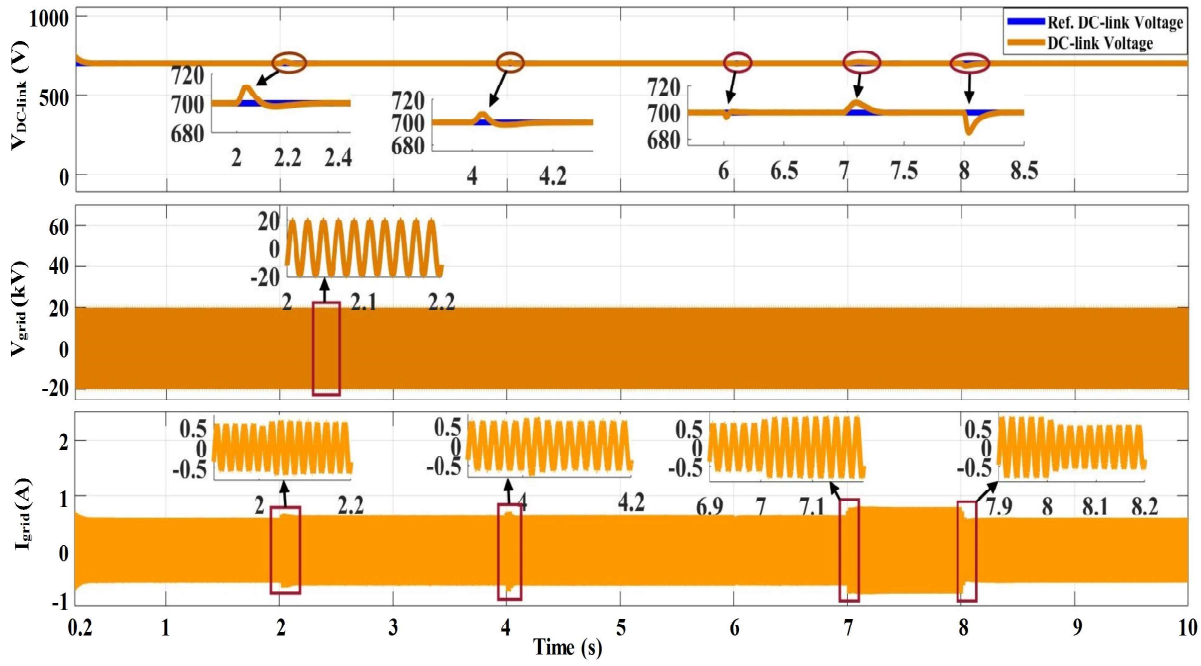

Figure 5.15: Dynamic behaviour of the proposed control scheme in terms of $V_{DC-link}^{ref}$, $V_{DC-link}$, V_{grid} and I_{grid}

Simultaneously, the inverter is transferring active power at the rated capacity and does not have enough margin to generate the reactive power as presented in (5.8). In this case, the maximum apparent power ($S_{inv,max}$) is equal to the active power so, the margin to generate the reactive power is zero. Therefore, to create the margin for inverter the active power is derated as discussed in (5.10) where P_{limit} depends upon the load demand as discussed in (5.6). The active power is derated using proposed MP&O algorithm at considered irradiance conditions (G_1, G_2 and G_3). The generated active power at G_1 (or at t=0s & 8s) and G_2 (or at t=2s & 6s) are 17.72 and 23.80, respectively which are within the limit and inverter have enough margin to generate the reactive power. Whenever, the system reaches to irradiance condition G_3 (or at t=4s), the system generates active power *i.e.* 25 kW instead of 30.02 kW due to MP&O algorithm as we can see in Fig. 5.12. Simultaneously, the active power and reactive power exchanges of the system with the grid is shown in Fig. 5.13 and Fig. 5.14, respectively. Fig. 5.14 depicts that there is no reactive power exchange from the grid at any time instant which justifies the need of proposed control scheme. Moreover, the performance of the DC-link capacitor in terms of voltage ($V_{DC-link}$), system grid voltage (V_{grid}) and injected grid current (I_{grid}) with respect to change in irradiance conditions and connected load is presented in Fig. 5.15. Further, the performance of the proposed control scheme is verified in real-time environment with real-time

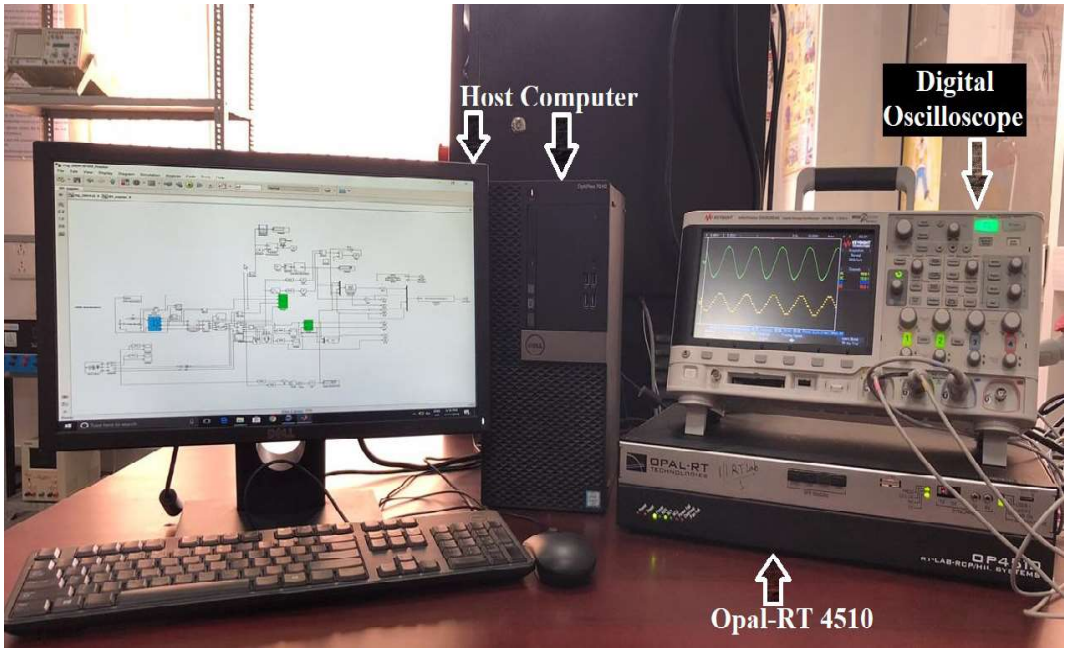

Figure 5.16: Setup for SIL operation in the real-time environment

simulator (RTS).

5.4.2 System performance in real-time environment

The RTS of the GIPV system with proposed control scheme provides parallel computing hardware capability for complex model over various processors. It improvises the computation and realizes high accuracy with low cost real-time execution. In addition, it improves the system reliability in abnormal operating conditions in software-in-the-loop (SIL) mode. A SIL mode of operation utilizes the powerful computation of the RTS where physical system and the controller are in same RTS. The proposed system is modelled by the RTS of Opal-RT 4510. In Opal-RT, a human interfaced software called RT-Lab provides users to execute models using SimPowerSystems blockset and ARTEMiS plug-in. The proposed system is modelled in a host computer and transferred to the Opal-RT hardware through RT-lab software. Further, the RT-Lab performs SIL operation and respective results are illustrated on digital oscilloscope (DSO) as shown in Fig. 5.16. To perform the SIL operation, a host computer with Intel core i7 at 1.80-GHz is performing with 2 Intel processors (targets) at 3.3-GHz and Xilinx KINTEX 7 FPGA board. Whereas, a typical sampling time used for the SIL operation *i.e.* 50 μs and the performance of the proposed system is obtained on Keysight make DSOX2024A, a 4-channel DSO using DB37 connector. Furthermore, the robustness of the proposed system is validated

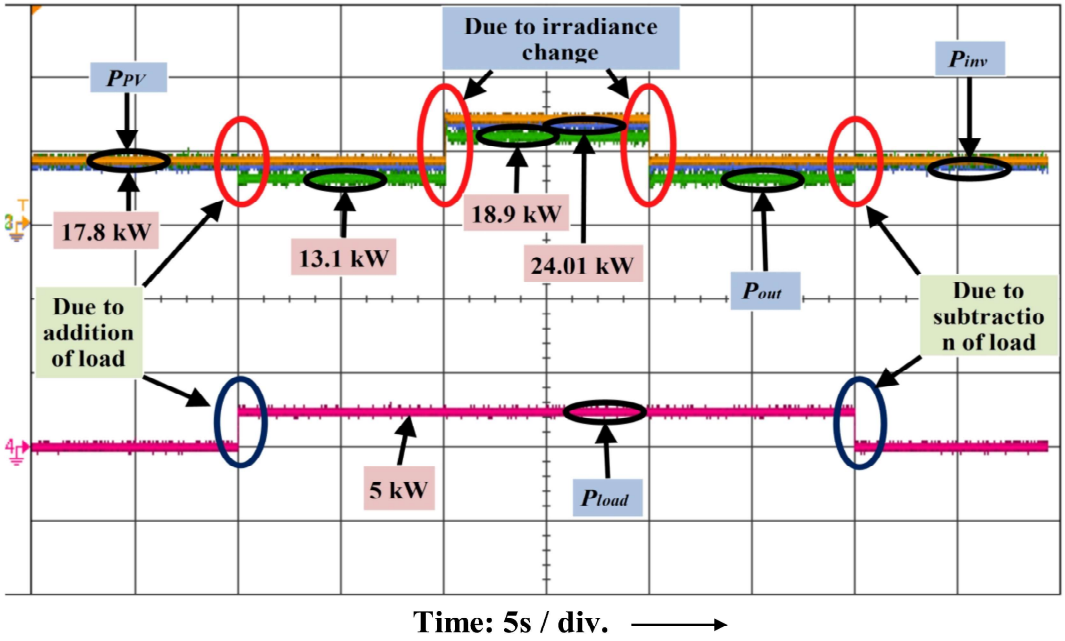

Figure 5.17: Dynamic performance of P_{PV}, P_{inv}, P_{out} and P_{load} of the proposed control scheme in real-time scenario

under two irradiance conditions G_1 and G_3. At G_1, the PV source is generating 17.8 kW, during this time, load is not connected. Therefore, the active power from PV and inverter are the same as the power transfer to the grid, as shown in Fig. 5.17. On the other hand, when load is connected, some power get absorbed hence, transferred power to the grid has reduced. Further, after 10s the irradiance condition changes from G_1 to G_3, at this time, the rated power P_{PV}= 30.02 kW should have generated. However, due to the presence non linear load, it generates only P_{PV}=25 kW using derating mode of proposed control algorithm. Thereby, the inverter gets margin and generates the reactive power to fulfil the demand of the non linear load. In Fig. 5.18, it is evident that the reactive power demand is only fulfilled from the inverter, not from the grid, which justify the need of proposed control. In this support, the performance of the DC-link voltage, grid voltage and injected current under variable irradiance condition and local load are presented in Fig. 5.19.

5.5 Conclusion

A 30 kW two-stage, three-phase GIPV system is designed to generate the PV power and compensate the reactive power demand from the local non-linear loads. Therefore, a MP&O, MPPT technique with IBC is implemented to extract power from the PV source. Additionally, the

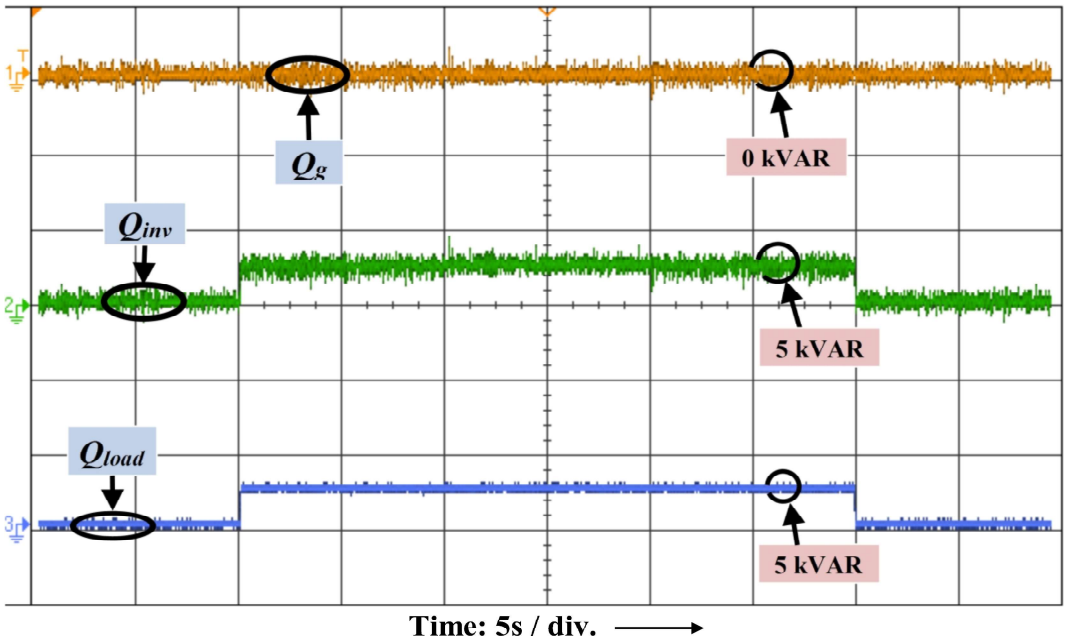

Figure 5.18: Dynamic behaviour of Q_g, Q_{inv} and Q_{load} of the proposed control in real-time scenario

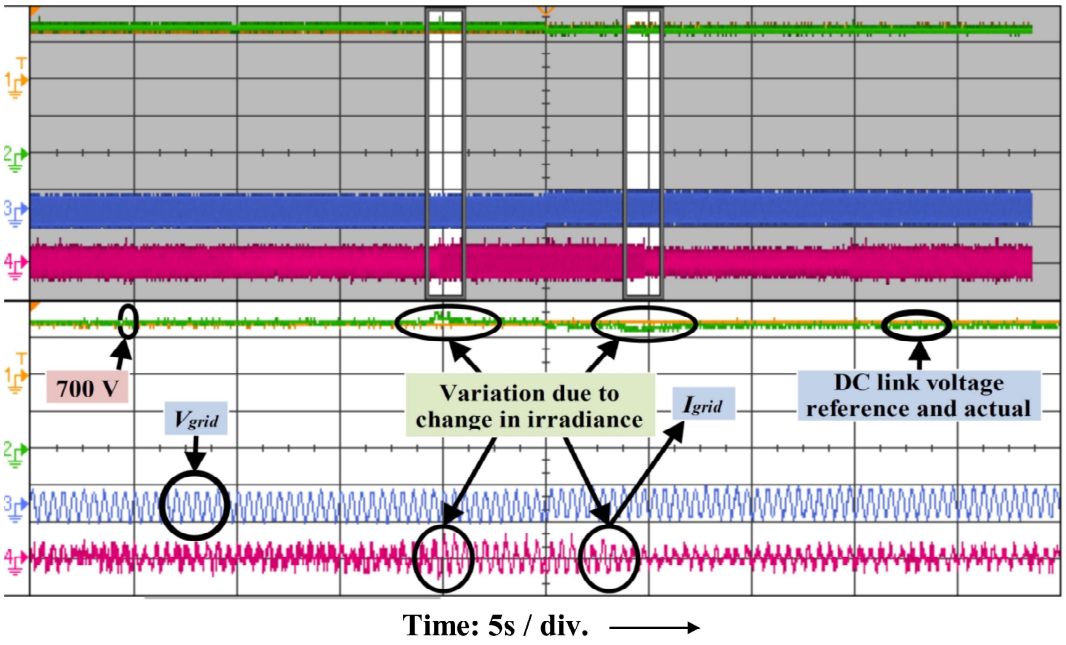

Figure 5.19: Dynamic performance of the proposed control in terms of $V_{DC-link}^{ref}, V_{DC-link}, V_{grid}$ and I_{grid} in real-time scenario under variable irradiance conditions

MP&O technique works in derated mode when reactive power demand is available and inverter transfers the active power at rated capacity. Thus, there is no margin for the inverter to generate the reactive power. Hence, the MP&O, MPPT addresses the problem and derates the PV power generation. Herewith, the inverter gets margin to generate the reactive power which reduces

the dependency of the system on the grid for the reactive power compensation. As a result, the burden of the grid reduces without increasing the size of inverter. Further, the dynamic performance clearly depicts the effectiveness of the proposed technique in terms of PV power extraction and MPP tracking under normal as well as variable irradiance condition. Whereas, it is tested and verified in SIL mode using Opal-RT 4510.

Chapter 6

PV BASED CHARGING STATION FOR ELECTRIC VEHICLES

6.1 Introduction

The need for the electric vehicle (EV) is rising exponentially if the present Indian scenario is taken into account. The statement can be validated by considering India′s atmospheric pollution level. According to the report in [147], India is one of the main fossil fuels consuming country for the transportation purposes. However, the quantity of fossil fuels is expected to reduce at a great extent in the future. Therefore, the presence of EVs in the automobile industry is the need of the present scenario. These EVs are powered through the grid i.e., grid to vehicle (G2V). As a result, the number of EVs and hence energy demand increases. Therefore, to overcome this issue, Prof. Kempton [148] had proposed the idea of vehicle to grid (V2G) which states that the energy stored in the EV battery can be transferred back to the grid. In addition, the battery storage may support the frequency regulation while the EV is transferring energy to the grid. Therefore, the V2G and G2V mode of operation presents the bi-directional behaviour of a grid-connected EV charger.

A grid-connected bi-directional (GCBD) charger requires bi-directional converters (rectifier/inverter and buck/boost). It operates in two modes i.e., G2V and V2G mode [149–151]. In G2V mode, grid side converter works as a rectifier while the battery side is used as a buck converter. On the other hand, the battery side is used as a boost converter and grid side is used as an inverter in V2G mode. However, the energy source of the GCBD charger is fossil fuel which results in pollution of the environment. Hence, the EVs are required for the pollution-free transportation. Thus, there is a need to shift from grid-based EV charging stations to the clean energy based or PV based charging station (PVBCS) [152].

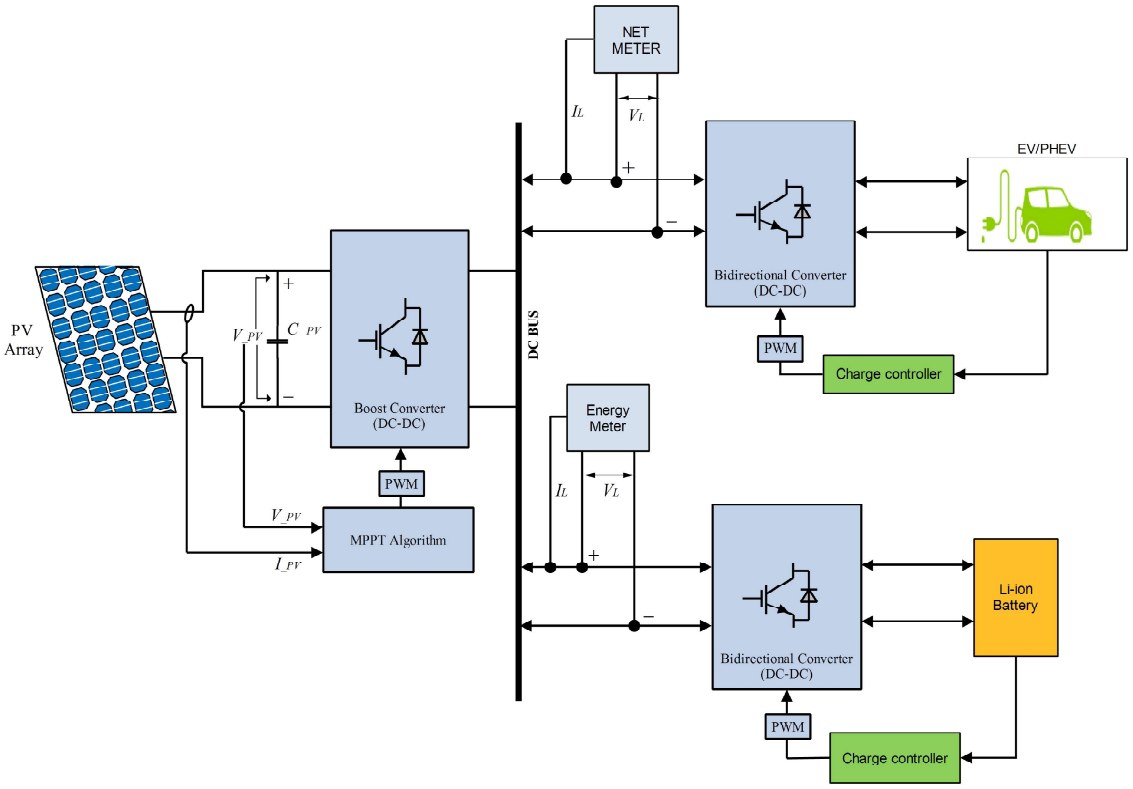

Figure 6.1: Block diagram of the proposed PV based charging station

The above-mentioned issue i.e. a self generated / off-grid charging station is a requirement of the present scenario. Although, the rapid increase of EVs imposes the burden on the grid. RESs based charging station (CS) is required especially in the highways and at the remote locations for the successful implementation of the EVs [153, 154]. Therefore, a PV based off-grid CS is proposed. To make the proposed system sustainable, an involvement of energy storage system (ESS) is a suitable approach amongst the possibilities mentioned in the preliminary research [155, 156]. The PV source coordinated with ESS are efficiently used during variable irradiance condition. Further, during surplus power condition and unavailability of EVs, ESS utilizes the maximum RES. Thus, the system results in an efficient and eco-friendly CS.

The above discussion contributes some preliminary findings which are as follows.

- To reduce the burden on the grid and use of EVs at remote locations, a renewable energy source based off-grid EV charging station is introduced.
- The reliability of the PV based charging station is improved by using ESS.
- The charging and discharging of the energy storage system is governed on the basis of PV irradiance.

6.2 Proposed System Framework

The proposed PV based charging station consists of three subcomponents, they are PV generation, EV charger and ESS. The first section is PV generation system which includes a PV array, maximum power point (MPPT) and a intermediate boost converter. The PV array converts solar energy into clean electrical energy and provides voltage V_{PV} and current I_{PV}. The V_{PV} and I_{PV} are given to the boost converter which fluctuates due to change in irradiance. Therefore, an MPPT technique is proposed to manage the fluctuations in V_{PV} and I_{PV}. The MPPT extracts maximum power P_{PV} from the PV array and provides corresponding operating voltage and current to the boost converter. The boost converter regulates the output voltage according to the desired DC-link voltage by generating the pulse width modulation (PWM) signals from the MPPT. This DC-link voltage at the DC bus is connected to the EV charger and ESS as shown in Fig. 6.1. The EV charger consists of a DC-DC bi-directional converter (BDC) and EVs. The operation of BDC depends on the charging and discharging of the EV battery. During charging mode, BDC acts as a buck converter. On other hand, it works as a boost converter during discharging mode. Similarly, the ESS also consists of a BDC and a battery bank. This battery bank is used as the energy saver during excess energy generation and is utilized at the maximum extent. The power that is stored in the ESS is fed back to the DC-link through BDC which is operated in boost mode. The mode of conversion is carried out with the help of constant current (CC) control strategy. This control strategy generates PWM signals to switch on the BDC. The mode (boost or buck) of converter changes according to the control signal generated by the control strategy. In this way, the operation of an PV based EV charging is carried out. Further, the brief modelling and control of PV array, boost converter, bi-directional converter, ESS and EV have been discussed in subsection 6.3.

6.3 System Formulation and Control

6.3.1 PV array

The main energy source of the off-grid charging station is the PV array. The PV array is made up of solar cells. The series combination of solar cells is called module. These modules are connected in many combinations to achieve a desired voltage and current as shown in Fig. 6.2.

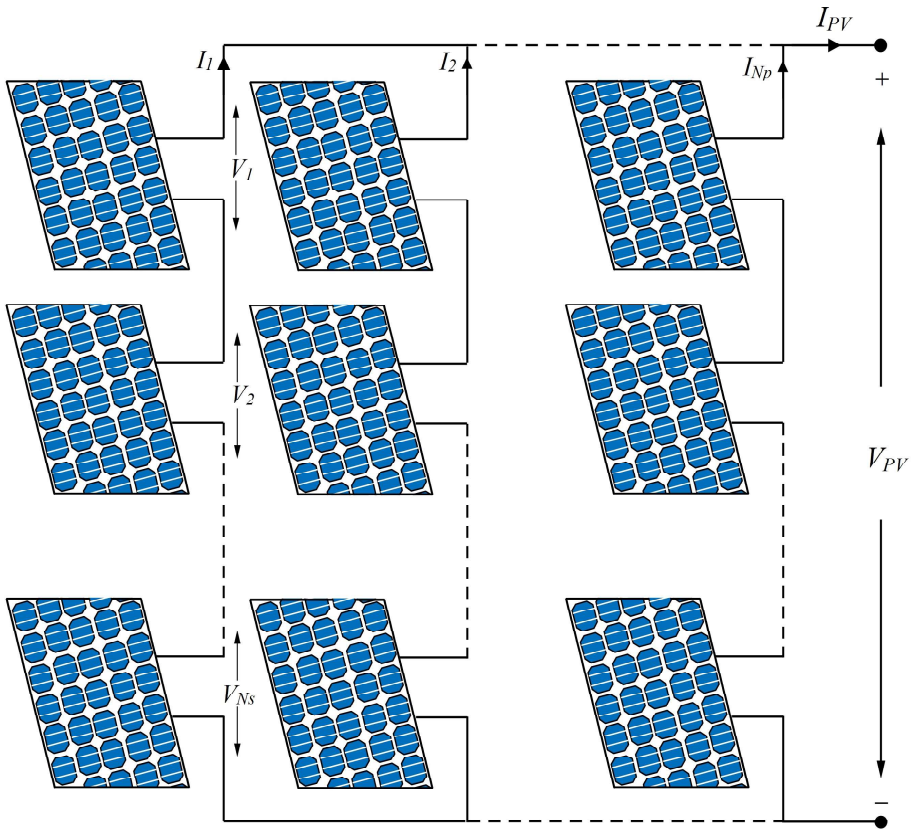

Figure 6.2: Arrangement of the modules as a PV array

In this figure, N_{ser} and N_{par} are the number of modules in series and parallel respectively. The voltage V_{PV} and current I_{PV} of the PV array are presented by [121] and illustrated as follows.

$$I_{PV} = N_{par}I - N_{par}I_d\left[\exp(\frac{q\alpha}{\beta}) - 1\right] - \frac{\alpha}{\gamma} \tag{6.1}$$

$$V_{PV} = N_{par}n_s\left(V_d - IR_s\right) \tag{6.2}$$

where

$$\alpha = V + IR_s\frac{N_{ser}}{N_{par}}; \beta = N_sKTAN_{ser}; \gamma = R_{sh}\frac{N_{ser}}{N_{par}}$$

simultaneously, $I, I_d, V_d, q, R_s, R_{sh}, n_s, K, T$ and A are the PV short circuit current, diode saturation current, diode voltage, electron charge, series resistance, shunt resistance, number of PV cells, Boltzmann constant, cell temperature and diode ideality factor of the array respectively. Further, the generated V_{PV} ad I_{PV} from the PV array is transferred to the boost converter.

6.3.2 Intermediate boost converter

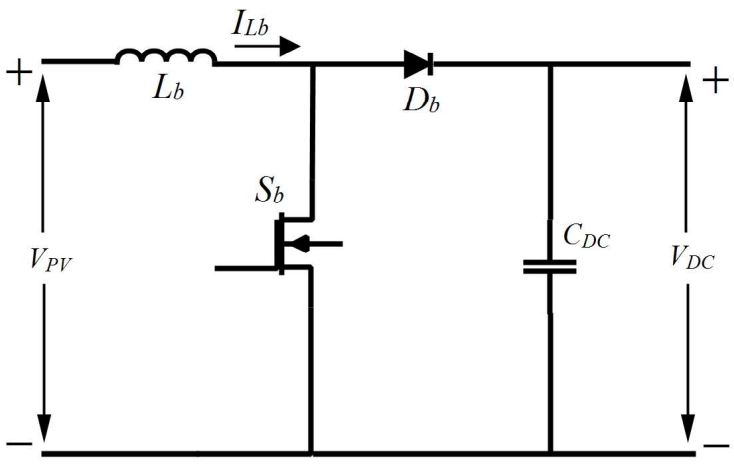

Figure 6.3: Boost converter used in the proposed system

The transfer capability of boost converter depends upon the inductor (L_b) and capacitor (C_{DC}) as shown in Fig. 6.3. The output voltage (V_{DC}), L_b and C_{DC} value is obtained as,

$$V_{DC} = \frac{1}{1-D_b} V_{PV} \tag{6.3}$$

$$L_b = \frac{V_{DC} D_b}{\Delta I_L f} \tag{6.4}$$

$$C_{DC} = \frac{V_{PV} D_b}{R_o \Delta V_{PV} f} \tag{6.5}$$

where $V_{PV}, \Delta I_L, f, \Delta V_{PV}$ and R_o are the input voltage, inductor ripple current, switching frequency, capacitor ripple voltage and output impedance of boost converter, respectively. Other than this, D_b is the duty ratio of boost converter, obtained by the control strategy as shown below.

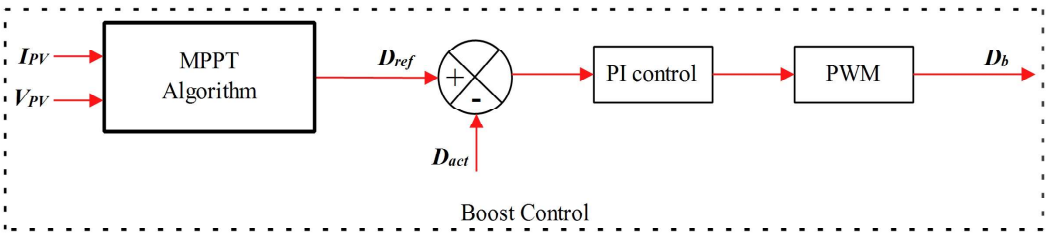

Figure 6.4: Control structure of the boost converter

The D_b is used to maintain the desired DC-link voltage through boost converter. The obtained DC-link voltage is used as input for the bi-directional converter in EV charger and ESS.

6.3.3 Bi-directional converter

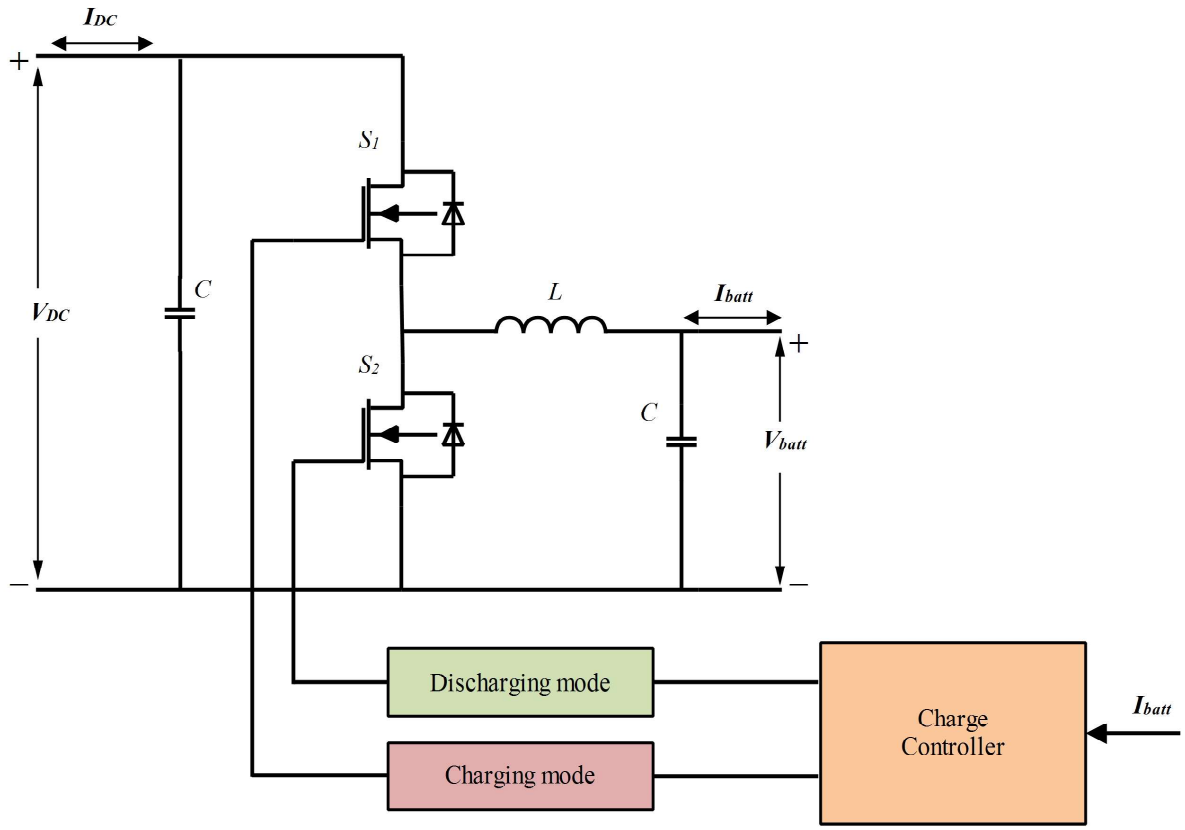

Figure 6.5: Circuit diagram of a bi-directional converter with control used in the proposed system

The proposed system consists of two BDC of the same power rating as shown in Fig. 6.1. One is used in EV charger and other is used in ESS. In Fig. 6.5, a BDC model is presented which operate in two modes i.e. charging and discharging. During charging mode it acts as a buck converter, on other hand, it behaves as a boost converter during discharging mode.

Charging mode

In charging mode, DC-link is connected as an input of BDC and battery is connected as a load on the output side. To achieve the voltage level of the battery (V_{batt}) at the output side, BDC operates in buck mode with components as an inductor (L_{buck}) and capacitor (C_{buck}). The

values of (L_{buck}) and (C_{buck}) depends upon the corresponding voltage and current rating of the converter. These values are calculated as follows.

$$L_{buck} = \frac{(V_{DC} - V_{batt})D_{buck}}{\Delta I_L f} \tag{6.6}$$

$$C_{buck} = \frac{(1 - D_{buck})V_{batt}}{8L_{buck}\Delta V_{batt} f^2} \tag{6.7}$$

where ΔI_L and f are the ripple current and switching frequency for the buck mode, respectively.

Discharging mode

Similarly, in discharging mode, BDC is interfacing the DC-link and battery. In this mode, battery act as an input source and DC-link as the output. The DC-link voltage level is higher than the battery terminal voltage. Therefore, the BDC operates in boost mode with the help of the corresponding components value. The components such as inductor (L_{boost}) and capacitor (C_{boost}) values in boost mode is calculated as follows.

$$L_{boost} = \frac{V_{batt} D_{boost}}{\Delta I_L f} \tag{6.8}$$

$$C_{boost} = \frac{V_{DC} D_{boost}}{R_o \Delta V_{DC} f} \tag{6.9}$$

where ΔV_{DC} and R_o are the ripple voltage and output impedance for the boost mode, respectively. However, the BDC operates in both modes. The values of inductor L_{BDC} and capacitor C_{BDC} are considered as follows.

$$L_{BDC} = max\,(L_{buck}, L_{boost}) \tag{6.10}$$

$$C_{BDC} = max\,(C_{buck}, C_{boost}) \tag{6.11}$$

Further, the operation of the BDC depends on the duty ratio such as D_{buck} and D_{boost} which are obtained during charging and discharging control respectively. There are various control methods such as constant current (CC), constant voltage (CV), pulse, reflex and con-

stant current/constant voltage (CC/CV) method. Among all these methods, CC and CC/CV method are mostly preferred for high C-rate charging so that charging time can be reduced. Therefore, for the ease of simulation, we have carried out a CC method which is shown in Fig. 6.6.

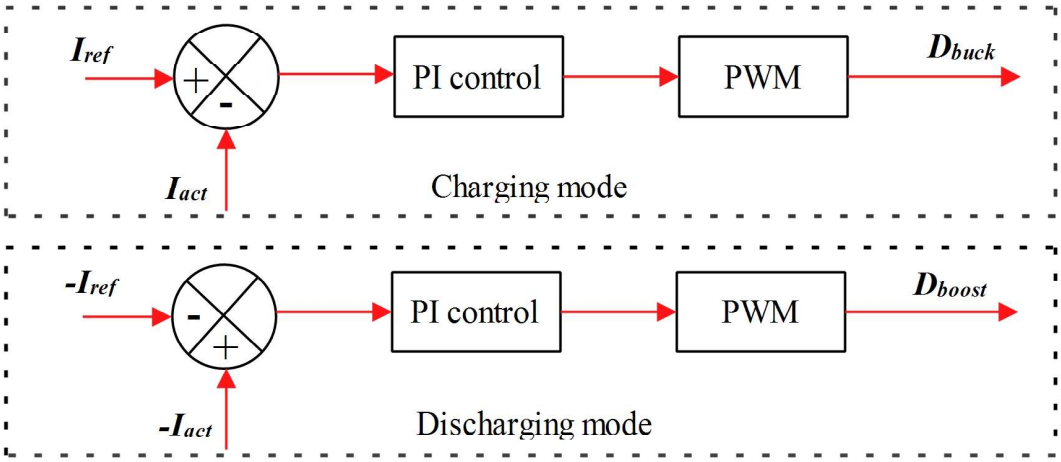

Figure 6.6: Constant current method of the bi-directional converter during (i) charging and (ii) discharging mode

Further, the obtained duty ratios are used for the charging and discharging operation of EV and ESS batteries for the proposed system. The performance of the proposed system is carried out by assuming modes. The characteristic analysis of the system during these modes are depicted in section.

6.4 Results and Discussions

The proposed PV based charging station (PVBCS) consists of a 24 kWp PV generation for the EV batteries of 15 kWh capacity. Additionally, an ESS of 15 kWh capacity is added to the proposed system. It has been used as an emergency supply to the EV batteries in case of low PV generation and stores the energy during the time of high PV generation. Further, the system has been designed in MATLAB/Simulink. The performance of the proposed system analysed by considering three modes. These modes are categorized such as EV battery charging (i) with PVBCS in absence of ESS, (ii) with PVBCS in the presence of ESS and (iii) with ESS in the absence PV generation. Every mode is analysed for 12s. on the basis of charging rate (C-rate) which replicate the power demand at a time of EV battery. Initially, the EV battery is charged at 0.5 C-rate for 3s. and a step of 0.5 C-rate is added at every 3s. up to 12s. Whenever the

power demand increases or decreases in terms of C-rate, the connected ESS and PV generation are participating accordingly in the aforementioned modes. The performance of every mode is discussed in terms of power, SoC, terminal voltage and current of the battery in following subsections.

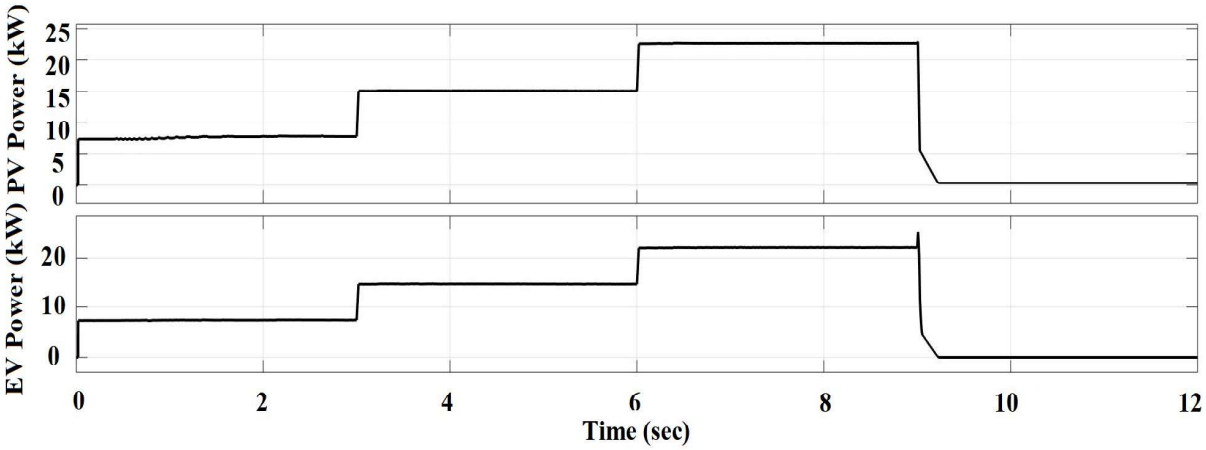

Figure 6.7: Power response curve of PV and EV

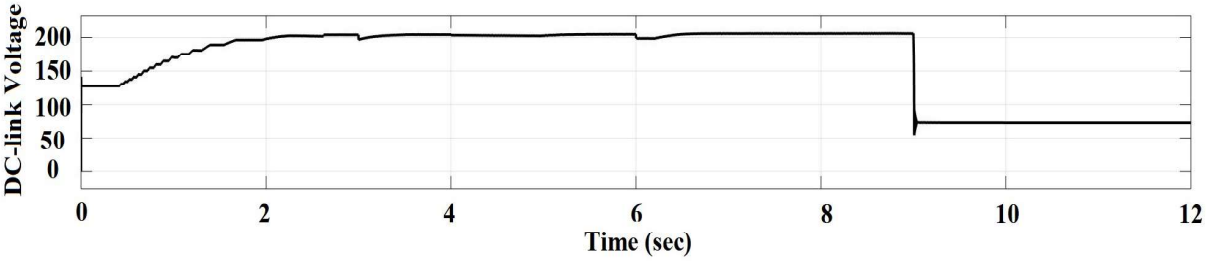

Figure 6.8: DC-link voltage at DC bus of the system

6.4.1 Charging of EV battery with PVBCS in the absence of ESS:

In this mode, Fig. 6.7 states that PV generation is sufficient to charge the EV battery till 1.5 C-rate. Further, the increase in EV battery C-rate indicates that PV generated is not sufficient to charge the EV battery. The increase in the C-rate of EV battery leads to decrease in DC-link voltage. Therefore, the DC-link voltage is maintained constant during power fluctuations with the proposed control strategy as shown in Fig. 6.4. This constant DC-link voltage provides desired terminal voltage for EV batteries continuously. The SoC, current and terminal voltage of the EV battery response are shown in Fig. 6.9. As the energy demand increases from the

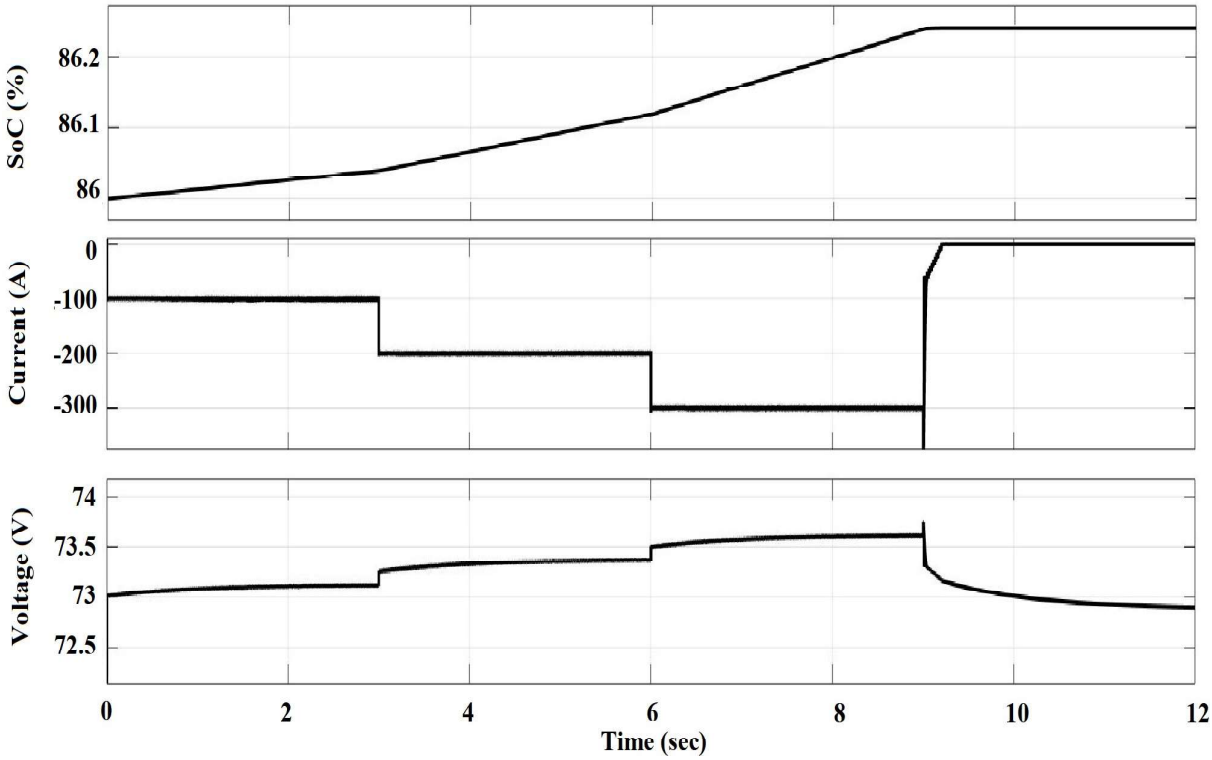

Figure 6.9: Response of the EV battery in terms of SoC, current and voltage

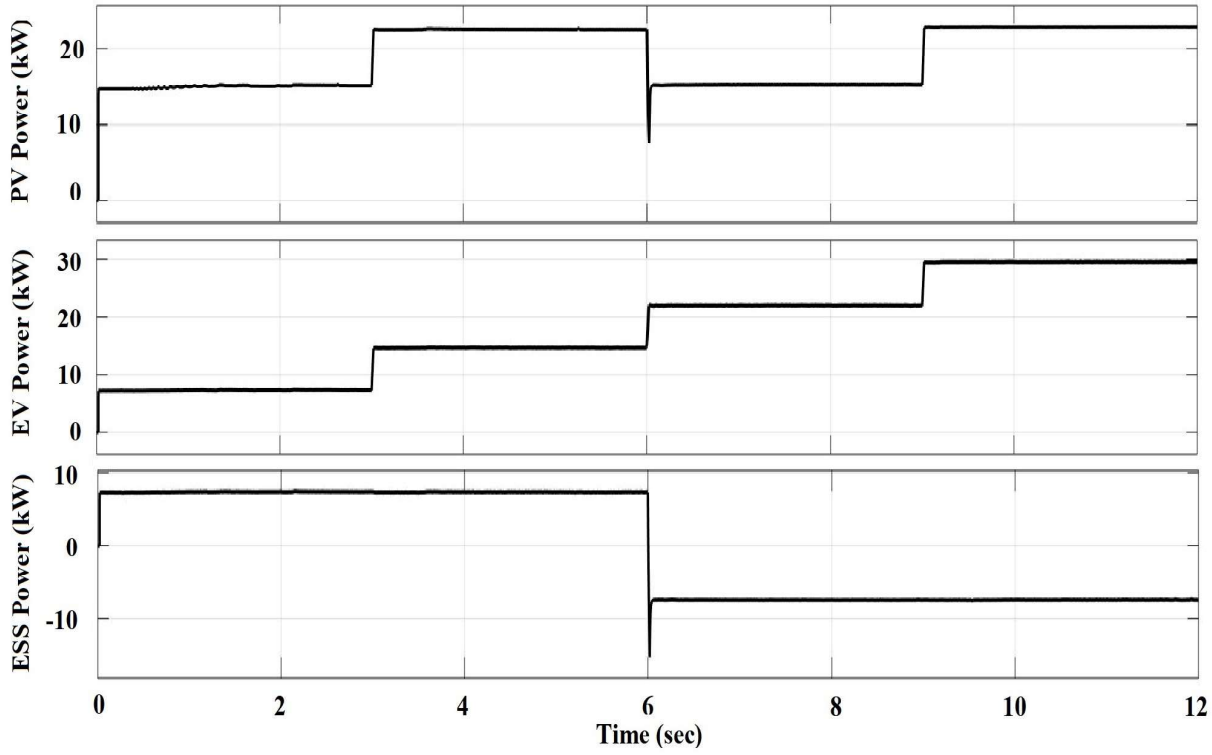

Figure 6.10: Power response curve of PV, EV and ESS

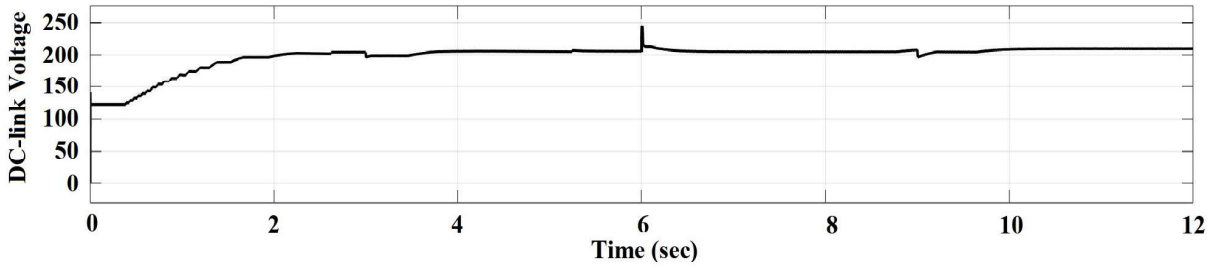

Figure 6.11: DC-link voltage response when PV and ESS charging the EV

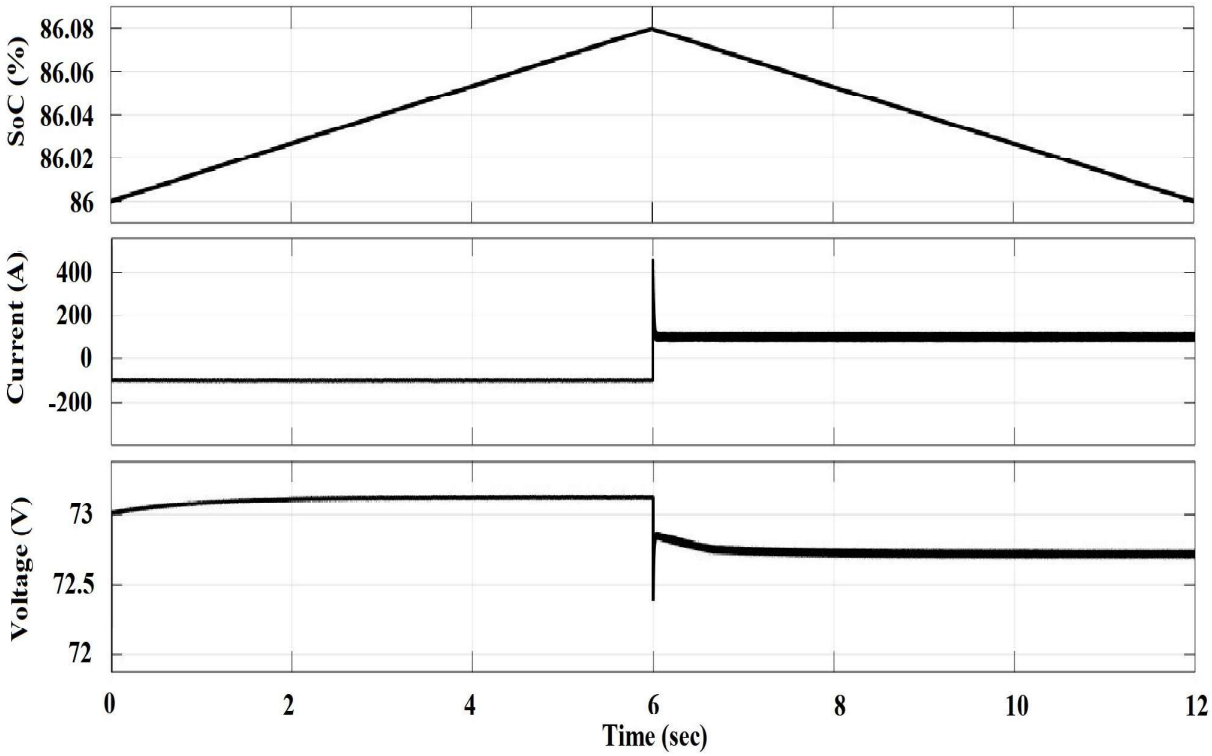

Figure 6.12: EV Battery response such as SoC, current and voltage

EV battery (from 1.5 to 2 C-rate), only PV is unable to fulfil the demand. Therefore, an ESS is connected with PV to fulfil the requirement which is shown in the next case.

6.4.2 Charging of EV battery with PVBCS in the presents of ESS:

For this mode, the PV generation is sufficient to charge the EV and ESS battery until EV battery reaches to 1 C-rate. Further, the rise in C-rate of EV battery indicates the PV generated power is not sufficient to charge the battery. Therefore, the ESS battery discharges the stored energy to charge the EV battery along with PV generation. As a result, the EV battery can be charged up to 2 C-rate as shown in Fig. 6.10. The corresponding SoC, current and terminal voltage of

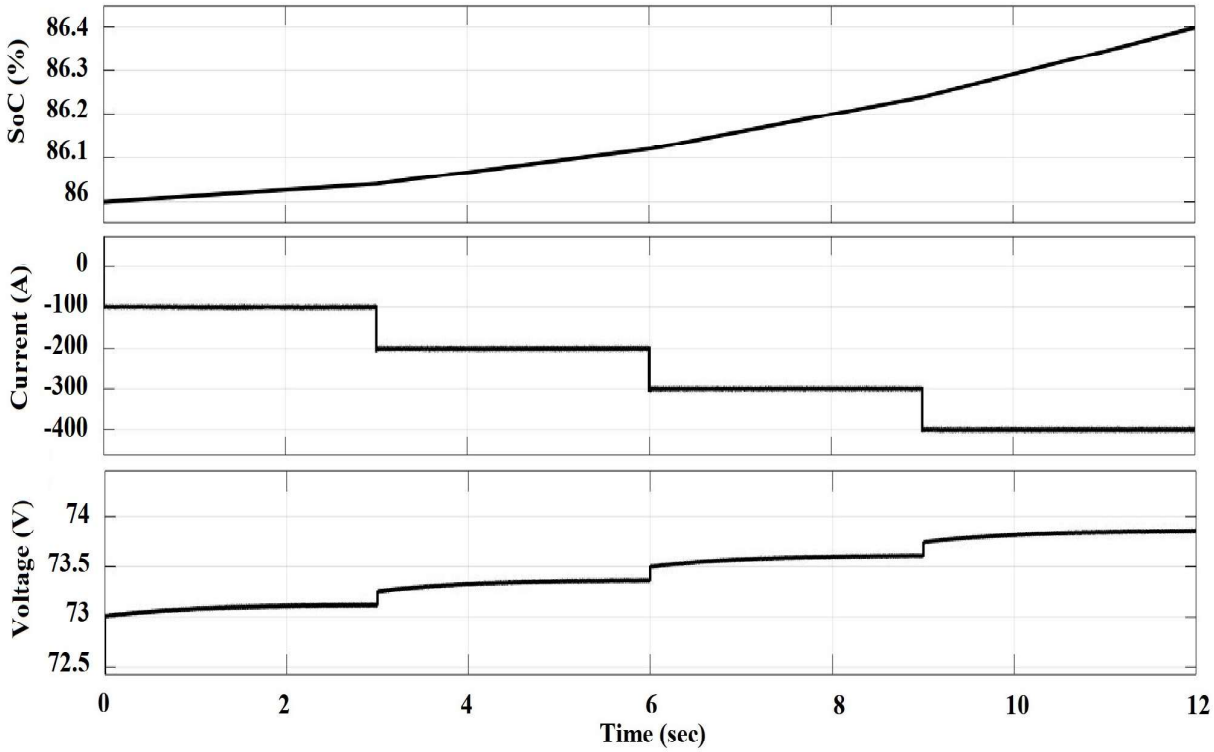

Figure 6.13: ESS Battery responses such as SoC, current and voltage

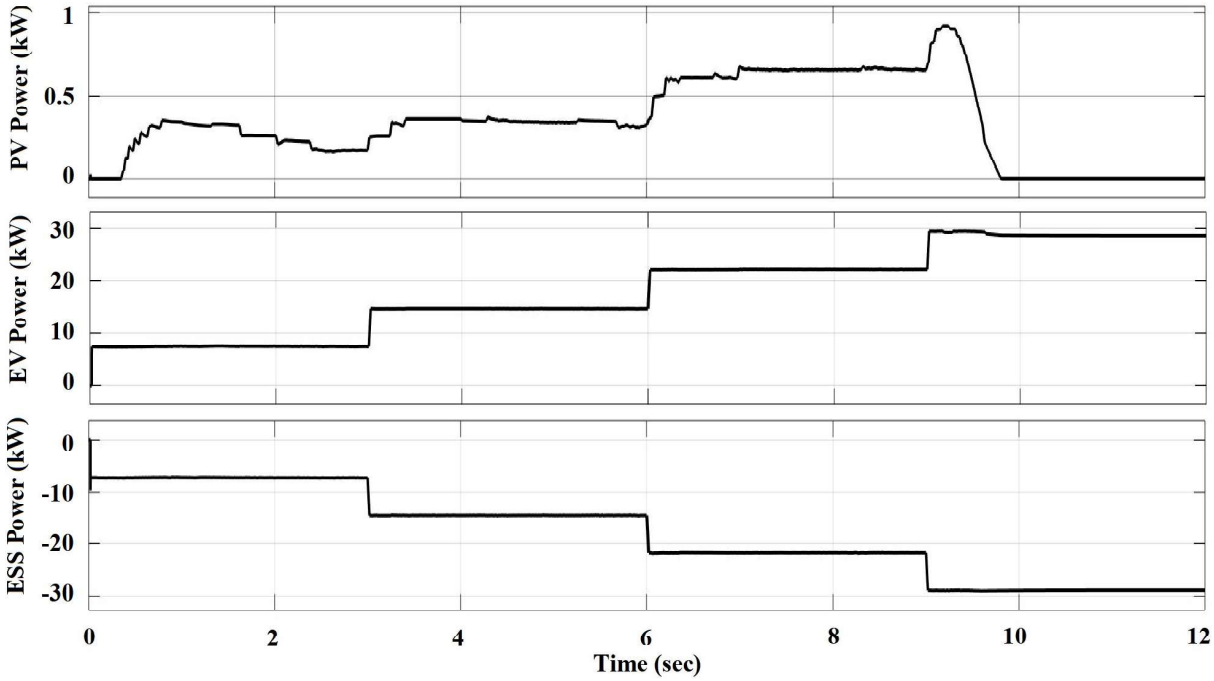

Figure 6.14: Power response for EV and ESS

EV and ESS battery response are shown in Fig. 6.12 and 6.13 respectively. The system DC-link voltage is maintained constant which is shown in Fig. 6.11. This arrangement serves the system when PV generation is not sufficient. The worst scenario of this condition is when the

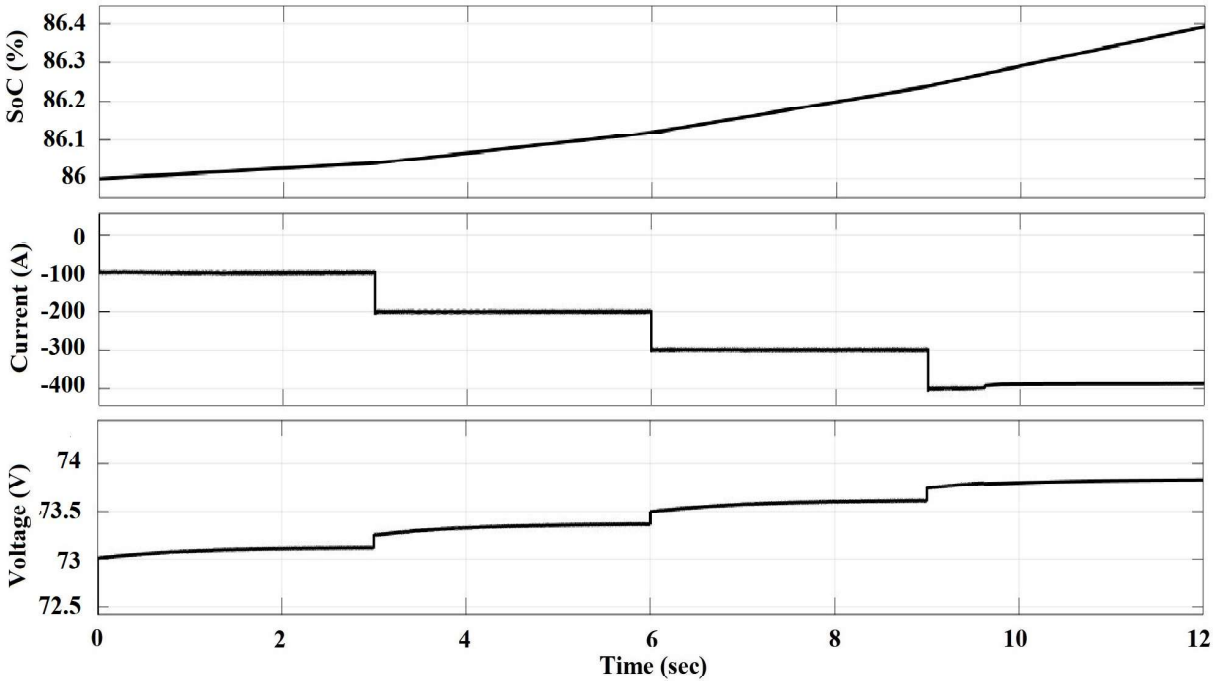

Figure 6.15: Response of the EV battery in terms of SoC, current and voltage

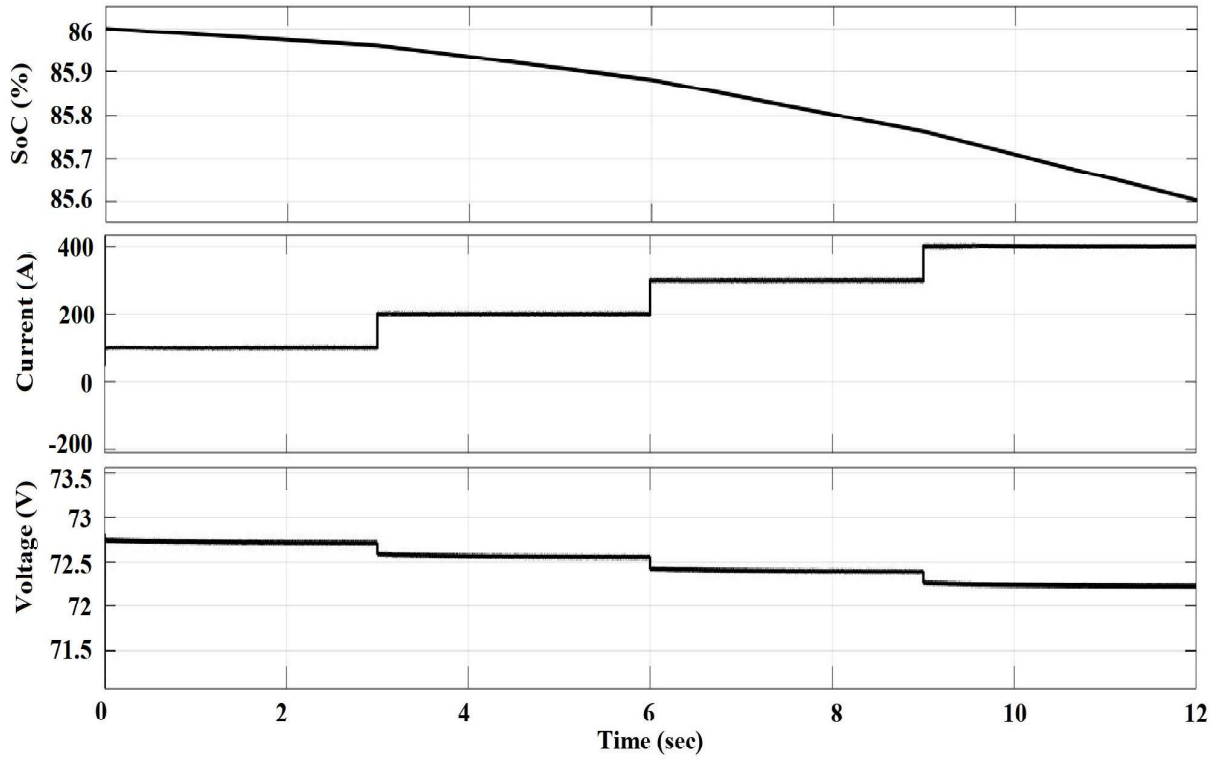

Figure 6.16: Response of the ESS battery in terms of SoC, current and voltage

PV is absent. Thus, in such a situation, the ESS will fulfil the requirement of the EV battery.

6.4.3 Charging of EV battery with ESS in the absence of PV:

In this mode, the EV battery is charged only from ESS battery. In Fig. 6.14, the PV generation is almost zero and simultaneously, EV and ESS power increase and decrease with the change in C-rate respectively. The corresponding SoC, current and terminal voltage of the EV and ESS batteries are increasing and decreasing at the equal rate which is shown in Fig. 6.15 and 6.16 respectively.

These modes reveal that the proposed PVBCS is capable of charging the EV battery at any circumstances and it also increases utilization of renewable energy sources to the maximum extent.

6.5 Conclusion

In this chapter, a PV based charging station (PVBCS) is proposed to charge the EV battery. This minimizes the grid burden and increases the EVs utilization at remote locations by using the PV. Moreover, an ESS is connected to the PVBCS which make the system work in any circumstances. The PVBCS with ESS exchange the power to charge the EV battery during the absence or reduced sunlight. Further, a constant current method is used to charge the EV battery at various C-rate. Altogether, this chapter presents a more sustainable and efficient CS as well as fervours pollution-free transportation.

Chapter 7

CONCLUSIONS AND FUTURE SCOPE

This chapter gives concluding remarks of the proposed schemes to resolve the research challenges such as the cost-effective structure of the system, handling of surplus power, implementation of effective MPPT techniques, reactive power compensation and energy source for charging stations. Additionally, it also suggests future research goals for the researchers in GIPV system domain for the betterment of electricity users as well as suppliers.

7.1 Conclusions

The core concept of using a PV system is to enhance the clean power production and support the utility grid. This thesis introduces the chronology of PV systems, involved power processing stages, various topologies of converters used for power conversion and the role of the GIPV system in the present electricity scenario. Moreover, it also highlights the various research challenges involved during power generation process from the GIPV systems. In this respect, preliminary research works are analyzed and compared to find out the research goals while interfacing the PV system to the grid. Moreover, the research challenges such as large system structure, the performance of maximum power extracting techniques, handling of surplus power, utilization of PV system for reactive power compensation and uses for an electric vehicle energy source have also discussed. In this thesis, four different schemes have been proposed to resolve these research challenges and each is summarised as follows.

In the first scheme, a sensorless control scheme has been proposed, which minimizes the control complexity and cost of the system and improves the dynamic response. The sensorless control eliminates the high-cost DC-link voltage sensors, correspondingly avoids the outer control loop, which used to be implemented while using the conventional control scheme. At the place of a conventional outer control loop, a feed-forward control loop is introduced, which

deals with the estimated DC-link voltage and generates the reference current for active power generation. This scheme also works in variable irradiance conditions and on these conditions, the analysis of transient and harmonic gives a very close result, which proves the practicability of the proposed scheme.

In the second scheme, the surplus feed-in PV power is curtailed during peak hours of generation using the proposed modified P&O MPPT algorithm. Additionally, it resolves the operating point problem of drifting and oscillation near MPP. The proposed algorithm works in modified mode during non-peak hours. In this mode, the algorithm achieves the shortest path to reach the MPP using PV current information regarding irradiance change. On the other hand, during peak-hours, it works in a derated mode, which curtails the extra feed-in power to prevent the overvoltage problem at PCC and damage of grid-connected network's equipment such as circuit breakers, transformers and others. Additionally, the large step size used to improve the time response. The performance of the modified P&O has been compared with the conventional P&O algorithm at variable irradiance condition. The results show that the proposed algorithm responds faster and more accurately for MPP tracking, which proves the effectiveness of the modified P&O technique.

In the third scheme, a reactive power compensation scheme has been proposed using a MP&O algorithm for the locally connected non-linear loads. This proposed scheme utilizes the reactive power delivery aspect of the grid-interfaced VSI used in GIPV system. In this scheme, when VSI transfers the PV power at rated capacity, the MP&O derates the PV power generation and creates the margin to generate the reactive power for local non-linear loads. As a result, the dependency on grid for reactive power compensation minimizes without increasing the rating of the grid-interfaced VSI. The simulation results shows the effectiveness of the proposed MP&O algorithm which are tested in simulation-in-loop mode using Opal-RT 4510.

In the fourth scheme, to reduce the pollution and dependency on grid dependent charging stations, a PVBCS is proposed to charge the EV. In the proposed scheme, ESS is added in the system to make the system more reliable. The ESS stores the unexploited PV power and It utilized when irradiance is low or the sun is not available to supply energy for the EV charging. To charge the EVs, a constant current method is used at different charging-rates for various conditions such as PVBCS in the absence of ESS, PVBCS in the presence of ESS and the presence of ESS only. In the above conditions, the performance of the scheme has been found

satisfactory.

7.2 Future Scope

In the future, the demand for electricity is increasing gradually. Therefore, the contributions provided in this thesis are not enough to increase the participation of the GIPV system for grid support. There are still some research areas that need to be focused in the future. Therefore, in near future the researchers can be focused on the following aspects.

- To increase PV power generation using GIPV systems, some more effective converter (DC-DC and DC-AC) topologies need to be developed.
- To make the converters more functional, some better and efficient MPPT and VSI control strategy are needed to be developed.
- To eliminate the harmonics injections into the utility grid, an improved conditioning unit is required which avoids or minimizes the use of power filters. Simultaneously, the improved conditioning unit also able to handle the power quality issues which arise due to the sudden change in irradiance conditions.
- To be a part of the smart grid, existing GIPV system needs to synchronized with information and communications technology (ICT) and the internet of things (IoT).

Bibliography

[1] IEO(2019), "International energy outlook 2019," Tech. Rep., 2019 (accessed March 5, 2020).

[2] R. Singh, Y. Sood, and N. Padhy, "Development of renewable energy sources for indian power sector moving towards competitive electricity market," *in 2009 IEEE Power Energy Society General Meeting*, pp. 1–6, Jul. 2009.

[3] A. Singla, K. Singh, V. Yadav, and N. Padhy, "Development of distributed solar photovoltaic energy market in india," *in 2015 IEEE Power Energy Society General Meeting*, pp. 1–5, Jul. 2015.

[4] IEA(2018). (2019 (accessed March 5, 2020)) World energy outlook 2018.

[5] O. Ellabban, H. Rub, and F. Blaabjerg, "Renewable energy resources: Current status, future prospects and their enabling technology," *Renewable and Sustainable Energy Reviews*, vol. 39, pp. 748–764, Nov. 2014.

[6] J. Carrasco, L. Franquelo, J. Bialasiewicz, E. Galvan, R. Guisado, M. Prats, J. Leon, and N. Alfonso, "Power-electronic systems for the grid integration of renewable energy sources: A survey," *IEEE Transactions on Industrial Electronics*, vol. 53, no. 4, pp. 1002–1016, Jun. 2006.

[7] E. Romero, G. Spagnuolo, L. Franquelo, C. Ramos, T. Suntio, and W. Xiao, "Grid-connected photovoltaic generation plants: Components and operation," *IEEE Industrial Electronics Magazine*, vol. 7, no. 3, pp. 6–20, Sep. 2013.

[8] G. Quesada, F. Gispert, R. Lopez, M. Lumbreras, and A. Roca, "Electrical PV array reconfiguration strategy for energy extraction improvement in grid-connected PV systems," *IEEE Transactions on Industrial Electronics*, vol. 56, no. 11, pp. 4319–4331, Nov. 2009.

[9] S. Kouro, J. Leon, D. Vinnikov, and L. Franquelo, "Grid-connected photovoltaic systems: An overview of recent research and emerging PV converter technology," *IEEE Industrial Electronics Magazine*, vol. 9, no. 1, pp. 47–61, Mar. 2015.

[10] L. Hassaine, E. Olias, J. Quintero, and V. Salas, "Overview of power inverter topologies and control structures for grid-connected photovoltaic systems," *Renewable and Sustainable Energy Reviews*, vol. 30, pp. 796–807, Feb. 2014.

[11] F. Blaabjerg, Z. Chen, and S. Kjaer, "Power electronics as efficient interface in dispersed power generation systems," *IEEE Transactions on Power Electronics*, vol. 19, no. 5, pp. 1184–1194, Sep. 2004.

[12] D. Debnath and K. Chatterjee, "Two-stage solar photovoltaic based stand-alone scheme having battery as energy storage element for rural deployment," *IEEE Transactions on Industrial Electronics*, vol. 62, no. 7, pp. 4148–4157, Jul. 2015.

[13] S. Malla and C. Bhende, "Enhanced operation of stand-alone photovoltaic-diesel generator-battery system," *Electric Power Systems Research*, vol. 107, pp. 250–257, Feb. 2014.

[14] C. Bhende and S. Malla, "Voltage control of stand-alone wind and solar energy system," *International Journal of Electrical Power & Energy Systems*, vol. 56, pp. 361–373, Mar. 2014.

[15] S. Jain and V. Agarwal, "A single-stage grid-connected inverter topology for solar PV systems with maximum power point tracking," *IEEE Transactions on Power Electronics*, vol. 22, no. 5, pp. 1928–1940, Sep. 2007.

[16] S. Kjaer, J. Pedersen, and F. Blaabjerg, "A review of single-phase grid-connected inverters for photovoltaic modules," *IEEE Transactions on Industry Applications*, vol. 41, no. 5, pp. 1292–1306, Sep. 2005.

[17] M. Calais, J. Myrzik, T. Spooner, and V. Agelidis, "Inverters for single-phase grid-connected photovoltaic systems-an overview," *in Proc. IEEE 33rd Annual IEEE Power Electronics Specialists Conf.*, vol. 4, pp. 1995–2000, Jun. 2002.

[18] M. Meinhardt and G. Cramer, "Past, present and future of grid-connected photovoltaic and hybrid power systems," *in Proc. Power Engineering Society Summer Meeting*, vol. 2, pp. 1283–1288, Jul. 2000.

[19] D. Martins, "Analysis of a three-phase grid-connected PV power system using a modified dual-stage inverter," *ISRN Renewable Energy*, Jan. 2013.

[20] R. Gonzalez, J. Lopez, P. Sanchis, and L. Marroyo, "Transformerless inverter for single-phase photovoltaic systems," *IEEE Transactions on Power Electronics*, vol. 22, no. 2, pp. 693–697, Mar. 2007.

[21] W. Libo, Z. Zhengming, and L. Jianzheng, "A single-stage three-phase grid-connected photovoltaic system with modified MPPT method and reactive power compensation," *IEEE Transactions on Energy Conversion*, vol. 22, no. 4, pp. 881–886, Dec. 2007.

[22] Y. Zhou, W. Huang, P. Zhao, and J. Zhao, "A transformerless grid-connected photovoltaic system based on the coupled inductor single-stage boost three-phase inverter," *IEEE Transactions on Power Electronics*, vol. 29, no. 3, pp. 1041–1046, Mar. 2014.

[23] A. Yazdani, A. Fazio, H. Ghoddami, M. Russo, M. Kazerani, J. Jatskevich, K. Strunz, S. Leva, and J. Martinez, "Modeling guidelines and a benchmark for power system simulation studies of three-phase single-stage photovoltaic systems," *IEEE Transactions on Power Delivery*, vol. 26, no. 2, pp. 1247–1264, Apr. 2011.

[24] T. Wu, C. Chang, L. Lin, and C. Kuo, "Power loss comparison of single and two-stage grid-connected photovoltaic systems," *IEEE Transactions on Energy Conversion*, vol. 26, no. 2, pp. 707–715, Jun. 2011.

[25] R. Erickson and D. Maksimovic, *Fundamentals of power electronics*. Springer Science & Business Media, 2007.

[26] IEEE-Std-2003, "IEEE standard for interconnecting distributed resources with electric power systems," *IEEE Std 1547-2003*, pp. 1–28, Jul. 2003.

[27] O. Kulkarni, S. Doolla, and B. Fernandes, "Mode transition control strategy for multiple inverter based distributed generators operating in grid-connected and stand-alone mode," *in 2016 IEEE Applied Power Electronics Conference and Exposition (APEC)*, pp. 3376–3382, Mar. 2016.

[28] N. Rahim, J. Selvaraj, and C. Krismadinata, "Five-level inverter with dual reference modulation technique for grid-connected PV system," *Renewable Energy*, vol. 35, no. 3, pp. 712–720, Mar. 2010.

[29] N. Rahim, K. Chaniago, and J. Selvaraj, "Single-phase seven-level grid-connected inverter for photovoltaic system," *IEEE Transactions on Industrial Electronics*, vol. 58, no. 6, pp. 2435–2443, Jun. 2011.

[30] R. Teodorescu, M. Liserre, and P. Rodriguez, *Grid converters for photovoltaic and wind power systems*. John Wiley & Sons, 2011.

[31] I. Patrao, E. Figueres, F. González, and G. Garcerá, "Transformerless topologies for grid-connected single-phase photovoltaic inverters," *Renewable and Sustainable Energy Reviews*, vol. 15, no. 7, pp. 3423–3431, Sep. 2011.

[32] E. Koutroulis and F. Blaabjerg, "Design optimization of transformerless grid-connected PV inverters including reliability," *IEEE Transactions on Power Electronics*, vol. 28, no. 1, pp. 325–335, Jan. 2013.

[33] A. Darwish, D. Holliday, S. Ahmed, A. Massoud, and B. Williams, "A single-stage three-phase inverter based on cuk converters for PV applications," *IEEE Journal of Emerging and Selected Topics in Power Electronics*, vol. 2, no. 4, pp. 797–807, Dec. 2014.

[34] T. Kerekes, R. Teodorescu, P. Rodríguez, G. Vázquez, and E. Aldabas, "A new high efficiency single-phase transformerless PV inverter topology," *IEEE Transactions on Industrial Electronics*, vol. 58, no. 1, pp. 184–191, Jan. 2011.

[35] Z. Zhao, M. Xu, Q. Chen, J. Lai, and Y. Cho, "Derivation, analysis, and implementation of a boost-buck converter based high efficiency PV inverter," *IEEE Transactions on Power Electronics*, vol. 27, no. 3, pp. 1304–1313, Aug. 2012.

[36] V. Araújo, P. Zacharias, and R. Mallwitz, "Highly efficient single-phase transformerless inverters for grid-connected photovoltaic systems," *IEEE Transactions on Industrial Electronics*, vol. 57, no. 9, pp. 3118–3128, Sep. 2010.

[37] Y. Zhou and H. Li, "Analysis and suppression of leakage current in cascaded multilevel inverter based PV systems," *IEEE Transactions on Power Electronics*, vol. 29, no. 10, pp. 5265–5277, Oct. 2014.

[38] R. Selvamuthukumaran, A. Garg, and R. Gupta, "Hybrid multicarrier modulation to reduce leakage current in a transformerless cascaded multilevel inverter for photovoltaic systems," *IEEE Transactions on Power Electronics*, vol. 30, no. 4, pp. 1779–1783, Apr. 2015.

[39] W. Li, Y. Gu, H. Luo, W. Cui, X. He, and C. Xia, "Topology review and derivation methodology of single-phase transformerless photovoltaic inverters for leakage current suppression," *IEEE Transactions on Industrial Electronics*, vol. 62, no. 7, pp. 4537–4551, Jul. 2015.

[40] B. Yang, W. Li, Y. Gu, W. Cui, and X. He, "Improved transformerless inverter with common-mode leakage current elimination for a photovoltaic grid-connected power system," *IEEE Transactions on Power Electronics*, vol. 27, no. 2, pp. 752–762, Feb. 2012.

[41] Y. Yang, F. Blaabjerg, and H. Wang, "Low-voltage ride-through of single-phase transformerless photovoltaic inverters," *IEEE Transactions on Industry Applications*, vol. 50, no. 3, pp. 1942–1952, May 2014.

[42] F. Mattos, V. Lacerda, R. Valle, A. Ferreira, P. Barbosa, and H. Braga, "Contribution to the study of a single-phase and single-stage photovoltaic system," *IEEE Latin America Transactions*, vol. 13, no. 5, pp. 1265–1271, May 2015.

[43] T. Freddy, N. Rahim, W. Hew, and H. Che, "Comparison and analysis of single-phase transformerless grid-connected PV inverters," *IEEE Transactions on Power Electronics*, vol. 29, no. 10, pp. 5358–5369, Oct. 2014.

[44] S. Jain and V. Agarwal, "Comparison of the performance of maximum power point tracking schemes applied to single-stage grid-connected photovoltaic systems," *IET Electric Power Applications*, vol. 1, no. 5, pp. 753–762, Sep. 2007.

[45] B. Singh, C. Jain, and S. Goel, "ILST control algorithm of single-stage dual purpose grid connected solar PV system," *IEEE Transactions on Power Electronics*, vol. 29, no. 10, pp. 5347–5357, Oct. 2014.

[46] C. Jain and B. Singh, "Single-phase single-stage multifunctional grid interfaced solar photovoltaic system under abnormal grid conditions," *IET Generation, Transmission & Distribution*, vol. 9, no. 10, pp. 886–894, Jun. 2015.

[47] Y. Zhou, W. Huang, F. Hong, and C. Wang, "Modelling analysis and power loss of coupled inductor single-stage boost inverter based grid-connected photovoltaic power system," *IET Power Electronics*, vol. 9, no. 8, pp. 1664–1674, Jun. 2016.

[48] D. Casadei, G. Grandi, and C. Rossi, "Single-phase single-stage photovoltaic generation system based on a ripple correlation control maximum power point tracking," *IEEE Transactions on Energy Conversion*, vol. 21, no. 2, pp. 562–568, Jun. 2006.

[49] F. Neves, M. Carrasco, F. Mancilla, G. Azevedo, and V. Santos, "Unbalanced grid fault ride-through control for single-stage photovoltaic inverters," *IEEE Transactions on Power Electronics*, vol. 31, no. 4, pp. 3338–3347, Apr. 2016.

[50] R. Agarwal, I. Hussain, and B. Singh, "Three-phase single-stage grid tied solar PV ECS using PLL-less fast CTF control technique," *IET Power Electronics*, vol. 10, no. 2, pp. 178–188, Feb. 2017.

[51] Y. Chen and K. Smedley, "A cost-effective single-stage inverter with maximum power point tracking," *IEEE Transactions on Power Electronics*, vol. 19, no. 5, pp. 1289–1294, Sep. 2004.

[52] L. Chen, A. Amirahmadi, Q. Zhang, N. Kutkut, and I. Batarseh, "Design and implementation of three-phase two-stage grid-connected module integrated converter," *IEEE Transactions on Power Electronics*, vol. 29, no. 8, pp. 3881–3892, Aug. 2014.

[53] Z. Wang, L. Chang, and M. Mao, "DC voltage sensorless control method for three-phase grid-connected inverters," *IET Power Electronics*, vol. 3, no. 4, pp. 552–558, Jul. 2010.

[54] N. Naidu and B. Singh, "Sensorless control of single voltage source converter-based doubly fed induction generator for variable speed wind energy conversion system," *IET Power Electronics*, vol. 7, no. 12, pp. 2996–3006, Dec. 2014.

[55] A. Mallik and A. Khaligh, "DC-link voltage sensorless control of a three-phase boost power factor correction rectifier," *in 2016 IEEE Transportation Electrification Conference and Expo (ITEC)*, pp. 1–6, Jun. 2016.

[56] N. Zakzouk, A. Abdelsalam, A. Helal, and B. Williams, "PV single-phase grid-connected converter: DC-link voltage sensorless prospective," *IEEE Journal of Emerging and Selected Topics in Power Electronics*, vol. 5, no. 1, pp. 526–546, Mar. 2017.

[57] S. Taghizadeh, M. Ghartemani, M. Hossain, and J. Lu, "A fast and robust DC-bus voltage control method for single-phase voltage-source DC/AC converters," *IEEE Transactions on Power Electronics*, vol. 34, no. 9, pp. 9202–9212, Sep. 2019.

[58] S. Taghizadeh, M. Hossain, J. Lu, and M. Ghartemani, "An enhanced DC-bus voltage-control loop for single-phase grid-connected DC/AC converters," *IEEE Transactions on Power Electronics*, vol. 34, no. 6, pp. 5819–5829, Jun. 2019.

[59] O. Wasynezuk, "Dynamic behavior of a class of photovoltaic power systems," *IEEE transactions on power apparatus and systems*, vol. PER-3, no. 9, pp. 3031–3037, Sep. 1983.

[60] A. Ahmed, L. Ran, S. Moon, and J. Park, "A fast PV power tracking control algorithm with reduced power mode," *IEEE Transactions on Energy Conversion*, vol. 28, no. 3, pp. 565–575, Sep. 2013.

[61] Z. Salam and J. Ahmed, "A modified P&O maximum power point tracking method with reduced steady-state oscillation and improved tracking efficiency," *IEEE Transactions on Sustainable Energy*, vol. 7, no. 4, pp. 1506–1515, Oct. 2016.

[62] L. Zhang, S. Yu, T. Fernando, H. Iu, and K. Wong, "An online maximum power point capturing technique for high-efficiency power generation of solar photovoltaic systems," *Journal of Modern Power Systems and Clean Energy*, vol. 7, no. 2, pp. 357–368, Mar. 2019.

[63] T. Esram and P. Chapman, "Comparison of photovoltaic array maximum power point tracking techniques," *IEEE Transactions on Energy Conversion*, vol. 22, no. 2, pp. 439–449, Jun. 2007.

[64] B. Subudhi and R. Pradhan, "A comparative study on maximum power point tracking techniques for photovoltaic power systems," *IEEE Transactions on Sustainable Energy*, vol. 4, no. 1, pp. 89–98, Jan. 2013.

[65] A. Amir, A. Amir, C. Seng, A. Khateb, J. Selvaraj, and N. Rahim, "Application of modified classical numerical methods for DMPPT on buck and boost converters," *Solar Energy*, vol. 173, pp. 437–448, Oct. 2018.

[66] R. Kadri, P. Gaubert, and G. Champenois, "An improved maximum power point tracking for photovoltaic grid-connected inverter based on voltage-oriented control," *IEEE Transactions on Industrial Electronics*, vol. 58, no. 1, pp. 66–75, Jan. 2011.

[67] M. Killi and S. Samanta, "Modified perturb and observe MPPT algorithm for drift avoidance in photovoltaic systems," *IEEE Transactions on Industrial Electronics*, vol. 62, no. 9, pp. 5549–5559, Sep. 2015.

[68] S. Lyden and M. Haque, "A simulated annealing global maximum power point tracking approach for PV modules under partial shading conditions," *IEEE Transactions on Power Electronics*, vol. 31, no. 6, pp. 4171–4181, Jun. 2016.

[69] Y. Wang, Y. Li, and X. Ruan, "High-accuracy and fast-speed MPPT methods for PV string under partially shaded conditions," *IEEE Transactions on Industrial Electronics*, vol. 63, no. 1, pp. 235–245, Jan. 2016.

[70] S. Mohanty, B. Subudhi, and P. Ray, "A new MPPT design using grey wolf optimization technique for photovoltaic system under partial shading conditions," *IEEE Transactions on Sustainable Energy*, vol. 7, no. 1, pp. 181–188, Jan. 2016.

[71] M. Ghasemi, H. Forushani, and M. Parniani, "Partial shading detection and smooth maximum power point tracking of PV arrays under PSC," *IEEE Transactions on Power Electronics*, vol. 31, no. 9, pp. 6281–6292, Sep. 2016.

[72] Y. Yang and H. Wen, "Adaptive perturb and observe maximum power point tracking with current predictive and decoupled power control for grid-connected photovoltaic inverters," *Journal of Modern Power Systems and Clean Energy*, vol. 7, no. 2, pp. 422–432, Mar. 2019.

[73] F. Liu, S. Duan, F. Liu, B. Liu, and Y. Kang, "A variable step size INC MPPT method for PV systems," *IEEE Transactions on Industrial Electronics*, vol. 55, no. 7, pp. 2622–2628, Jul. 2008.

[74] A. Ghamrawi, J. Gaubert, and D. Mehdi, "A new dual-mode maximum power point tracking algorithm based on the perturb and observe algorithm used on solar energy system," *Solar Energy*, vol. 174, pp. 508–514, Nov. 2018.

[75] Y. Yang, P. Enjeti, F. Blaabjerg, and H. Wang, "Wide-scale adoption of photovoltaic energy: Grid code modifications are explored in the distribution grid," *IEEE Industry Applications Magazine*, vol. 21, no. 5, pp. 21–31, Sep. 2015.

[76] M. Braun, T. Stetz, R. Bründlinger, C. Mayr, K. Ogimoto, H. Hatta, H. Kobayashi, B. Kroposki, B. Mather, M. Coddington, K. Lynn, G. Graditi, A. Woyte, and I. Macgill, "Is the distribution grid ready to accept large-scale photovoltaic deployment ? state of the art, progress, and future prospects," *Progress in photovoltaics: Research and applications*, vol. 20, no. 6, pp. 681–697, Nov. 2012.

[77] F. Blaabjerg, R. Teodorescu, M. Liserre, and A. Timbus, "Overview of control and grid synchronization for distributed power generation systems," *IEEE Transactions on industrial electronics*, vol. 53, no. 5, pp. 1398–1409, Oct. 2006.

[78] P. Mishra, A. Pradhan, and P. Bajpai, "Voltage control of PV inverter connected to unbalanced distribution system," *IET Renewable Power Generation*, vol. 13, no. 9, pp. 1587–1594, Jun. 2019.

[79] A. Cagnano, E. Tuglie, M. Liserre, and R. Mastromauro, "Online optimal reactive power control strategy of PV inverters," *IEEE Transactions on Industrial Electronics*, vol. 58, no. 10, pp. 4549–4558, Oct. 2011.

[80] G. Tsengenes and G. Adamidis, "Investigation of the behavior of a three phase grid-connected photovoltaic system to control active and reactive power," *Electric Power Systems Research*, vol. 81, no. 1, pp. 177–184, Jan. 2011.

[81] S. Mishra, D. Ramasubramanian, and P. Sekhar, "A seamless control methodology for a grid-connected and isolated PV-diesel microgrid," *IEEE Transactions on Power Systems*, vol. 28, no. 4, pp. 4393–4404, Nov. 2013.

[82] Y. Bae, T. Vu, and R. Kim, "Implemental control strategy for grid stabilization of grid-connected PV system based on german grid code in symmetrical low to medium voltage network," *IEEE Transactions on Energy Conversion*, vol. 28, no. 3, pp. 619–631, Sep. 2013.

[83] V. Kumar, K. Reddy, and D. Thukaram, "Coordination of reactive power in grid-connected wind farms for voltage stability enhancement," *IEEE Transactions on Power Systems*, vol. 29, no. 5, pp. 2381–2390, Sep. 2014.

[84] C. Chang, Y. Lin, Y. Chen, and Y. Chang, "Simplified reactive power control for single-phase grid-connected photovoltaic inverters," *IEEE Transactions on Industrial Electronics*, vol. 61, no. 5, pp. 2286–2296, May 2014.

[85] Y. Han, H. Li, P. Shen, E. Coelho, and J. Guerrero, "Review of active and reactive power sharing strategies in hierarchical controlled microgrids," *IEEE Transactions on Power Electronics*, vol. 32, no. 3, pp. 2427–2451, Mar. 2017.

[86] S. Jain, M. Shadmand, and R. Balog, "Decoupled active and reactive power predictive control for PV applications using a grid-tied quasi-Z-source inverter," *IEEE Journal of Emerging and Selected Topics in Power Electronics*, vol. 6, no. 4, pp. 1769–1782, Dec. 2018.

[87] S. Weckx, C. Gonzalez, and J. Driesen, "Combined central and local active and reactive power control of PV inverters," *IEEE Transactions on Sustainable Energy*, vol. 5, no. 3, pp. 776–784, Jul. 2014.

[88] A. Haque, "Chapter 3 - solar energy," in *Electric Renewable Energy Systems*, M. Rashid, Ed. Boston: Academic Press, 2016, pp. 40–59.

[89] P. Zarina, S. Mishra, and P. Sekhar, "Exploring frequency control capability of a PV system in a hybrid PV-rotating machine-without storage system," *International Journal of Electrical Power & Energy Systems*, vol. 60, pp. 258–267, Sep. 2014.

[90] Q. Zhou and J. Bialek, "Generation curtailment to manage voltage constraints in distribution networks," *IET Generation, Transmission & Distribution*, vol. 1, no. 3, pp. 492–498, May. 2007.

[91] R. Tonkoski, L. Lopes, and T. El, "Coordinated active power curtailment of grid connected PV inverters for overvoltage prevention," *IEEE Transactions on Sustainable Energy*, vol. 2, no. 2, pp. 139–147, Apr. 2011.

[92] W. Omran, M. Kazerani, and M. Salama, "Investigation of methods for reduction of power fluctuations generated from large grid-connected photovoltaic systems," *IEEE Transactions on Energy Conversion*, vol. 26, no. 1, pp. 318–327, Mar. 2011.

[93] Y. Yang, H. Wang, F. Blaabjerg, and T. Kerekes, "A hybrid power control concept for PV inverters with reduced thermal loading," *IEEE Transactions on Power Electronics*, vol. 29, no. 12, pp. 6271–6275, Dec. 2014.

[94] A. Sangwongwanich, Y. Yang, and F. Blaabjerg, "High-performance constant power generation in grid-connected PV systems," *IEEE Transactions on Power Electronics*, vol. 31, no. 3, pp. 1822–1825, Mar. 2016.

[95] A. Sangwongwanich, Y. Yang, F. Blaabjerg, and H. Wang, "Benchmarking of constant power generation strategies for single-phase grid-connected photovoltaic systems," *IEEE Transactions on Industry Applications*, vol. 54, no. 1, pp. 447–457, Jan. 2018.

[96] H.Tafti, A. Maswood, G. Konstantinou, J. Pou, and F. Blaabjerg, "A general constant power generation algorithm for photovoltaic systems," *IEEE Transactions on Power Electronics*, vol. 33, no. 5, pp. 4088–4101, May 2018.

[97] M. Singh, P. Kumar, I. Kar, and N. Kumar, "A real-time smart charging station for EVs designed for V2G scenario and its coordination with renewable energy sources," *in 2016 IEEE Power and Energy Society General Meeting (PESGM)*, pp. 1–5, Jul. 2016.

[98] A. Bhatti and Z. Salam, "Charging of electric vehicle with constant price using photovoltaic based grid-connected system," *in 2016 IEEE International Conference on Power and Energy (PECon)*, pp. 268–273, Nov. 2016.

[99] P. Tulpule, V. Marano, S. Yurkovich, and G. Rizzoni, "Economic and environmental impacts of a PV powered workplace parking garage charging station," *Applied Energy*, vol. 108, pp. 323–332, Aug. 2013.

[100] P. Goli and W. Shireen, "PV integrated smart charging of PHEVs based on DC-link voltage sensing," *IEEE Transactions on Smart Grid*, vol. 5, no. 3, pp. 1421–1428, May 2014.

[101] J. Hernandez and F. Sutil, "Electric vehicle charging stations feeded by renewable: PV and train regenerative braking," *IEEE Latin America Transactions*, vol. 14, no. 7, pp. 3262–3269, Jul. 2016.

[102] X. Li, D. Hui, and X. Lai, "Battery energy storage station (BESS)-based smoothing control of photovoltaic (PV) and wind power generation fluctuations," *IEEE Transactions on Sustainable Energy*, vol. 4, no. 2, pp. 464–473, Apr. 2013.

[103] B. Biegel, D. Madjidian, V. Spudić, A. Rantzer, and J. Stoustrup, "Distributed low-complexity controller for wind power plant in derated operation," *in 2013 IEEE International Conference on Control Applications (CCA)*, pp. 146–151, Aug. 2013.

[104] T. Fiedler, "Simulation of a power system with large renewable penetration," *Renewable Energy*, vol. 130, pp. 319–328, Jan. 2019.

[105] T. Shimizu, O. Hashimoto, and G. Kimura, "A novel high-performance utility interactive photovoltaic inverter system," *IEEE Transactions on Power Electronics*, vol. 18, no. 2, pp. 704–711, Mar. 2003.

[106] R. Panigrahi, S. Mishra, S. Srivastava, A. Srivastava, and N. Schulz, "Grid integration of small - scale photovoltaic systems in secondary distribution network - A review," *IEEE Transactions on Industry Applications*, vol. 56, no. 3, pp. 3178–3195, 2020.

[107] Z. Ahmad and S. Singh, "Comparative analysis of single-phase transformerless inverter topologies for grid-connected PV system," *Solar Energy*, vol. 149, pp. 245–271, Jun. 2017.

[108] D. Talavera, F. Munoz, G. Jimenez, and C. Rus, "A new approach to sizing the photovoltaic generator in self-consumption systems based on cost competitiveness, maximizing direct self consumption," *Renewable Energy*, vol. 130, pp. 1021–1035, Jan. 2019.

[109] R. Bálint, A. Fodor, and A. Magyar, "Model-based power generation estimation of solar panels using weather forecast for microgrid application," *Acta Polytechnica Hungarica*, vol. 16, no. 7, pp. 149–165, 2019.

[110] R. Bálint, A. Fodor, I. Szalkai, Z. Szalkai, and A. Magyar, "Modeling and calculation of the global solar irradiance on slopes," *Hungarian Journal of Industry and Chemistry*, vol. 47, no. 1, pp. 57–63, 2019.

[111] A. Anzalchi and A. Sarwat, "Overview of technical specifications for grid-connected photovoltaic systems," *Energy Conversion and Management*, vol. 152, pp. 312–327, Nov. 2017.

[112] M. Singh, V. Khadkikar, A. Chandra, and R. Varma, "Grid interconnection of renewable energy sources at the distribution level with power-quality improvement features," *IEEE Transactions on Power Delivery*, vol. 26, no. 1, pp. 307–315, Jan. 2011.

[113] X. Wang, F. Zhuo, J. Li, L. Wang, and S. Ni, "Modeling and control of dual-stage high-power multifunctional PV system in d - q - *o* coordinate," *IEEE Transactions on Industrial Electronics*, vol. 60, no. 4, pp. 1556–1570, Apr. 2013.

[114] C. Jain and B. Singh, "A three-phase grid tied SPV system with adaptive DC-link voltage for CPI voltage variations," *IEEE Transactions on Sustainable Energy*, vol. 7, no. 1, pp. 337–344, Jan. 2016.

[115] C. Trujillo, F. Santamaría, and E. Gaona, "Modeling and testing of two-stage grid-connected photovoltaic micro-inverters," *Renewable Energy*, vol. 99, pp. 533–542, Dec. 2016.

[116] F. Blaabjerg and Y. Yang, "Chapter 3 - overview of single-phase grid-connected photovoltaic systems," in *Renewable Energy Devices and Systems with Simulations in MATLAB® and ANSYS®*. Boca Raton: CRC Press, 2017, pp. 41–66.

[117] H. Athari, M. Niroomand, and M. Ataei, "Review and classification of control systems in grid-tied inverters," *Renewable and Sustainable Energy Reviews*, vol. 72, pp. 1167–1176, May 2017.

[118] N. Guerrero, A. Rey, and E. Reyes, "Overview and comparative study of two control strategies used in 3-phase grid-connected inverters for renewable systems," *Renewable Energy Focus*, vol. 19-20, pp. 75–89, Jun. 2017.

[119] N. Guerrero, A. Bueno, O. Ortiz, and E. Reyes, "Synchronization algorithms for grid-connected renewable systems: Overview, tests and comparative analysis," *Renewable and Sustainable Energy Reviews*, vol. 75, pp. 629–643, Aug. 2017.

[120] G. Masters, "Chapter 9 - photovoltaic systems," in *Renewable and Efficient Electric Power Systems*. New Jersey: John Wiley & Sons, 2005, pp. 505–604.

[121] A. Nordin and A. Omar, "Modeling and simulation of photovoltaic (PV) array and maximum power point tracker (MPPT) for grid-connected PV system," *in 2011 3rd International Symposium Exhibition in Sustainable Energy Environment (ISESEE)*, pp. 114–119, Jun. 2011.

[122] S. Kumar, A. Verma, I. Hussain, B. Singh, and C. Jain, "Better control for a solar energy system: Using improved enhanced phase-locked loop-based control under variable solar intensity," *IEEE Industry Applications Magazine*, vol. 23, no. 2, pp. 24–36, Mar. 2017.

[123] S. Chander, P. Agarwal, and I. Gupta, "Design, modeling and simulation of DC-DC converter," *in 2010 Conference Proceedings IPEC*, pp. 456–461, Oct. 2010.

[124] R. Krishan, A. Verma, and B. Prasad, "Small signal stability analysis of grid connected distributed PV and wind energy system," *in 2014 6th IEEE Power India International Conference (PIICON)*, pp. 1–6, Dec. 2014.

[125] N. Jayaram, P. Agarwal, and S. Das, "Mathematical model of five-level AC/DC converter in abc reference frame," *International Journal of Electrical Power & Energy Systems*, vol. 62, pp. 469–475, Nov. 2014.

[126] G. Franklin, J. Powell, and A. Emami, *Feedback Control of Dynamic Systems*, 7th ed. Pearson, 2014.

[127] Y. Du, W. Xiao, Y. Hu, and D. Lu, "Control approach to achieve burst mode operation with DC-link voltage protection in single-phase two-stage PV inverters," *in 2014 IEEE Energy Conversion Congress and Exposition (ECCE)*, pp. 47–52, Sep. 2014.

[128] Y. Du, D. Lu, G. Chu, and W. Xiao, "Closed-form solution of time-varying model and its applications for output current harmonics in two-stage PV inverter," *IEEE Transactions on Sustainable Energy*, vol. 6, no. 1, pp. 142–150, Jan. 2015.

[129] D. Kumar and F. Zare, "Harmonic analysis of grid connected power electronic systems in low voltage distribution networks," *IEEE Journal of Emerging and Selected Topics in Power Electronics*, vol. 4, no. 1, pp. 70–79, Mar. 2016.

[130] O. Abedinia, D. Raisz, and N. Amjady, "Effective prediction model for hungarian small-scale solar power output," *IET Renewable Power Generation*, vol. 11, no. 13, pp. 1648–1658, Nov. 2017.

[131] O. Abedinia, N. Amjady, and N. Ghadimi, "Solar energy forecasting based on hybrid neural network and improved metaheuristic algorithm," *Computational Intelligence*, vol. 34, no. 1, pp. 241–260, Oct. 2018.

[132] M. Biswal, B. Pati, and A. Pradhan, "Adaptive distance relay setting for series compensated line," *International Journal of Electrical Power & Energy Systems*, vol. 52, pp. 198–206, Nov. 2013.

[133] F. Olivier, P. Aristidou, D. Ernst, and T. Cutsem, "Active management of low-voltage networks for mitigating overvoltages due to photovoltaic units," *IEEE Transactions on Smart Grid*, vol. 7, no. 2, pp. 926–936, Mar. 2016.

[134] M. Shayestegan, "Overview of grid-connected two-stage transformer-less inverter design," *Journal of Modern Power Systems and Clean Energy*, vol. 6, no. 4, pp. 642–655, Jul. 2018.

[135] A. Ali, M. Sayed, and E. Mohamed, "Modified efficient perturb and observe maximum power point tracking technique for grid-tied PV system," *International Journal of Electrical Power & Energy Systems*, vol. 99, pp. 192–202, Jul. 2018.

[136] A. Ramyar, H. Iman, and S. Farhangi, "Global maximum power point tracking method for photovoltaic arrays under partial shading conditions," *IEEE Transactions on Industrial Electronics*, vol. 64, no. 4, pp. 2855–2864, Apr. 2017.

[137] S. Liu, P. Liu, and X. Wang, "Stochastic small-signal stability analysis of grid-connected photovoltaic systems," *IEEE Transactions on Industrial Electronics*, vol. 63, no. 2, pp. 1027–1038, Feb. 2016.

[138] V. Kumar and M. Singh, "Sensorless DC-link control approach for three-phase grid integrated PV system," *International Journal of Electrical Power & Energy Systems*, vol. 112, pp. 309–318, Nov. 2019.

[139] A. Singh, I. Hussain, and B. Singh, "Double-stage three-phase grid-integrated solar PV system with fast zero attracting normalized least mean fourth based adaptive control," *IEEE Transactions on Industrial Electronics*, vol. 65, no. 5, pp. 3921–3931, May 2018.

[140] M. Molina, "Energy storage and power electronics technologies: A strong combination to empower the transformation to the smart grid," *Proceedings of the IEEE*, vol. 105, no. 11, pp. 2191–2219, Nov. 2017.

[141] K. Hussein, I. Muta, T. Hoshino, and M. Osakada, "Maximum photovoltaic power tracking: An algorithm for rapidly changing atmospheric conditions," *IEE Proceedings - Generation, Transmission and Distribution*, vol. 142, no. 1, pp. 59–64, Jan. 1995.

[142] J. Ahmed and Z. Salam, "An enhanced adaptive P&O MPPT for fast and efficient tracking under varying environmental conditions," *IEEE Transactions on Sustainable Energy*, vol. 9, no. 3, pp. 1487–1496, Jul. 2018.

[143] Y. Mahmoud, W. Xiao, and H. Zeineldin, "A simple approach to modeling and simulation of photovoltaic modules," *IEEE Transactions on Sustainable Energy*, vol. 3, no. 1, pp. 185–186, Jan. 2012.

[144] N. Femia, G. Petrone, G. Spagnuolo, and M. Vitelli, "Optimization of perturb and observe maximum power point tracking method," *IEEE Transactions on Power Electronics*, vol. 20, no. 4, pp. 963–973, Jul. 2005.

[145] A. Verma, R. Krishan, and S. Mishra, "A novel PV inverter control for maximization of wind power penetration," *in 2016 IEEE 7th Power India International Conference (PIICON)*, pp. 1–5, Nov. 2016.

[146] A. Sangwongwanich, A. Abdelhakim, Y. Yang, and K. Zhou, "Chapter 6 - control of single-phase and three-phase DC/AC converters," in *Control of Power Electronic Converters and Systems*. Academic Press, 2018, pp. 153–173.

[147] S. Choudhary, "9 most polluted Indian cities to get electric vehicles ecosystem," *Business Today*, Aug. 1997.

[148] W. Kempton and S. Letendre, "Electric vehicles as a new power source for electric utilities," *Transportation Research Part D: Transport and Environment*, vol. 2, no. 3, pp. 157–175, Sep. 1997.

[149] I. Subotic, N. Bodo, and E. Levi, "Single-phase on-board integrated battery chargers for EVs based on multiphase machines," *IEEE Transactions on Power Electronics*, vol. 31, no. 9, pp. 6511–6523, Sep. 2016.

[150] I. Subotic and E. Levi, "A review of single-phase on-board integrated battery charging topologies for electric vehicles," *in 2015 IEEE Workshop on Electrical Machines Design, Control and Diagnosis (WEMDCD)*, pp. 136–145, Mar. 2015.

[151] H. Nunna, S. Battula, S. Doolla, and D. Srinivasan, "Energy management in smart distribution systems with vehicle-to-grid integrated microgrids," *IEEE Transactions on Smart Grid*, vol. 9, no. 5, pp. 4004–4016, Sep. 2018.

[152] M. Kumar, S. Srivastava, and S. Singh, "Control strategies of a DC microgrid for grid connected and islanded operations," *IEEE Transactions on Smart Grid*, vol. 6, no. 4, pp. 1588–1601, Jul. 2015.

[153] P. Görbe, A. Magyar, and K. Hangos, "Reduction of power losses with smart grids fueled with renewable sources and applying EV batteries," *Journal of Cleaner Production*, vol. 34, pp. 125–137, Oct. 2012.

[154] A. Göllei, P. Görbe, and A. Magyar, "Modeling and optimization of electrical vehicle batteries in complex clean energy systems," *Journal of Cleaner Production*, vol. 34, pp. 138–145, Oct. 2012.

[155] S. Mandelli, M. Molinas, E. Park, M. Leonardi, E. Colombo, and M. Merlo, "The role of storage in emerging country scenarios," *Energy Procedia*, vol. 73, pp. 112–123, Jun. 2015.

[156] A. Boveri, F. Silvestro, M. Molinas, and E. Skjong, "Optimal sizing of energy storage systems for shipboard applications," *IEEE Transactions on Energy Conversion*, vol. 34, no. 2, pp. 801–811, Jun. 2019.

[157] S. Chattopadhyay, "Electric power quality in power system," Ph.D. dissertation, University of Calcutta, 2009.

Appendix A

Clarke and Park Transformation

The Clarke and Park transformation is used to transform a three phase to a two phase quantity. The Clarke and Park transformations are used to transform from the natural (abc) to stationary ($\alpha\beta$) reference frame and from stationary ($\alpha\beta$) to rotating (dq) reference frame, respectively [157]. Therefore, Lets suppose I_a, I_b and I_c are the instantaneous balanced three phase current. Then,

$$I_a + I_b + I_c = 0 \tag{A.1}$$

Thus, transformation from three phase (a,b,c) to two phase $(\alpha\beta)$is commonly known as Clarke transformation which is illustrated as follows.

$$\begin{bmatrix} I_\alpha \\ I_\beta \end{bmatrix} = \frac{2}{3} \times \begin{bmatrix} 1 & -\frac{1}{2} & -\frac{1}{2} \\ 0 & \frac{\sqrt{3}}{2} & -\frac{\sqrt{3}}{2} \end{bmatrix} \times \begin{bmatrix} I_a \\ I_b \\ I_c \end{bmatrix} \tag{A.2}$$

Now, the transformation from $\alpha\beta$ to dq-reference frame is using Park's transformation which is illustrated as follows.

$$\begin{bmatrix} I_d \\ I_q \end{bmatrix} = \begin{bmatrix} cos\theta & sin\theta \\ -sin\theta & cos\theta \end{bmatrix} \times \begin{bmatrix} I_\alpha \\ I_\beta \end{bmatrix} \tag{A.3}$$

where θ is obtained from the phase lock loop (PLL).